Technical Report

TR-10-59

Aspects of geochemical evolution of the SKB near field in the frame of SR-Site

Clara Sena, Joaquín Salas, David Arcos
Amphos 21

September 2010

Svensk Kärnbränslehantering AB
Swedish Nuclear Fuel
and Waste Management Co

Box 250, SE-101 24 Stockholm
Phone +46 8 459 84 00

ISSN 1404-0344
SKB TR-10-59
ID 1257823
Updated 2014-01

Aspects of geochemical evolution of the SKB near field in the frame of SR-Site

Clara Sena, Joaquín Salas, David Arcos
Amphos 21

September 2010

Update notice

The original report, dated September 2010, was found to contain both factual and editorial errors which have been corrected in this updated version. The corrected factual errors are presented below.

Updated 2014-01

Location	Original text	Corrected text
Page 10, paragraph 2, line 5	/Fernández and Villar et al. 2006/	/Fernández and Villar 2010/
Page 13, paragraph 1, line 5	/Olsson and Karnland, in press/	/Olsson and Karnland 2009/
Page 19, Table 3-2, footnote 2 and 3	/Olsson and Karnland in press/	/Olsson and Karnland 2009/
Page 24, Table 4-1, footnote (e) and (h)	/Åkesson et al. 2009/	/Åkesson et al. 2010/
Page 33, paragraph 4, line 2	/Åkesson et al. 2009/	/Åkesson et al. 2010/
Page 105, Reference Hartley et al. 2006	SKB R-06-99	SKB R-06-98
Page 106, Reference Olsson and Karnland, in press	Olsson S, Karnland O (in press). Characterisation of bentonites from Kutch, India and Milos, Greece – some candidate tunnel back-fill materials?	Olsson S, Karnland O, 2009. Characterisation of bentonites from Kutch, India and Milos, Greece – some candidate tunnel back-fill materials? SKB R-09-53, Svensk Kärnbränslehantering AB.
Page 106, Reference Villar et al. 2008	Behaviour of a bentonite barrier in the laboratory: Experimental results up to 8 years and numerical simulation.	Behaviour of a bentonite barrier in the laboratory: Experimental results up to 8 years and numerical simulation. Physics and Chemistry of the Earth, 33, S476-S485.
Page 106, Reference Åkesson et al. 2009	Åkesson M, Kristensson O, Börgesson L, 2009. THM modelling of buffer, backfill and other system components. Critical processes and scenarios.	Åkesson M, Kristensson O, Börgeson L, Dueck A, Hernelind J, 2010. THM modelling of buffer, backfill and other system components. Critical processes and scenarios. SKB TR-10-11, Svensk Kärnbränslehantering AB

Abstract

The concept for the final disposal of high level nuclear waste (HLNW) developed by the Swedish Nuclear Waste Management Company (SKB) entails a multi-barrier system that surrounds the HLNW, which is also known as the near-field.

In the near-field, the buffer is initially subject to a high thermal gradient induced by the heat generated by the radioactive decay of the HLNW. During this period, the buffer is also subject to a hydrodynamic pressure induced by the surrounding water saturated rock massif which progressively leads to the saturation of the buffer. After saturation and cooling of the near-field, the interaction of groundwater with the bentonite buffer may result in an evolving distribution of some aqueous species in the bentonite porewater, as well as the redistribution of accessory minerals and the cation exchanger composition in the montmorillonite interlayer. The distribution of aqueous and solid species in the buffer can affect, directly or indirectly, some of the relevant safety function indicators defined by /SKB 2006/. In this context, the work developed by /Arcos et al. 2006/ is revisited in the present work and, based on new data from SKB, additional models are developed for the SR-Site Safety Assessment. The work presented here represents an update of the model conducted within the SR-Can exercise /Arcos et al. 2006/ and, therefore, similar simulation cases are developed.

Three aspects must be considered regarding the geochemical evolution of the near field: (1) the effect of the thermal period; (2) the processes during the saturation of bentonite; and, (3) the interaction of the water-saturated bentonite with the local groundwater. In this numerical exercise, two types of bentonite are analysed: the MX-80 and the Deponit CA-N.

The effect of the thermal period and the water saturation are analysed in a series of one-dimensional radial-symmetric simulations performed using TOUGHREACT /Xu et al. 2008/ which is a reactive transport code that accounts for variably saturated multi-phase flow under non-isothermal conditions. These simulations are based on the outcomes of a previous numerical model built with the same code for the simulation of the LOT-A2 experiment /Sena et al. 2010/.

The interaction of the fully water-saturated bentonite with groundwater is assessed through a series of tree-dimensional (3D) numerical models performed in PHAST /Parkhurst et al. 2004/.

In order to assess the thermo-hydraulic and geochemical evolution of the near-field, a fracture in the granitic host rock is considered to intersect the deposition hole in which bentonite buffer surrounds the copper canister containing the spent fuel. The main achievements obtained in the numerical models developed for the saturation of the bentonite buffer during the thermal period indicate that although the model predicts a temporary evaporation of water near the copper canister, no chloride salt reaches saturation, and therefore, chloride is considered to behave conservatively. In addition, if the advective flow rate through the fracture is relatively low, the chemical composition of the groundwater in the fracture around the buffer could be influenced by the bentonite chemistry. Anhydrite, the high-temperature stable Ca-sulphate mineral, is predicted to precipitate around the copper canister when the higher temperatures are established (above 56ºC). Nevertheless, as the temperature in the near-filed tends to decrease towards the regional value of 15ºC, anhydrite previously precipitated progressively dissolves, and in turn, gypsum tends to replace the higher temperature Ca-sulphate mineral.

During the thermal period, the primary quartz of the bentonite tends to dissolve close to the copper canister and re-precipitate close to the contact between the bentonite buffer and the granite. The evolution of this mineral is a function of the thermal conditions as its solubility increases with temperature.

Computed results for the water-saturated period of the near-field indicate that the interaction between the minerals that constitute the MX-80 bentonite and the Forsmark groundwater that occurs nowadays at the depth of the future repository leads to an overall depletion in gypsum in favour of calcite precipitation. In addition, the initially Na-rich montmorillonite interlayer is predicted to enrich in calcium.

In the case that the bentonite buffer is composed of Deponit CA-N bentonite, the inflow of Forsmark groundwater leads to the dissolution of gypsum and dolomite in favour of more calcite precipitated. In addition, the initially Mg and Ca-rich montmorillonite interlayer becomes depleted in these cations and enriched in sodium.

In both bentonite types considered, the inflow of Forsmark groundwater leads to relatively small changes on the pH of the near-field with respect to the values expected for the initial porewater of the engineered barriers.

Sammanfattning

Det koncept för hantering av högaktivt kärnavfall som utvecklats av Svensk Kärnbränslehantering AB (SKB) består av ett multi-barriärsystem som omger avfallet. De tekniska barriärerna tillsammans med det närmaste berget benämns närområdet.

I närområdet utsätts bufferten initialt för en termisk gradient orsakat värmen från det radioaktiva sönderfallet i avfallet. Under denna period utsätts bufferten också för ett hydrodynamiskt tryck från grundvattnet i berget. Detta leder till att bufferten successivt mättas med vatten. I perioden efter vattenmättnad och nerkylning, kan interaktionen med grundvattnet leda till en förändrad fördelning av specier i porvattnet i bufferten samt en omfördelning av accessoriska mineral och sammansättning i jonbytespositionerna i montmorilloniten. Fördelningen av fasta ämnen och lösta specier i bufferten kan direkt eller indirekt påverka några av dess definierade säkerhetsfunktioner/SKB 2006/. För att belysa detta har det arbete som presenterades i /Arcos et al. 2006/ vidareutvecklats i denna studie och, baserat på nya data och instruktioner från SKB, har nya modeller tagits fram för att användas i säkerhetsanalysen SR-Site. Arbetet i denna rapport är en uppdatering av modelleringen från SR-Can /Arcos et al. 2006/ och därför presenteras liknande modelleringsfall.

Hänsyn måste tas till tre aspekter i beskrivningen av den geokemiska utvecklingen i närområdet:

1. Effekten av perioden med förhöjd temperatur.
2. Effekten av mättnadsförloppet.
3. Interaktionen med det lokala grundvattnet.

I den här numeriska studien har två olika bentoniter beaktats: MX-80 and Deponit CA-N.

Effekten av perioden med förhöjd temperatur och mättnadsförloppet har studerats i en serie endimensionella radialsymmetriska simuleringar med TOUGHREACT /Xu et al. 2008/, som är ett reaktiv-transport datorprogram som kan hantera flerfas transport i ett variabelt mättat medium under icke-isotermiska förhållanden. Simuleringarna baseras på slutsatserna från en tidigare modellering av LOT-A2 experimentet med samma program /Sena et al. 2010/.

Interaktionen mellan den vattenmättade bufferten och det lokala grundvattnet ha studerats med en serie av tredimensionella (3D) modeller i PHAST /Parkhurst et al. 2004/.

För att studera den termohydrauliska och geokemiska utvecklingen i närområdet har en det antagits att en vattenförande spricka skär deponeringshålet med kapsel och buffert. De viktigaste observationerna i de numeriska simuleringarna i är att, även om modellen förutsäger en förångning när vatten kommer i kontakt med kopparkapseln, inga kloridsalter når mättnad och därför kan klorid antas att uppföra sig som ett konservativt spårämne. Till detta visas också, om flödet i sprickan som skär deponeringshålet är tillräckligt lågt, att grundvattnet sammansättning kan påverkas av buffertens kemi. Anhydrit, den stabila kalciumsulfaten vid högre temperaturer, faller ut runt kopparkapseln vid temperaturer över 56 °C. När temperaturen i närområdet sjunker löser sig den utfällda anhydriten och gips bildas i dess ställe.

Under perioden med förhöjd temperatur kan primär kvarts lösa sig nära kapseln och falla ut i kontaktzonen mellan berg och buffert. Detta styrs av de termiska förhållandena eftersom lösligheten ökar med temperaturen.

Beräknade resultat för den vattenmättade perioden i närområdet indikerar att interaktionen mellan mineralen i MX-80 och dagens grundvatten på förvarsdjup i Forsmark leder till en utlakning av gips och en utfällning av kalcit. Den tidigare natriumdominerade bentoniten kommer också att successivt anrikas med kalcium.

Om bufferten består av Deponit CA-N bentonit kommer interaktionen med grundvattnet i Forsmark att leda till en upplösning av gips och dolomit samt en utfällning av kalcit. I det här fallet kommer jonbytet att gå åt andra hållet jämfört med MX-80 eftersom initialt kalcium och magnesium kommer att bytas mot natrium.

För båda bentoniterna kommer dock interaktionen med vattnet i Forsmark att leda till relativt små förändringar i sammansättning och pH i porvattnet jämfört med de värden som förväntas råda initialt.

Contents

1 Introduction

The interaction of groundwater with the bentonite buffer will result in an evolving distribution of some aqueous species in bentonite pore water, as well as the redistribution of accessory minerals. This distribution of aqueous and solid species in the buffer can affect, directly or indirectly, some of the relevant safety functions defined by SKB.

1.1 Objectives

The main objective of the present work is to develop numerical simulations that help us to understand the main features that influence the hydro-geochemical evolution of the near-field of a high level nuclear waste (HLNW), according to the KBS-3 repository design by SKB. These numerical simulations are an update of the work presented in /Arcos et al. 2006/.

Three aspects will be considered in the geochemical evolution of the near field: (1) the interaction of bentonite with groundwater, (2) the effect of bentonite water saturation, and (3) the effect of the thermal period.

1.2 Motivation and context

In the KBS-3 design for the HLNW repository, there are two main safety functions that must be maintained by the components of the repository /SKB 2006/:

1. The isolation of spent nuclear fuel within the copper canisters, and
2. to retard any releases from the canister, in case of failure of canister isolation.

These two main safety functions are described by a number of subordinate safety function indicators /SKB 2006/: pH, redox conditions (oxygen concentration), concentration of corroding agents (like aqueous sulphide), concentration of cations participating in montmorillonite transformation reactions (like iron and potassium), and concentration of major divalent cations that could affect the bentonite erosion through the formation of bentonite colloids. The thermal-hydro-geochemical models developed in the present work are intended to supply a quantitative assessment of the concentrations for those chemical species that are considered either as safety function indicators, or directly affecting them, like pH, aqueous carbonate, aqueous sulphide and divalent cation concentration /SKB 2006/. The evolution of the redox conditions of the near-field will not be assessed in the present work. No disturbances on the porewaters redox are expected to occur during the thermal stage and during the long-term evolution of the bentonite. The reactivity processes included in our conceptual model don't affect the redox capacity of the buffer. Oxygen has been previously exhausted and, in absence of oxidizing condition, the buffer capacity of smectite is the key factor controlling the redox evolution of the system /Arcos et al. 2008/. Pyrite, that is considered to be in equilibrium in porewaters, is not oxidized under anoxic conditions.

In 2006, /Arcos et al. 2006/ developed geochemical models based on hydrological, engineering design, and geological information of Forsmark, to evaluate the behaviour of the bentonite barrier and also the backfill material that fills the access tunnels of a KBS-3 repository (Figure 1-1). The models developed by these authors include a set of geochemical processes that are important for the interaction between groundwater and the engineered barriers of the near-filed, such as precipitation/dissolution of solid phases, cation exchange and surface acidity reactions in the clay fraction of the bentonite.

Regarding the possible paths for groundwater to reach the near-field, /Arcos et al. 2006/ developed two cases: Case I where groundwater-buffer interaction is simulated in a 3D model, and Case II, where groundwater-backfill-buffer interaction is simulated in a 2D model. In Case I, groundwater is considered to reach the near-filed through a pre-existing fracture that intersects a deposition hole and, therefore, the circulating groundwater is put in direct contact with the bentonite buffer. In Case

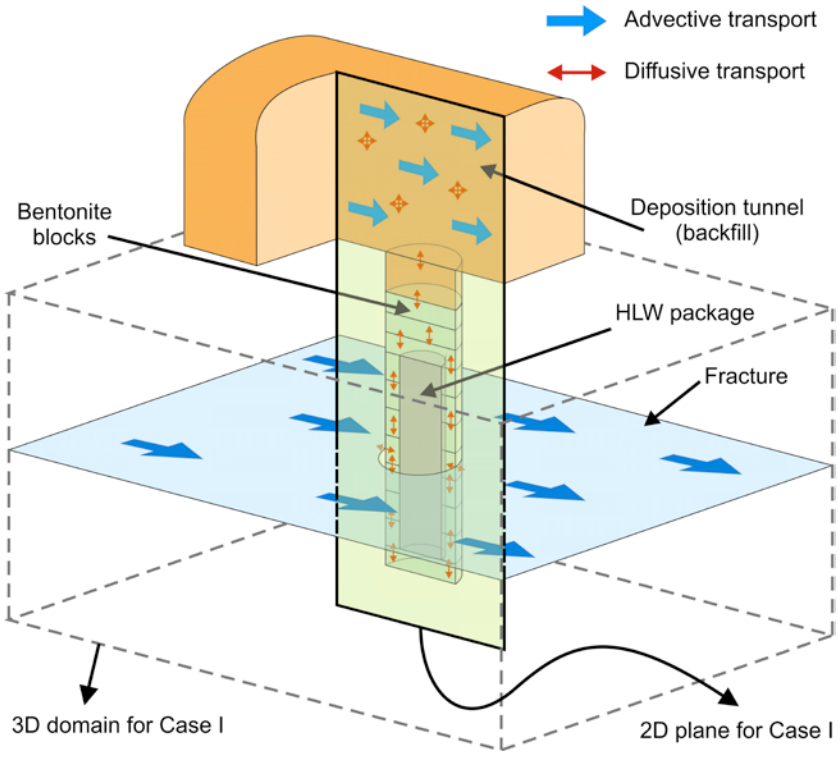

Figure 1-1. *Schematic view of the near field of a KBS-3 repository showing the transport mechanisms in the different parts of the system, from /Arcos et al. 2006/. The modelled domains for Cases I and II are also shown.*

II, a pre-existing fracture is considered to intersect an access tunnel. In this case, the groundwater that circulates in the fracture flows through the backfill of the access tunnel and, then, contact the buffer in a deposition hole.

In the present work, Cases I and II are revisited and additional hydro-geochemical scenarios are simulated using the corresponding modelled domains.

1.3 Scope

As it has been previously commented, the work presented here concerns the development of numerical simulations of the geochemical and thermo-hydrological processes that are likely to occur in the near-field of a KBS-3 repository. These simulations are basically split in two important stages of the near-field:

1. The thermal period corresponding to the early stages of the near-field evolution. During this period, the bentonite buffer is progressively water saturated by the surrounding granitic groundwater, due to the hydrodynamic pressure of the granitic host rock at 500 m depth. The simulations performed for this period are based on the main achievements of the modelling exercise performed for the LOT-A2 test /Sena et al. 2010/.
2. The fully water-saturated period, during which the temperature at the near-field has decreased to values close to the undisturbed temperature of the granitic host rock. The possible external changes that the granitic groundwater might undergo in the long-term, can affect the geochemistry of the bentonite buffer and the backfilled tunnel. The simulations performed for this period are based on the modelling exercise performed by /Arcos et al. 2006, 2008/.

In order to obtain information on the redistribution of the aqueous and solid species in the long-term, it was revisited the model performed in /Arcos et al. 2006/. However, some differences will be incorporated into the model. First, the thermal period includes the period of bentonite water saturation. The overall process has been based on the LOT experiment conducted in the Äspö HRL, where a

modelling task is being performed. In this way, these calculations have allowed the estimation of the composition of the initial pore water for the saturated stage. On the other hand, a sensitivity analysis has been conducted on transport parameters (advection in the fracture intersecting the deposition hole, advection in the bentonite during saturation, and diffusivity in the saturated bentonite), and on the Ca-C(IV)-pH system, mainly regarding the calcite content of bentonite. Consequently, the initial and boundary conditions has been the same as in /Arcos et al. 2006/, except for initial pore water composition in bentonite, transport parameters, and calcite content, as stated above.

The same scenarios as in /Arcos et al. 2006/ have been considered. However, the scenarios considered in /Arcos et al. 2006/ have not been explicitly considered in the sensitivity analysis performed here. Instead, the whole range of chemical compositions considered for the sensitivity analysis performed in the present work implicitly account for the scenarios developed by /Arcos et al. 2006/.

For the saturation and thermal period, the results specially focus on the following issues:

- Calculation of the initial pore water composition: based on initial water content and composition, regarding the effect of saturation. Comparison with other modelling data from experiments (i.e. LOT at Äspö, experiments conducted by Ciemat within NF-PRO).
- Redistribution of sulphur and carbonate phases.
- Cementation due to precipitation of SiO_2 (input to the mechanical properties model).
- During the saturated stage (long-term), the mainprocesses simulated have been:
  - Sensitivity analysis of the previous model (mainly related to the effect of hydraulic properties of the fractures around the near field, the groundwater composition and the diffusion mechanism).
  - Sensitivity of the Ca-HCO_3^--pH system for both MX-80 and Deponit CA-N bentonites.
  - Sensitivity analysis of the ion-exchange composition in the buffer close to the fracture.

1.4 Approach

As it has been previously commented, the bentonite-groundwater interaction has been conducted by two different types of reactive transport models: for the thermal period, and for the saturated stage of the bentonite, and accounting for the long-term evolution of the system. In the first case, the reactive transport calculations have been performed using the code TOUGHREACT /Xu et al. 2008/, and ithas been validated with the experimental data from the LOT experiment conducted in the Äspö HRL. The second case has been evaluated with the code PHAST /Parkhurst et al. 2004/, using the results from the former model as initial conditions.

1.4.1 Software

TOUGHREACT /Xu et al. 2008/ results from coupling the calculation of geochemical reactions to the THOUGH2 code /Xu et al. 2008/, which solves multiphase, non-isothermal fluid flow, heat flow and multi-component transport. TOUGHREACT accommodates chemical species present in liquid, gas and solid phases. Aqueous complexation, gas dissolution/ex-solution, and cation exchange are modelled under local equilibrium. On the other hand, mineral precipitation/ dissolution may be modelled either under equilibrium or kinetics assumptions. Additionally, changes in porosity, permeability, and capillary pressure, owing to mineral precipitation/dissolution, may be computed /Xu et al. 2008/.

TOUGHREACT encompasses two relevant phenomena for the models included in the present study: (1) gas phase is active for multiphase flow, mass transport and chemical reactions, and (2) the effects of heat include heat-driven fluid flow and temperature-dependant thermodynamic physical and geochemical properties, such as fluid density and viscosity, and thermodynamic and kinetic data for geochemical reactions. Advection and diffusion processes are considered for both the liquid and gas phases, and their coefficients are assumed to be the same for all species /Xu and Pruess 2001/.

TOUGHREACT does not account for (1) the deformation of the porous skeleton either due to mechanical stress or swelling processes; (2) fluid pressure effects owing to porosity changes; and (3) heat effects from chemical reactions, such as changes in thermo-physical properties of fluids (viscosity, surface tension and density).

PHAST v.1 /Parkhurst et al. 2004/ simulates multi-component, reactive transport in 3D saturated groundwater flow systems. PHAST is a versatile groundwater flow and solute transport simulator with capabilities to model a wide range of equilibrium and kinetic geochemical reactions. The flow and the transport calculations are based on a modified version of HST3D /Kipp 1997/ that is restricted to constant fluid density and constant temperature. The geochemical reactions are simulated with the geochemical code PHREEQC /Parkhurst and Appelo 1999/, which is imbedded in PHAST. PHAST has been used in the SR-Can assessment for modelling different aspects of the near-field (canister and the engineered systems) behaviour /SKB 2006/. The version of the code used has been updated as the authors release new versions in the web (http://wwwbrr.cr.usgs.gov/projects/GWC_coupled/phast/). The last version is PHAST v.1.5.

As a possible alternative, it was envisaged to use the code RETRASO-CODE_BRIGHT /Saaltink et al. 2004/ instead to TOUGHREACT. In order to improve our understanding of the process occurring during bentonite saturation, and the associated transport of conservative solutes, it was decided to build a numerical model using, alternativelly, both codes. The test was performed with an experiment conducted by CIEMAT with the FEBEX bentonite /Fernández and Villar 2010/, where data at different time intervalswere available and, therefore, provided an additional instrument to test and validate our conceptual model. Although /Villar et al. 2008/ applied the van Genuchten equation for the capillary pressure function to simulate the evolution of water saturation in the FEBEX experiment by using the numerical code CODE-BRIGHT /Olivella et al. 1996/, we attained better results with the Leverett's function and using the numerical code TOUGHREACT.

1.4.2 Input data

The main input data for the models using both codes are the same: transport data, geochemical data and thermodynamics and kinetics data. In addition, for the first model there are some additional input data: thermal gradient (thermal conductivity and heat generation rate), bentonite suction data under unsaturated conditions, and gas transport properties.

The deliverable for the bentonite – groundwater interaction will be a report including input files for the codes used as annexes. The inputs files are not included in this report due to the considerable size of the present report. Instead, the input files will be provided in a separate file.

Transport data (Table 1-1 and Table 1-2). Input data needed to simulate groundwater flow through the fracture will be set in order to be in agreement with the equivalent groundwater flow rate ($Q_{eq\ 1}$; Equation 1-1) as defined in /SKB 2006/ and /Hartley et al. 2006/. A value of $5 \cdot 10^{-6}$ m^3/yr has been selected for the reference case, although a higher value ($5.44 \cdot 10^{-3}$ m^3/yr) as that calculated in /Arcos et al. 2006/ will be used as an upper value and to determine the sensitivity of the model to this parameter. However, many deposition holes will not be intersected by any fracture at all, and the geochemical evolution will be determined by diffusion alone.

Table 1-1. Hydraulic parameters selected to be implemented in the model.

Parameter	Value	Units	Source
w_c	5.0	m	/Hartley et al. 2006/
L_f	5.5	m	Calculated from KBS-3 design
U_{r1}	10^{-5}	m/yr	/SKB 2006/
Fracture thickness	0.116	m	/Arcos et al. 2006, Dershowitz et al. 2003/
D_w	$2.8 \cdot 10^{-10}$	m^2/s	/Arcos et al. 2006/

Table 1-2. Hydraulic conductivity and porosity values of bentonite and backfill /Arcos et al. 2006/.

	Buffer	Backfill (IBECO-RWC-BF)
K (m/s)	$<10^{-12}$	10^{-12}
Porosity	0.43	0.45

The equivalent groundwater flow rate for $Q_{eq\,1}$ can be written as:

$$Q_{eq1} = \sum_f \left(2\frac{Q_f}{\sqrt{a_f}} \sqrt{\frac{4D_w t_{w,f}}{\pi}} \right), \textit{where } t_{w,f} = \frac{L_f \cdot e_{t,f}}{Q_f / \sqrt{a_f}} \quad (1\text{-}1)$$

where D_w is the diffusivity in water, [m^2/yr], $t_{w,f}$ is the time the water is in contact with the deposition hole within each fracture, [yr], L_f is the length of the fracture intersection with the wall of the deposition hole, [m], Q_f is the volumetric flux in the fracture adjacent to the deposition hole [m^3/yr], $e_{t,f}$ is the transport aperture of the fracture adjacent to the deposition hole [m], and a_f is the area of the fracture plane intersecting the hole [m^2].

If there are several fractures intersecting a single deposition hole, then a conservative approach to calculate the equivalent groundwater flow-rate requires the flow to be summed across all the fractures. Hence, the equivalent Darcy velocity, U_{r1}, for all fractures intersecting the deposition hole is:

$$U_{r1} = \frac{1}{w_c} \sum_f \frac{Q_f}{\sqrt{a_f}} \quad (1\text{-}2)$$

where U_{r1} is the average initial Darcy velocity in the fracture system averaged over the rock volume adjacent to the canister (water flux) [m/yr], and w_c is the canister height [m].

With these data values the following parameters can be calculated:

$$a_f = 0.6377\ m^2 \quad (1\text{-}3)$$

and:

$$Q_f = U_{r1} \cdot w_c \cdot \sqrt{a_f} = 3.99 \cdot 10^{-5}\ m^3/yr \quad (1\text{-}4)$$

In the PHAST code, the input parameters for the transport in the fracture are porosity (ε), fracture thickness, diffusion coefficient in water (D_w), hydraulic conductivity (K), and hydraulic head gradient (i). A value for K of $5 \cdot 10^{-10}$ m/s has been selected according to /Follin et al. 2005/, which allows to calculate the hydraulic gradient ($i = U_{r1}/K$). Therefore, as fracture thickness, D_w, K, and i are fixed values, the only input parameter that needs to be calculated is porosity (ε). From Equation 1-1, the value of $t_{w,f}$ to obtain $Q_{eq\,1}$ as $5 \cdot 10^{-6}$ m^3/yr is 4.46 years, and, therefore, $e_{t,f}$ is $4.06 \cdot 10^{-5}$ m. Assuming that $e_{t,f}$ is the fracture thickness times the porosity, then the calculated porosity is 0.00035, which is in agreement with the porosity values from Äspö /Dershowitz et al. 2003/.

As the important parameter in the model is the groundwater flow for advective transport through the fracture, any relationship of porosity (ε), hydraulic conductivity (K) and hydraulic head gradient (i), resulting in the target $Q_{eq\,1}$ value could be valid. Therefore, for the extreme case, where $Q_{eq\,1}$ is taken as $5.44 \cdot 10^{-3}$ m^3/yr /Arcos et al. 2006/, the following parameters have been modified: $U_{r1} = 0.11$ m/yr, and $i = 0.688$.

As the code only allows a single value for diffusion coefficient in water, regardless of the material considered, we calculated a value of $2.8 \cdot 10^{-10}$ m^2/s. This value is used by the code to calculate the effective diffusion in each material through the following expression:

$$D_w \cdot \varepsilon = D_e \quad (1\text{-}5)$$

In fact, the selected values for the bentonite buffer are a porosity of 0.43 /SKB 2006/ and $D_e = 1.2 \cdot 10^{-10}$ m^2/s, which is calculated according to /Ochs and Talerico 2004/ by:

$$D_e = 6.7785 \cdot 10^{-9} \cdot e^{-0.0025671 \cdot \rho} \quad (1\text{-}6)$$

and considering a dry density of 1.570 kg·m^{-3} /SKB 2006/.

In any case, the diffusion coefficient should be modified in a further revision previous to the model, which can lead to slight modifications of all previous parameters accordingly.

Other transport input data, as hydraulic conductivity of bentonite and backfill, and porosity of backfill will be the same as selected in /Arcos et al. 2006/ (Table 1-2).

Geochemical data and initial water content. The main geochemical parameters needed in the calculations performed in the present work are: groundwater composition for the different scenarios considered, initial water composition in bentonite (and its content), fracture-filling minerals (especially those that can have an impact on the geochemical evolution of the system), bentonite mineral composition, cation exchange capacity and cation distribution, and montmorillonite surface area for protonation/deprotonation reactions.

In the Table 1-3, the groundwater composition used in /Arcos et al. 2006/ are presented. However, new groundwater compositions with their corresponding uncertainties will be delivered by SKB.

The initial water content in the bentonite buffer prior to saturation is given by a saturation degree of 0.61 /SKB 2006/. The composition of such initial water will be calculated to be in equilibrium with mineral and cation exchange distribution in bentonite. The resulting composition from the first model will be used as initial pore water composition for the second modelling case. The initial porewater composition of the bentonite buffer in the saturated (long-term) period has been set by equilibrating Forsmark groundwater with the bentonite minerals.

Fracture-filling minerals in the geosphere will be obtained from /Sandström et al. 2004/ and /Sandström et al. 2008/ whereas mineral composition, as well as CEC and montmorillonite surface area data of bentonite buffer and backfill will be those reported in /SKB 2006/ which are equivalent to those used in /Arcos et al. 2006/. However, no minerals have been considered in the fracture in order to understand the consequences of the different groundwater compositions considered in the sensitivity analysis on the geochemical evolution of the bentonite buffer. In spite of the kinetically-controlled reactivity of the granitic lithologies could slightly modify groundwater composition along of the fracture zone, only conservative transport and precipitation of secondary minerals will be modelled within the fracture in the vicinity of the buffer. In the framework of this study, the thermal-hydraulic effects of the fracture (and its influence on the boundary conditions) will be treated.

Thermodynamic and kinetic data. The thermodynamic database used in TOUGHREACT is the EQ3/6 database, developed by /Worely 1992/, which is commonly used in geochemical models. The thermodynamic database includes reaction stoichiometries, dissociation constants, and regression coefficients of dissociation constants as a function of temperature. On the other hand, in PHAST calculations we will use the thermodynamic database from SKB's Trac system.

Data for cation exchange and protonation/deprotonation reactions will be discussed and selected as part of the modelling process.

Table 1-3. Groundwater composition used in /Arcos et al. 2006/.

moles/L	Forsmark	Laxemar saline[(1)]	Grimsel Ice-melting
pH	7.2	7.9	9.6
pe	–2.42	–5.08	–3.38
HCO_3^-	$2.20\cdot10^{-3}$	$1.00\cdot10^{-4}$	$4.50\cdot10^{-4}$
Ca	$2.33\cdot10^{-2}$	$4.64\cdot10^{-1}$	$1.40\cdot10^{-4}$
Cl	$1.53\cdot10^{-1}$	1.28	$1.60\cdot10^{-4}$
Fe (tot)	$3.31\cdot10^{-5}$	$8.00\cdot10^{-6}$	$3.00\cdot10^{-9}$
K	$8.75\cdot10^{-4}$	$7.00\cdot10^{-4}$	$5.00\cdot10^{-6}$
Mg	$9.30\cdot10^{-3}$	$1.00\cdot10^{-4}$	$6.20\cdot10^{-7}$
Na	$8.88\cdot10^{-2}$	$3.49\cdot10^{-1}$	$6.90\cdot10^{-4}$
SO_4^{2-}	$6.80\cdot10^{-3}$	$9.00\cdot10^{-3}$	$6.10\cdot10^{-5}$
Si	$1.85\cdot10^{-4}$	$8.00\cdot10^{-5}$	$2.05\cdot10^{-4}$

[(1)] Data for saline water as reported in /SKB 2006/, except for pe and silica, which come from /Laaksoharju et al. 1995/.

2 Description of the conceptual model

The bentonite blocks that will be placed in the deposition holes of the KBS-3 repository are prepared with a mixture of a natural bentonite powder and water which is then subject to uniaxial compression /SKB 2004a/. The type of bentonite to be used by SKB in the future repository is still under consideration. In this context and taking into account the types of bentonite that have been analysed by SKB (/SKB 2004a/ and /Olsson and Karnland 2009/), two types of bentonite have been considered in the numerical simulations: Wyoming MX-80 and Deponit CA-N. Both bentonite types are rich in montmorillonite. Nevertheless, MX-80 is composed of a Na-montmorillonite, while Deponit Ca-N is composed of a Mg-Ca-montmorillonite. In addition, the first is depleted in carbonates, while the second is not.

In order to assess the geochemical evolution of the near-field, a hypothetical fracture of the granitic host rock is considered to intersect the buffer surrounding a copper canister, so that Forsmark groundwater gradually will fill the partially saturated pores of the bentonite buffer. Subsequently, the mixing between the bentonite porewater and Forsmark groundwater will trigger geochemical modifications of the near-field towards a new thermodynamic equilibrium between minerals and porewater.

2.1 Hydro-geochemical processes during the thermal period

During the thermal period of a KBS-3 repository, the initially unsaturated compacted bentonite will progressively saturate due to the hydraulic pressure of the surrounding rock massif (Figure 2-1). Although the main transport mechanism in the low permeability compacted bentonite is diffusion, advective transport will be more important during the saturation stage due to the capillary pressure that is established during this stage. This process was already identified in /Sena et al. 2010/, and it will be dominant until full water saturation of bentonite, which can occur between 10 and more than 100 years after bentonite deposition /SKB 2004a/. In addition, during this period, water flow and transport of solutes will be affected by the thermal gradient imposed by the radioactive decay of nuclear waste.

In /Sena et al. 2010/, both the LOT-A2 experimental data and the numerical results have proven that the transport of chloride in the compacted bentonite is mainly influenced by (1) the advective flow of the water injected in the bentonite, which reflects a piston like flow, (2) the cyclic evaporation/con-

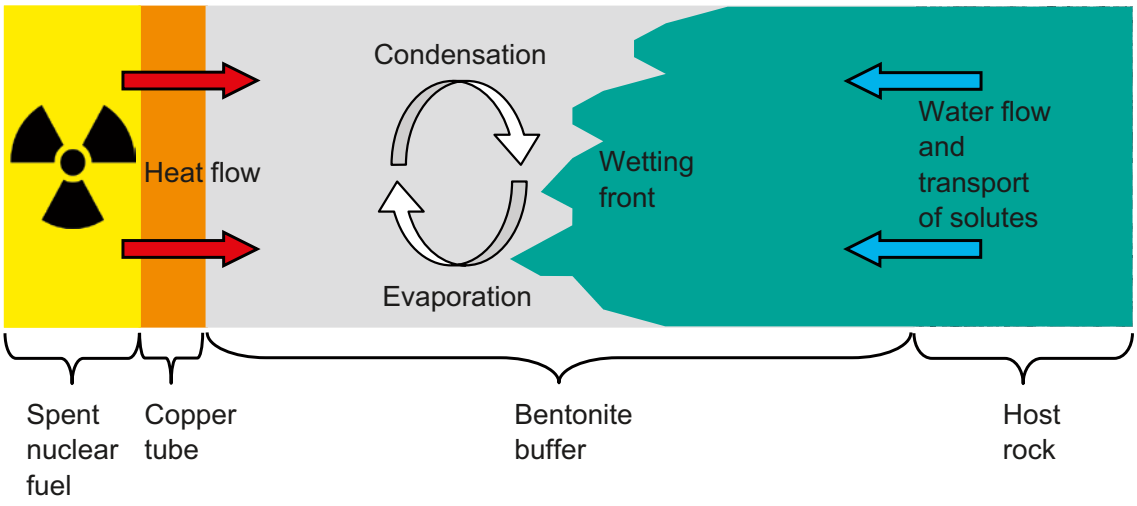

Figure 2-1. *Sketch of a vertical cross section of the near-field of a KBS-3 repository showing the thermo-hydraulic and transport processes that are believed to occur during the saturation period of the bentonite buffer.*

densation process that occurs in the migrating wetting front, and (3) water suction close to the heater. Although Donnan equilibrium and anion exclusion processes are known to influence the transport of chloride in compacted bentonite /Birgersson and Karnland 2009, Muurinen et al. 2004/, the numerical simulations performed have proven that, under the thermo-hydraulic conditions of the LOT-A2 test /Karnland et al. 2009/, these processes can be considered of low importance. In this context, the numerical simulations that are performed in the present work for the thermal period rely on the main outcomes obtained in the numerical models developed for the LOT-A2 experiment.

Besides being influenced by the same processes as chloride, sulphate is also influenced by the precipitation and dissolution of soluble calcium-sulphates which, in turn, are influenced by cation exchange in the montmorillonite interlayer, and evaporation and condensation of porewater. Although sulphate reduction could be significant in some environments due to bacterial activity, the presence and activity of such bacteria in compacted bentonite is very low and the data from the LOT experiment seems to confirm that sulphate is not being reduced.

The good agreement between computed results and experimental data from the LOT-A2 test has built confidence on the simulations developed in /Sena et al. 2010/. Therefore, the conceptual and numerical models built here for the thermal period of the near-field are based on the previous modelling exercise of the LOT-A2 experiment.

2.2 Hydro-geochemical processes during the water-saturated period

During the water saturated period, the permanent contact between the bentonite matrix and groundwater will favour geochemical modifications of the bentonite. In the cases modelled here, the geochemical conditions of the engineered barriers will change in order to approach a new thermodynamic equilibrium. In addition, the lower temperature prevailing during this period will favour the replacement of high temperature minerals that might have precipitated during the thermal period (e.g. anhydrite), by those minerals that are more stable under lower temperature conditions, such as gypsum. In spite that these processes could be kinetically inhibited, the large time frame considered and the slow transport processes enables to consider them under thermodynamic equilibrium assumptions.

Taking into account the main geochemical differences between the two bentonite types analysed here (MX-80 and Deponit CA-N), the geochemical reactions occurring in the near-filed, triggered by the contact between groundwater and the bentonite minerals, will vary. In the MX-80 bentonite, no carbonate minerals have been detected. Nevertheless, and since calcite is present in the fracture walls of the granitic host rock at Forsmark, calcite precipitation may occur in the near field, as a consequence of the interaction between groundwater and the bentonite minerals. The numerical results attained in /Arcos et al. 2006/ indicate that gypsum, which is present in minor amounts in the bentonite solid matrix, may dissolve due to the inflow of Forsmark groundwater. Further, by releasing calcium into solution, gypsum dissolution may be a key mechanism for calcite precipitation.

The backfill is one of the engineered barriers in the KBS-3 repository. The backfill is the material installed in deposition tunnels to fill them as soon as the corresponding repository sections are closed. The purpose and function of the backfill in the deposition tunnels is to sustain the multi-barrier principle by keeping the buffer in place, and restrict groundwater flow through the deposition tunnels /SKB 2006/. In order to assess the relative role of the bentonite and the backfill to buffer the hydro-geochemical changes induced by an intruding groundwater, two different cases are analysed here. Case I, where groundwater contacts directly the bentonite buffer through a fracture that intersects a deposition hole, and Case II, where groundwater circulates through the backfill before reaching a deposition hole.

Since the compacted bentonite that is used in a HLNW repository has a very low permeability, the transport of solutes in the bentonite pores, during the water-saturated period, will be most likely dominated by diffusive processes. Diffusion of solutes in compacted bentonite has been extensively studied /Birgersson and Karnland 2009, Bourg et al. 2003, Molera et al. 2003, Muurinen et al. 2004, Ochs et al. 2001, Van Loon et al. 2007/.

The diffusion of solutes in compacted bentonite is not straightforward, and therefore, different approaches are proposed to explain the diffusive process. Basically, there are two main approaches. One approach explains the diffusion of anions and cations by using different types of porosity for each other /Bourg et al. 2003, Molera et al. 2003, Muurinen et al. 2004, Ochs et al. 2001, Van Loon et al. 2007/, while another approach deals with only one type of porosity and applies an ion equilibrium term to explain the different transport behaviour of anions and cations in compacted bentonite /Birgersson and Karnland 2009/.

/Muurinen et al. 2004/ found that at high ionic strength, the Donnan equilibrium can predict the observed diffusion of solutes, while at low ionic strength, the effect of anion exclusion is higher and therefore the proposed model underestimates the observed concentration of solutes. If the microstructure of the bentonite, with different types of porosity, is taken into account, together with the Donnan equilibrium, the proposed model is able to predict observed solutes concentrations at low ionic strength. /Molera et al. 2003/ also found that two types of porosity are present in compacted bentonite, and both play an important role on the diffusion of solutes. The two types of porosity present in compacted bentonite are (Figure 2-2):

- Inter-particle porosity which corresponds to the voids present between the grains of minerals and montmorillonite aggregates.
- Interlayer porosity which corresponds to the voids present between the TOT montmorillonite layers. Each interlayer pores has a thickness of up to three water molecules /Fripiat et al. 1982 and Troilai et al. 1996 in Bourg et al. 2003/.

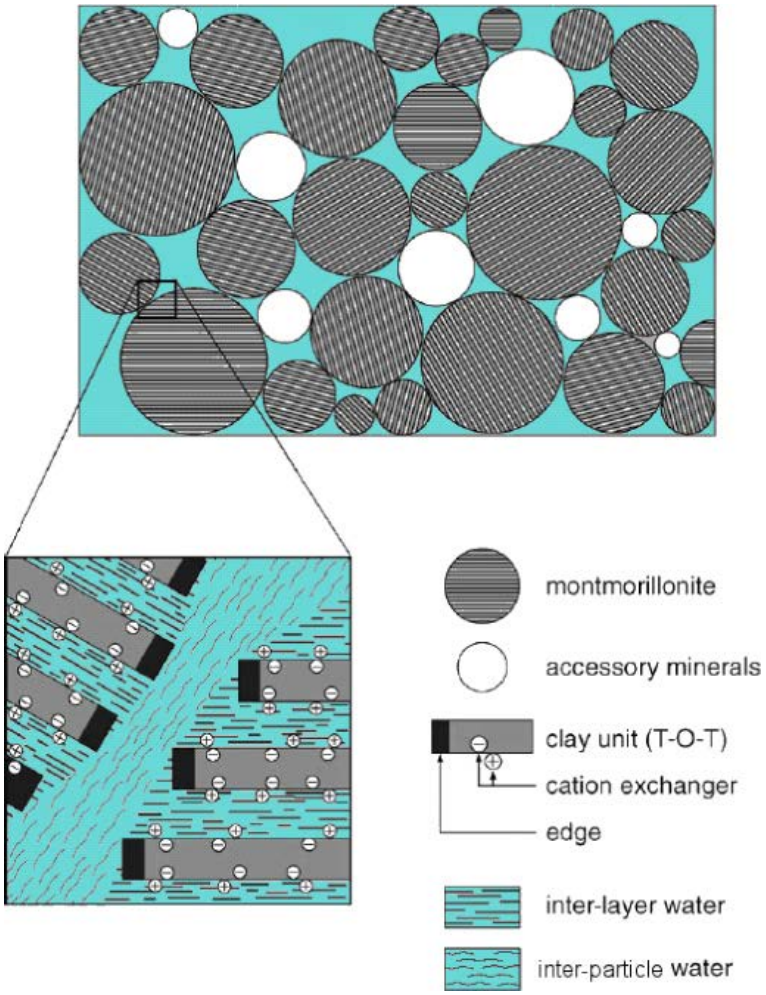

Figure 2-2. *Schematic picture of the microstructure of compacted bentonite. Modified from /Wersin 2003/.*

/Molera et al. 2003/ found that the interlayer diffusion seems to be affected by anion exclusion, while the inter-particle diffusion is retarded by ionic strength dependant sorption. In addition, in the interlayer porosity, cations are adsorbed on the negatively charged surfaces of montmorillonite layers /Bourg et al. 2003/. These authors found that diffusion of solutes through the interlayer pores is important only for dry densities of compacted bentonite above 1,800 kg/m^3. Below this value, diffusion in the interlayer can be negligible compared to inter-particle diffusion, and therefore the interlayer participates mainly as a charged surface that adsorbs cations. In highly compacted conditions, diffusion through the interlayer pores and the associated mechanisms of anion exclusion become important, and therefore, the bentonite acts as a semi-permeable membrane. /Ochs et al. 2001/ reached similar conclusions and stated that radionuclide migration can be predicted in compacted bentonite based on a consistent integration of mechanistic sorption reactions and diffusion models.

More recently, /Birgersson and Karnland 2009/ presented a new model to simulate the diffusion of solutes in compacted bentonite. These authors argued that the introduction of concepts such as the different types of pores, anion accessible porosity and cation exchange without considering ion equilibrium effects can lead to an erroneous description of the diffusion of solutes in compacted bentonite. In the model proposed by these authors, cation and anion diffusion are treated symmetrically with the use of an ion equilibrium coefficient. This coefficient explains the ion concentration discontinuities that are always present at the interface between the montmorillonite interlayer pores and an external solution. Two types of equilibrium contribute to these concentration discontinuities:

- Donnan equilibrium which affects both cations and anions in a symmetrical way, and leads to reduced concentration of excess ions in the interlayer pores compared to their concentration in the external solution.
- Cation exchange which involves thermodynamic exchange reactions between different cations.

From the scientific literature, it is seen that different approaches have been applied to explain the diffusion of solutes in the bentonite mainly in through-diffusion experiments and equilibration cells. Some important differences exist between the models developed so far which all tend to explain the transport of anions and cations in compacted bentonite.

In domains which are larger than the through-diffusion cells used in most of the works previously described (such as the bentonite rings that were used in the LOT-A2 test /Karnland et al. 2009/), the processes of Donnan equilibrium and anion exclusion seem to be relatively small compared with the diffusive transport of solutes, so that numerical codes that do not take into account these processes are able to correctly simulate the diffusive transport of anions in compacted bentonite. A good agreement between observed and simulated results for the transport of chloride and sulphate in the LOT-A2 test has been achieved by using the TOUGHREACT code /Sena et al. 2010/. These results support our decision to use the reactive transport codes Toughreact /Xu et al. 2008/ and PHAST /Parkhurst et al. 2004/ in the numerical models that have been developed in the present work for the simulation of solute transport coupled to geochemical reactions in the near-field of a HLNW repository.

3 Numerical model for the thermal period

3.1 Numerical tool and thermodynamic database

The numerical tool used in the calculations of the thermal period is TOUGHREACT /Xu et al. 2008/. This code results from coupling the calculation of geochemical reactions to the THOUGH2 code /Xu et al. 2008/, which solves multiphase, non-isothermal fluid flow, heat flow and multi-component transport. TOUGHREACT accommodates chemical species present in liquid, gas and solid phases. Aqueous complexation, gas dissolution/ex-solution, and cation exchange are modelled under local equilibrium. On the other hand, mineral precipitation/dissolution may be modelled either under equilibrium or kinetics assumptions. Additionally, changes in porosity, permeability, and capillary pressure, owing to mineral precipitation/dissolution, may be computed /Xu et al. 2008/.

In TOUGHREACT, the hydrodynamic dispersion is modelled through a spatial resolution on multiple scales, using multiple continua models to describe interactions between fluid regions with different velocities /Xu and Pruess 2001, and references therein/.

The activity coefficients of aqueous species are calculated from the Debye-Hückel equation. The activities of pure mineral phases and H_2O are assumed to be one, and gases are assumed ideal at atmospheric conditions. At higher temperatures and pressures such as boiling conditions, the fugacity coefficients of gases depend on the temperature and pressure of the system /Xu and Pruess 2001/.

Space discretization is made directly from the integral form of the basic conservation equations without converting them into partial differential equations. This method is called the integral finite difference /Xu et al. 2008, and references therein/, and is applicable to regular or irregular space discretization in one, two, and three dimensions. Time is fully implicitly discretized as a first-order backward finite difference, while flux is 100% upstream weighted. The coupling between fluid flow, mass transport and geochemical reactions is made using a sequential iterative approach.

The thermodynamic database used in TOUGHREACT is the EQ3/6 database, developed by /Worely 1992/ which is commonly used in geochemical models. The thermodynamic database includes reaction stoichiometries, dissociation constants (log(K)), and regression coefficients of log(K) as a function of temperature. The reason for using this thermodynamic database instead of database from SKB's Trac system (SKB-TDB) is related to the format database format used by TOUGHREACT. However, the data for the most relevant aqueous species and solids has been checked and compared against the values from the SKB-TDB for consistency.

3.2 Description of input data

3.2.1 Geometry of the modelled domain

The numerical model developed for the thermal period of the near-field is a 1D axis-symmetric model contained in a hypothetical fracture plane that intersects a deposition hole (Figure 3-1). The total length of the model domain is 2.84 m. Forsmark groundwater is considered to flow through the fracture aperture and the granitic walls of this fracture are considered impervious, i.e. matrix diffusion is obviated. In this context, the groundwater flowing through the fracture is conducted towards the buffer where it gradually fills the partially saturated pores of the bentonite.

3.2.2 Thermo-hydraulic processes and parameters

The thermo-hydraulic processes and parameters assigned to the three materials considered in the model domain set for the thermal period are those used in the numerical simulations performed for the LOT-A2 test /Sena et al. 2010/. The calibrated values of the thermo-hydraulic parameters are listed in Table 3-1. Although values are given in Table 3-1 for the canister, it has been considered and impervious and unreactive material, and considered only in reference of its thermal properties.

3.2.3 Geochemical processes and parameters

The geochemical processes and parameters implemented in the numerical simulations of the thermal period and water-saturated period of the near-field have been set based on the work developed by /Arcos et al. 2006/ and /Sena et al. 2010/.

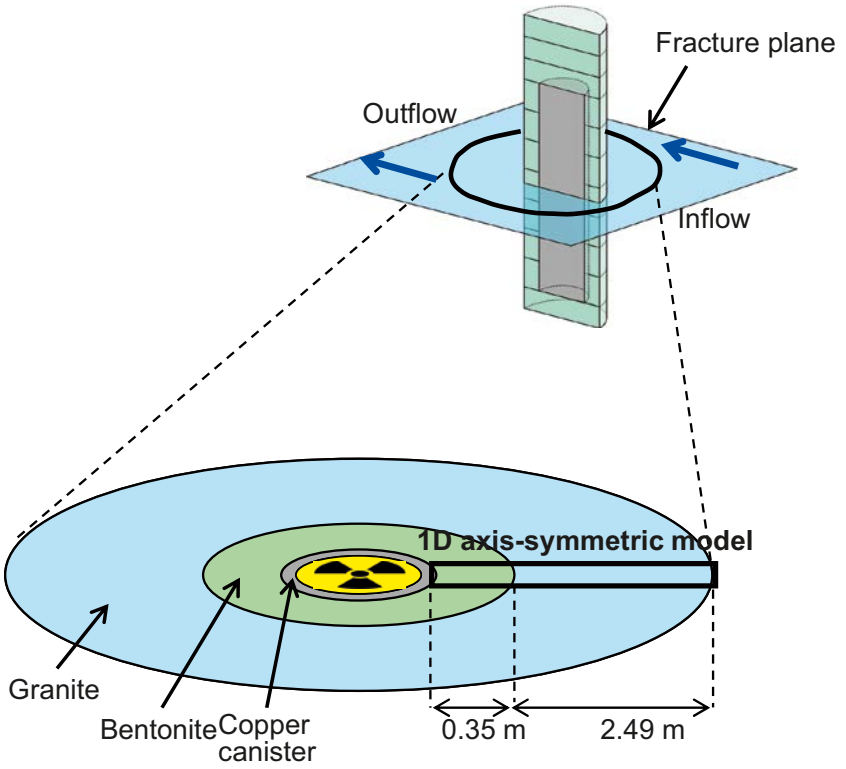

Figure 3-1. Geometry of the numerical model developed for the thermal period.

Table 3-1. Values of the thermo-hydraulic parameters assigned to the block materials (copper tube, bentonite, and granite) that constitute the numerical model of the near-field during the thermal period (data taken from /Sena et al. 2010/).

Parameter		Copper canister	Bentonite	Granite
Porosity	[–]	10^{-10} (a)	0.43 (b)	10^{-3} (c)
Absolute permeability	[m²]	10^{-21} (d)	10^{-21} (b)	$5 \cdot 10^{-17}$
*Molecular diffusion coef.	[m²/s]	$3 \cdot 10^{-8}$ (d)	$3 \cdot 10^{-8}$ (e)	$3 \cdot 10^{-8}$ (d)
Tortuosity	[–]	1.0 (d)	1.0 (e)	$5 \cdot 10^{-2}$ (e)
Thermal conductivity sat.	[W/(m·ºC)]	388 (f)	1.15 (g)	1.15 (d)
Specific heat capacity	[J/(kg·ºC)]	10^{20} (h)	964 (f)	964 (d)
Klinkenberg parameter	[MPa]	10^{1} (d)	10^{1} (e)	10^{1} (d)

(a) Considered very low; (b) from /Karnland et al. 2009/; (c) same as for the bentonite grid blocks; (d) same as for the bentonite grid blocks; (e) model calibration; (f) general literature; (g) from /Villar et al. 2008/; (h) set very high to prescribe constant temperature boundary condition in the modelled domain.

From the three materials present in the model domain of the thermal period, only the bentonite buffer is considered to have reactive minerals at the beginning of the simulation. The copper canister is considered to be inert throughout the simulation time, and no minerals are allowed to form on the canister, while the granite is considered to be depleted on reactive minerals at the beginning of the simulation, but, if any mineral present in the bentonite reaches oversaturation in the granite, it is allowed to precipitate on the fracture walls.

Since the selection of the type of bentonite to be used by SKB for the production of the bentonite blocks is still under consideration, two types of bentonite have been used in the numerical simulations:

- MX-80
- Deponit-CA-N

Both bentonite types are natural clayey materials rich in montmorillonite. The main feature distinguishing both bentonite types is the dominant cation of the montmorillonite interlayer. Deponit

CA-N has a Ca-Mg-montmorillonite where magnesium occupies approximately half of the cation exchange sites, while in the MX-80 bentonite sodium occupies 72% of the cation exchange sites (Table 3-2). In addition, the Deponit CA-N bentonite has calcite and dolomite as primary carbonates, while the MX-80 bentonite is apparently depleted in carbonates.

The cation exchange reactions implemented for the montmorillonite present in the bentonite buffer are listed in Table 3-3. Montmorillonite surface protonation – deprotonation process is not implemented within the TOUGHREACT code and, therefore, it has not been included in this models.

3.2.4 Space and time discretization

The numerical mesh representing the space discretization of the model domain is a one-dimensional axis-symmetric finite volume mesh (Figure 3-2), and has been built using the meshmaker option of the TOUGH2 program /Xu et al. 2008/. The mesh is composed of a total of 851 volumetric grid blocks which starts at 0.50 m from the axis in order to account for the radius of the copper canister (/SKB 2004/, Figure 3-2).

The thermal period has been simulated for 10,000 years. The initial time step is 10^3 seconds which is automatically increased until a maximum time step of 10^{11} seconds (approximately 3,170 years). The convergence criteria imposed in the calculations are as follows:

- 25 as the maximum number of sequential iterations between transport and chemistry,
- 20 as the maximum number of iterations allowed for solving the whole geochemical system,
- 10^{-4} as the relative tolerance of aqueous concentration for sequential transport/chemistry convergence, and
- 10^{-5} as the relative tolerance of aqueous concentration for the whole chemical system.

Table 3-2. Geochemical data of the two bentonite types considered in the numerical simulations developed for the thermal period and the water-saturated period.

	MX-80(1)	Deponit CA-N(2)
Minerals (wt%)		
Montmorillonite	87	58–70(3)
Calcite	0	8.48
Dolomite	0	16.
Gypsum	0.6	0.78
Quartz	5	0.7(3)
Pyrite	0.07	1.5(3)
Exchanger composition (%)		
CEC (meq/100 g)	75	72
Na	76	10
Ca	13(*)	37(**)
Mg	10	52
K	1	1

(1) Data from /SKB 2004/; (2) Taken from XRD data of sample Milos BF 04, Table 6 in /Olsson and Karnland 2009/; (3) Taken from XRD data of sample Milos BF 08, Table 6 in /Olsson and Karnland 2009/. (*) 18% for the fully-water saturated models; (**) 36% for the fully-water saturated models.

Table 3-3. Cation exchange reactions implemented for montmorillonite in the numerical simulations /Bradbury and Baeyens 2002/.

Cation exchange reactions	Log K
$X^- + Na^+ = NaX$	0.00
$X^- + K^+ = KX$	0.60
$2X^- + Ca^{2+} = CaX_2$	0.41
$2X^- + Mg^{2+} = MgX_2$	0.34

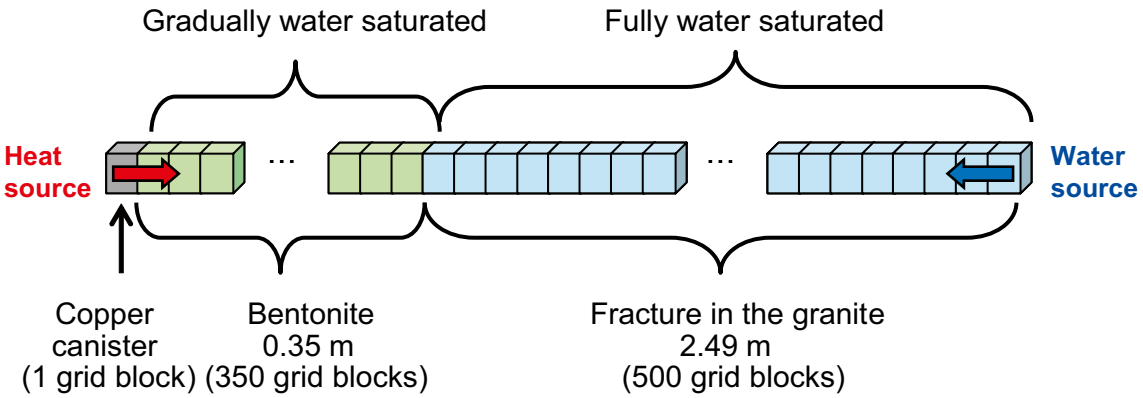

Figure 3-2. *Numerical mesh and boundary conditions set for the numerical simulations of the thermal period of the near-field.*

3.2.5 Initial and boundary conditions

The numerical simulations developed for the thermal period of the near-field reproduce the hydro-geochemical evolution of the system (1) under transient state and, (2) from well-known initial conditions. The initial water saturation conditions of the near-field are:

- The pores of the bentonite grid blocks are 62% saturated in water.
- The pores of the granite grid blocks are 100% saturated in water.
- The copper canister is considered impervious.

The composition of the different water types considered in the numerical models developed for the thermal period is presented in Table 3-4. The Forsmark water composition was adjusted by equilibrating the original composition /Laaksoharju et al. 2004/ (Table 3-4; Forsmark GW, measured) with the minerals identified. This adjustment results in slight variations to the original composition. The initial Deponit CA-N bentonite porewater has been estimated by equilibrating the Forsmark groundwater with the mineral phases and the cation exchanger from the bentonite. The initial porewater of the MX-80 bentonite has been defined from the water compositions measured in the LOT-A2 experiments (LOT A2-13-1, UniBern /Sena et al., 2010/).

Although these waters are relatively reducing, the estimated concentrations of the S(-II) aqueous species are 6 or 8 orders of magnitude lower than the S(VI) aqueous species. Therefore, only S(VI) aqueous species have been included in the thermal models.

Table 3-4. Initial and boundary waters considered in the numerical simulations of the thermal period (concentrations in mol/L).

Parameter	Forsmark GW (measured)	MX-80	Deponit CA-N
Temp. (ºC)	15	15	15
pH	7.2	7.86	7.15
Alk. (HCO_3^-)	$2.20\cdot10^{-3}$	$1.05\cdot10^{-3}$	$9.54\cdot10^{-4}$
Cl	$1.53\cdot10^{-1}$	$4.00\cdot10^{-2}$	$1.38\cdot10^{-1}$
SO_4^{2-}	$6.80\cdot10^{-3}$	$9.65\cdot10^{-2}$	$2.12\cdot10^{-2}$
Ca	$2.33\cdot10^{-2}$	$1.01\cdot10^{-2}$	$3.77\cdot10^{-2}$
Na	$8.88\cdot10^{-2}$	$2.12\cdot10^{-1}$	$2.89\cdot10^{-2}$
K	$8.75\cdot10^{-4}$	$1.40\cdot10^{-3}$	$2.35\cdot10^{-3}$
Mg	$9.30\cdot10^{-3}$	$5.81\cdot10^{-3}$	$3.72\cdot10^{-2}$
Si	$1.85\cdot10^{-4}$	$1.82\cdot10^{-3}$	$1.69\cdot10^{-4}$

As previously mentioned in Section 2.1 different scenarios for the time of saturation of the bentonite buffer and the flow regime in the fracture have been studied in the numerical simulations developed for the thermal period of the near-field. In this context, the different times of bentonite saturation (Table 3-5) have been set by calibrating the hydraulic pressure prescribed at the right border of the model domain in the granite (water source in Figure 3-2). The two advective flow regimes in the fracture have been set by defining a low and high transverse flux in the granite grid block located immediately at the right of the bentonite grid blocks, i.e. the left border of the granite section.

According to /SKB 2004b/ the thermal evolution of the bentonite buffer induced by the radioactive decay of the HLNW contained in the copper canister is expected to evolve from an initial temperature, ranging between 25 to 45ºC (outer and inner boundaries of the buffer, respectively), towards a a maximum temperature at the inner and outer boundaries of the buffer of 80º and 65ºC respectively. After the temperature peak which occurs approximately 10 to 30 years after bentonite deposition, the temperature of the buffer evolves towards the regional temperature of 15ºC (Figure 3-3), achieved after approximately 10,000 years.

The expected thermal evolution of the bentonite buffer as been set in the numerical simulations performed here, by defining 26 steps with different temperatures for the inner and outer boundaries of the buffer (Figure 3-3), so that the thermal evolution computed in the simulations is as similar as possible to the postulated thermal evolution /SKB 2004b/.

The temperature at the fracture in the granitic host rock is that of the rock massif, which is 15ºC. Therefore, from the right border of the model domain until the granite grid block located 1.50 m from the axis of the deposition hole, the temperature is fixed at 15ºC for the whole simulation period. Between the outer boundary of the buffer and the point in the fracture located 1.50 m from the axis of the deposition hole, the temperature gradient is calculated by the code TOUGHREACT (Figure 3-3). In the inner and outer boundaries of the buffer, the temperature is prescribed as shown in Figure 3-3, and within the buffer, the temperature gradient is calculated by TOUGHREACT.

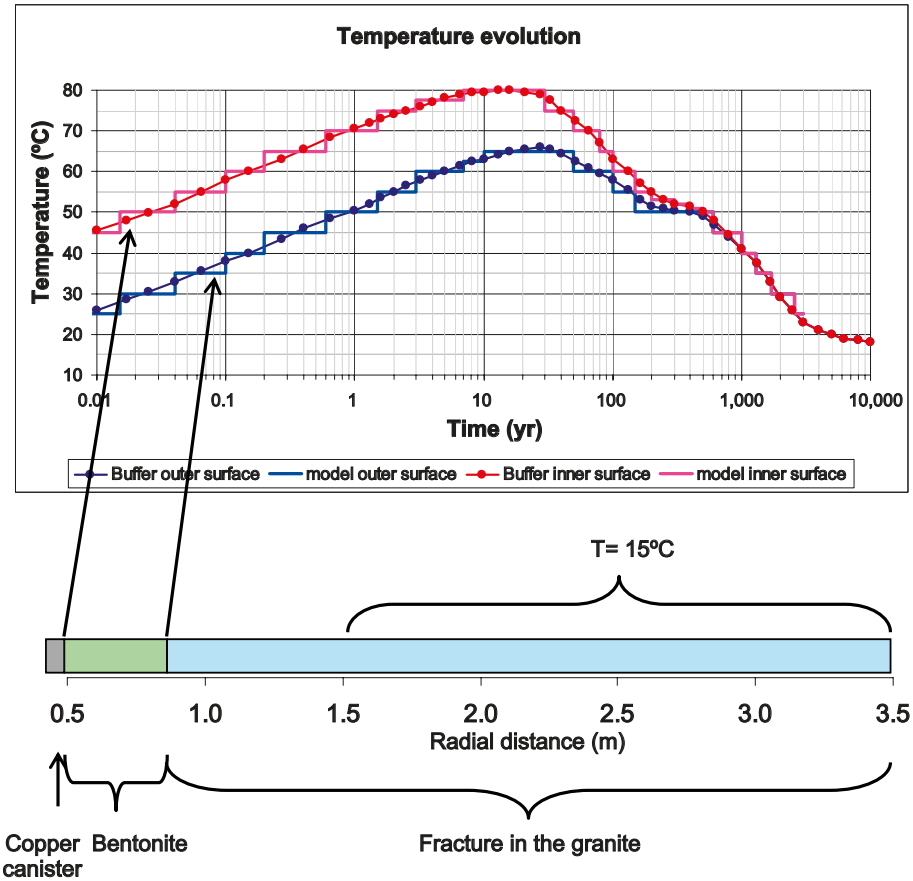

Figure 3-3. *Thermal boundary conditions for the thermal period of the near-field (data taken from /SKB 2004b/).*

3.2.6 Sensitivity analysis

During the thermal period of the near-field, the main processes that might disturb the geochemical evolution of the engineered barriers are: (1) the time of saturation of the bentonite buffer and (2) the efficiency of mixing between the granitic groundwater that flows through the fracture and the bentonite porewater. The first process depends mainly on the hydraulic pressure imposed over the deposition holes due to the regional hydraulic conditions of the granitic host rock, while the second process depends on the flow rate regime within the fracture.

Under a higher flow rate regime within the fracture, the effect of the diffusion of solutes from the bentonite porewater to the granite or vice versa on the chemical conditions of the granite around the deposition hole will be rapidly buffered by the supply of unaffected granitic groundwater. Under these conditions, the geochemical changes induced by the chemical reactions taking place in the buffer will be constrained to the buffer itself since any influence of these over the chemical conditions of the granite will be rapidly flushed due to granitic groundwater renewal (Figure 3-4). On the other hand, if the advective flow in the fracture is very low, diffusion will prevail and therefore, the chemical and diffusive processes occurring in the buffer will influence the chemical conditions of the fracture around the deposition hole (Figure 3-4).

In order to assess the influence of the magnitude of the two mains processes considered important during the thermal period, a sensitivity analysis has been set as shown in Table 3-5.

Table 3-5. Sensitivity analysis performed for the thermal period of the near-field, regarding the time of saturation of the bentonite buffer and the flow regime in the fracture.

Water saturation of the bentonite buffer after:	Low advective flow in the fracture	High advective flow in the fracture
10 years	X	X
100 years	X	X
1,000 years	X	
2,000 years	X	

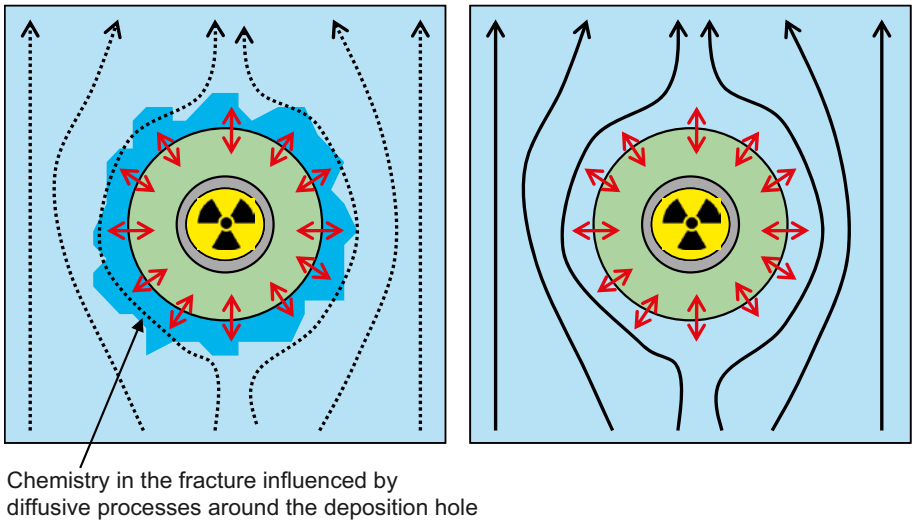

Figure 3-4. Sketch of the two scenarios considered for the flow regime in the hypothetical fracture that intersects a deposition hole, during the thermal period.

4 Numerical model for the water-saturated period

4.1 Numerical tool and thermodynamic database

The geochemical simulations for the water-saturated period have been performed with the reactive transport code PHAST /Parkhurst et al. 2004/. This code is the result of coupling a transport code, HST3D /Kipp 1997/ and a geochemical code, PHREEQC /Parkhurst and Appelo 1999/. Like PHREEQC, PHAST is able to simulate multicomponent, reactive solute transport in three-dimensional saturated groundwater flow systems. A number of boundary conditions are available (specified-head, flux and leaky conditions), and chemical reactions include homogeneous equilibria using an ion-association thermodynamic model, heterogeneous equilibria between the aqueous solution and minerals, gases, surface complexation sites, ion exchange sites, solid solutions, and kinetic reactions.

The thermodynamic database used in the simulations is the thermodynamic database from SKB's Trac system (SKB-TDB). This database is that developed by /Hummel et al. 2002/ with substantial modifications as reported in /Duro et al. 2006/.

4.2 Description of input data

4.2.1 Geometry of the modelled domain

Regarding the geometry of the modelled domain, two cases have been simulated for the water-saturated period (Figure 1-1). The first case is a 3D model domain where a pre-existing fracture of the granitic host rock intersects the deposition hole at its mid-height. The groundwater that circulates through the fracture contacts the bentonite, allowing diffusive transport between groundwater in the fracture and porewater from the bentonite (Figure 4-1).

In Case II, the granitic groundwater is considered to enter the backfilled tunnel through a fracture of the granitic host rock that intersects the tunnel. In addition, backfill groundwater is considered to enter the modelled domain through the right side of the backfilled tunnel that represents the contribution from the sections of the tunnel located upgradient from the modelled domain (Figure 4-2).

In the modelled domain of Case II, the groundwaters from the two sources (fracture and upgradient section of the backfilled tunnel) mix in the backfilled tunnel. This mixture then flows through the backfill domain. Groundwater contacts the buffer bentonite of the deposition hole located at the bottom of the backfilled tunnel, leading to diffusive transport. Then, groundwater that circulated through the backfill is leaving the modelled domain through the right boundary of the backfill (Figure 4-2).

4.2.2 Hydraulic processes and parameters

The hydraulic boundary conditions applied in the modelled domain of the two cases under study (Figure 4-1 and Figure 4-2) lead to the continuous flow of groundwater through the different materials that constitute each modelled domain. Since the flow rates defined for each boundary condition are constant over time, the simulations are modelled under steady state for flow. Depending on the hydraulic conductivity of each material, advective or diffusive flow will prevail in different areas of the modelled domain.

Taking into account the different hydraulic properties of the fracture, backfill and bentonite (Table 4-1), advective flow is expected to prevail in the first two material zones (fracture and backfill) whereas in the bentonite diffusive flow is expected to prevail. Under this premise and since the code PHAST allows only for a single value of diffusivity in water to be attributed to the whole modelled domain, the value of this parameter has been set in such a way that the effective diffusion coefficient (obtained by multiplying the diffusivity in water times the porosity) in the bentonite is $1.2 \cdot 10^{-10}$ m^2/s /Ochs and Talerico 2004/. Finally, diffusion in the granitic rock matrix has been neglected, and therefore, the fracture walls do not allow any exchange of mass between the groundwater flowing in the fracture and the granitic rock.

The hydraulic parameters of the compacted bentonite, fracture and backfill, applied in the modelled domains of Case I and Case II are listed in Table 4-1.

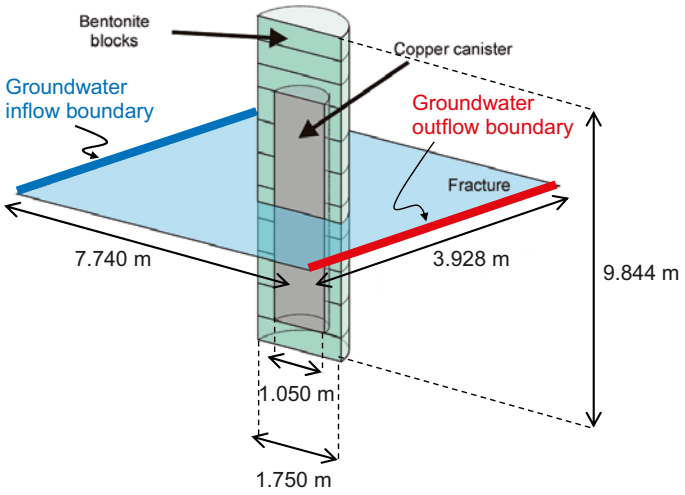

Figure 4-1. *Geometry and boundary conditions of the modelled domain for Case I (from /Arcos et al. 2006/).*

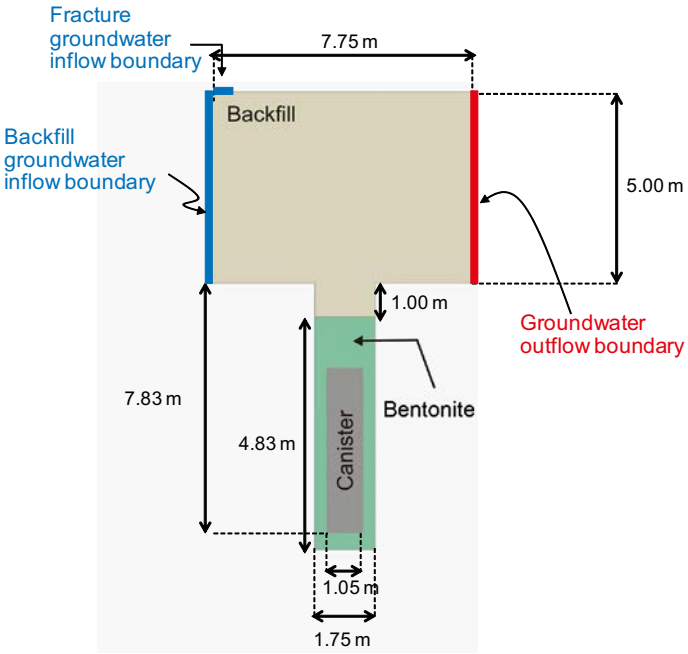

Figure 4-2. *Geometry and boundary conditions of the modelled domain for Case II (modified from /Arcos et al. 2006/).*

Table 4-1. Hydraulic parameters attributed to the three materials considered in the modelled domains of Case I and Case II.

Parameters	Units	Compacted bentonite	Fracture	Backfill
Hydraulic conductivity	[m/s]	10^{-14} (a)	$5 \cdot 10^{-10}$ (b)	10^{-10} (c)
Porosity	[–]	0.43 (a)	$3.5 \cdot 10^{-4}$ (d)	0.44 (e)
Diffusivity in water	[m^2/s]	$2.8 \cdot 10^{-10}$ (f)	$2.8 \cdot 10^{-10}$ (f)	$2.8 \cdot 10^{-10}$ (f)
Longitudinal dispersivity	[m]	0.15 (g)	0.15 (g)	0.15 (g)
Transverse dispersivity	[m]	0.001 (g)	0.001 (g)	0.001 (g)
Dry density	[g/L]	1,570 (a)	–	1,512 (h)
Fracture aperture	[m]	–	0.116 (i)	–

(a) /SKB 2006/; (b) /Follin et al. 2005/; (c) recommended maximum hydraulic conductivity according to /SKB 2006/; (d) Calculated using procedure from /Hartley et al. 2006/; (e) /Åkesson et al. 2010/; (f) /Arcos et al. 2006/; (g) To fulfil Peclet criterion ; (h) calculated from porosity and grain density given in /Åkesson et al. 2010/; (i) /Dershowitz et al. 2003/.

Porosity in the fracture zone has been chosen according to the calculations previously described in Section 1.4.2/Hartley et al. 2006/. This porosity is very low, and corresponds to a characteristic porosity of a granitic material. However, the estimated permeability is significantly higher than those estimated for the bentonite and the backfill.

The flow rate of the groundwater reaching the near-field has been set according to the procedure defined by /SKB 2006/ and /Hartley et al. 2006/ for the calculation of the equivalent groundwater flow rate for a fracture intersecting a deposition hole. On the other hand, the distribution of the relative heads is also controlled by the differences in permeabilities between the materials. The flow rate applied in the reference case of Case I is 10^{-3} m^3/yr. Three additional flow rates have been considered in a sensitivity analysis performed for this variable. Further information will be provided in Section 4.2.6, regarding the flow rates considered in Case I.

In Case II, the flow rate in the fracture was set to 10^{-4} m^3/yr, according to the recommendations given in the Backfill Production Report /SKB 2010/. The flow rate entering though the vertical cross section of the backfilled tunnel is $6.3 \cdot 10^{-4}$ m^3/yr which is obtained by multiplying the Darcy velocity ($3 \cdot 10^{-5}$ m/yr) recommended by /Hartley et al. 2004/ times the section of the tunnel (5 m × 4.2 m).

Other numerical parameters, as longitudinal and transverse dispersivities, have been selected according to the Peclet criterion.

4.2.3 Geochemical processes and parameters

The geochemical processes and parameters implemented in the numerical simulations of the near-field have been set based on the work developed by /Arcos et al. 2006, 2008/. In addition, whenever available, new geochemical and mineralogical data of the materials considered in the model have been used.

Regarding the geochemical features of the water-saturated period of the near-field, three materials have been considered: the bentonite buffer, the backfill, and the fracture of the granitic host rock.

The geochemical features of the two bentonite types considered in the numerical simulations are listed in Table 3-2, and the cation exchange reactions in the montmorillonite interlayer are listed in Table 3-3.

In the case that carbonate minerals are initially absent in the near-field (MX-80 bentonite), protonation of the montmorillonite surface is a well-known process that may have a relatively important role on the pH buffering /Arcos et al. 2008/. In this context and taking into account the geochemical processes considered by /Arcos et al. 2006, 2008/, surface protonation reactions have been considered in the numerical simulations (Table 4-2). Protonation reactions have not been implemented in the numerical models developed for the thermal period due to limitations of the code TOUGHREACT used for these simulations. Therefore, protonation reactions are only taken into account in the numerical models of the water-saturated period performed with the code PHAST.

The reference backfill material is a low grade bentonite, with 50–60% montmorillonite content /Börgesson 2008/. The bentonite to be used in the backfill production is the Deponit CA-N. According to /Börgesson 2008/, the target CEC for the backfill material is 50 meq/100 g. Therefore, and knowing that the CEC of Deponit CA-N is 72 meq/100 g /Olsson and Karnland 2009/, a weight fraction of 0.69 (50/72) of bentonite in the backfill is estimated. In Table 4-3 the mineralogy of the backfill material implemented in the numerical model is presented, based on the estimated fraction of Deponit CA-N bentonite in the backfill and considering that the material making up the 0.31 left (1–0.69) of the backfill is inert. Since the bentonite used in the production of the backfill is the Deponit CA-N, the relative occupancy of the exchanger of montmorillonite in the backfill is the same as the one shown in Table 3-2 for the Deponit CA-N.

In order to develop a sensitivity analysis on the main parameters of the groundwater that enters the modelled domains through the hypothetical fracture of the granitic host rock (for further details on the settings of the sensitivity analysis see Section 4.2.6), the fracture-filling minerals have been neglected.

Table 4-2. Protonation reactions implemented for montmorillonite in the numerical simulations /Bradbury and Baeyens 2002/ (ZOH and YOH denote the two weak site types which can protonate and deprotonate).

Site types	Site capacities
ZOH	$4.0 \cdot 10^{-2}$ mol/kg
YOH	$4.0 \cdot 10^{-2}$ mol/kg
Surface complexation reaction	**Log K**
$ZOH + H^+ = ZOH_2^+$	4.5
$ZOH = ZO^- + H^+$	–7.9
$YOH + H^+ = YOH_2^+$	6.0
$YOH = YO^- + H^+$	–10.5

Table 4-3. Mineralogical data of the backfill material considered in the numerical simulations.

Mineral	Weight (%)(1)
Calcite	5.56
Dolomite	11.11
Gypsum	0.56
Quartz	1.04
Pyrite	0.49

(1) Weight fraction of Deponit CA-N bentonite in the backfill is calculated by dividing the target CEC for the backfill (50 meq/100 g) by the average CEC of Deponit CA-N bentonite (72 meq/100 g).

In addition to the primary minerals that are considered for the bentonite and backfill material, secondary phases that could be relevant for the geochemical system under study have also been considered in the numerical simulations. These are amorphous ferrihydrite and siderite. If these phases precipitate, iron could be retained in the solid phase (iron is one of the geochemical parameters affecting the safety function indicators for the near-field, according to /SKB 2006/).

The construction of the initial porewater of the Deponit CA-N bentonite, which will be shown in Section 4.2.5, has been set in equilibrium with the primary minerals of this bentonite and also the exchanger composition as it is shown in Table 3-2. During these preliminary numerical equilibrations, it was concluded that the solubility constant for dolomite should be between that for disordered dolomite (Log K = 4.118) and that of ordered dolomite (Log K = 3.568). In Table 4-4, the solubility reactions for the minerals considered in the numerical simulations are listed.

The S(-II)/S(VI) and C(-IV)/C(IV) redox pairs have been decoupled from the thermodynamic database used in the numerical simulations. The production of both S(-II) and C(-IV) in the granitic host rock at depth is believed to be catalysed by microbial respiration /Pedersen 2000/ which is likely to undergo at a relatively low rate under the geochemical conditions that are modelled here. Therefore, since microbial respiration reactions are not considered, aqueous S(-II) can only be added or removed from the porewater in the modelled domain due to pyrite dissolution or precipitation.

Table 4-4. Solubility reactions for the minerals considered in the numerical simulations.

Mineral	Reaction	Log K
Calcite	$CaCO_3 + H^+ \leftrightarrow Ca^{2+} + HCO_3^-$	1.8490
Dolomite	$CaMg(CO_3)_2 + 2H^+ \leftrightarrow Ca^{2+} + Mg^{2+} + 2HCO_3^-$	3.8435(1)
Gypsum	$CaSO_4 \cdot 2H_2O \leftrightarrow Ca^{2+} + SO_4^{2-} + 2H_2O$	–4.5809
Quartz	$SiO_2 + 2H_2O \leftrightarrow Si(OH)_4$	–3.7460
Pyrite	$FeS_2 + 2H^+ + 2e^- \leftrightarrow Fe^{2+} + 2HS^-$	–16.5700
Amorphous ferrihydrite	$Fe(OH)_3(am) + 3H^+ \leftrightarrow Fe^{3+} + 3H_2O$	5.0000
Siderite	$FeCO_3 + H^+ \leftrightarrow Fe^{2+} + HCO_3^-$	–0.5585

(1) The Log K for dolomite solubility constant is between the Log K for ordered and disorder dolomites, and it has been calculated so that the exchanger of Deponit CA-N bentonite is in equilibrium with this mineral.

4.2.4 Space and time discretization

Since the modelled domains used for the simulations of Case I and Case II are those developed in /Arcos et al. 2006/, the space discretization is also the same as the one implemented by these authors. For more details the reader is referred to /Arcos et al. 2006/.

Knowing that the performance assessments for a deep geological repository must comprise at least 100,000 yr, this time lag was set as the total simulation time for the numerical simulations of Case I and Case II. The time discretization was set smaller at the beginning of the simulation time, when major geochemical changes are expected to occur due to the disturbance of the pre-existing equilibrium by the intrusion of the groundwater entering through the fracture. Then, the time discretization is set progressively coarser until the end of the simulation time (Table 4-5).

4.2.5 Initial and boundary conditions

The initial and boundary conditions of the modelled domains were set according to the possible groundwater flow rates that may occur in the near-field of a KBS-3 repository at Forsmark /SKB 2006, Hartley et al. 2006/, and also according to the geochemical features that have been previously described in Section 4.2.3 and may potentially affect the geochemical behaviour of the engineered barriers (bentonite and backfill).

In Case I, groundwater reaches the near-field through a hypothetical fracture of the granitic host rock that intersects a deposition hole. In this case, two waters mix in the near-field: the granitic groundwater flowing through the fracture and the initial porewater of the bentonite (Figure 4-3). According to /Hartley et al. 2006/, the flow rate of the granitic groundwater flowing through the fracture is calculated by means of the equivalent flow rate /SKB 2006/, where $Q_{eq\,1}$ and $Q_{eq\,3}$ represents the equivalent flows through a fracture intersecting the deposition hole and through the backfill respectively. According to /Hartley et al. 2006/ (see Section 1.4.2) a value of $Q_{eq\,1} = 10^{-4}$ m^3/yr has been selected for the reference case based on the DFN model as more than 70% of deposition holes will have equivalent flows below this value /SKB 2006/.

The data from Table 4-6 has been selected in order to calculate the needed input parameters for the model.

With this set of values, the Q_f value to obtain a $Q_{eq\,1}$ of 10^{-4} m^3/yr is 10^{-3} m^3/yr, for the reference case.

The sample for the Forsmark groundwater selected by /Arcos et al. 2006/ has also been used in the present simulations. Numerical calculations performed in PHREEQC indicate that this water sample is slightly oversaturated in calcite (Saturation Index, SI= 0.16) and undersaturated in pyrite (SI= –8.21). Nevertheless, for the purpose of the reactive transport calculations performed in the present work, the Forsmark granitic groundwater is assumed to be in equilibrium with the main reactive minerals present at the fracture walls. In this context, the pH and pe of the selected Forsmark groundwater sample ("Forsmark GW (measured)" in Table 4-7) have been set in equilibrium with calcite and pyrite, respectively, leading to the values shown in the column titled "Forsmark GW (Ref. Case)" of Table 4-7. This groundwater represents the Forsmark groundwater that circulates through the fracture in the numerical simulations.

Sodium and calcium are the dominant cations of Forsmark groundwater, while in the MX-80 porewater sodium is much more abundant that calcium. In addition, the dominant cations in Deponit CA-N porewater are magnesium and calcium.

Table 4-5. Time discretization implemented in the numerical simulations of Case I and Case II.

Time period	Time step (years)
From 0 to 10 years	1
From 10 to 100 years	10
From 100 to 1,000 years	50
From 1,000 to 5,000 years	250
From 5,000 to 100,000 years	1,000

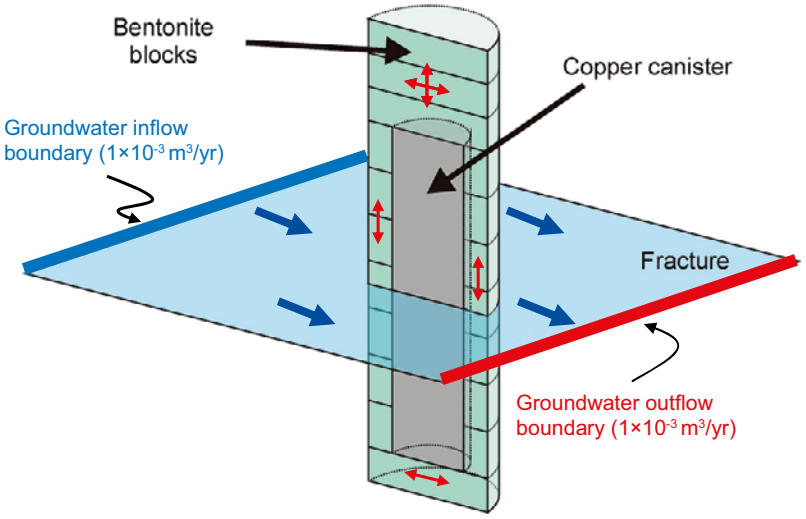

Figure 4-3. *Boundary conditions (flow rate shown for the reference case) and expected groundwater flow directions for Case II. Blue arrows indicate expected directions of groundwater flow. Red arrows indicate predominance of diffusive flow (modified from /Arcos et al. 2006/).*

Table 4-6. Selected data for the calculation of $Q_{eq\,1}$ according to /SKB 2006/.

Parameter	Value	Units	Source
D_w	$2.8 \cdot 10^{-10}$	[m^2/s]	/Arcos et al. 2006/
L_f	3.3	[m]	Calculated from KBS-3 design
U_{r1}	$3.35 \cdot 10^{-4}$	[m/yr]	/SKB 2006/
Porosity in fracture	$3.5 \cdot 10^{-4}$	[–]	/Dershowitz et al. 2003/
w_c	4.83	[m]	/Hartley et al. 2006/
Fracture thickness	0.116	[m]	/Arcos et al. 2006/

Table 4-7. Initial and boundary waters considered in the numerical simulations (concentrations in mol/L). These water compositions were defined by performing static geochemical calculations in PHREEQC with the original Forsmark groundwater and selected minerals (details in the text). The original Forsmark groundwater composition, as it was measured by /Laaksoharju et al. 2004 /, is also shown (Forsmark GW (measured)).

Parameter	Forsmark GW (measured)	Forsmark GW (Ref. Case)	MX-80	Deponit CA-N	Backfill
Temp. (ºC)	15	15	15	15	15
pH	7.2	7.05(1)	7.19	7.16	7.16
pe	–2.42	–2.83(1)	–2.78	–2.91	–2.78
Alk. (HCO_3^-)	$2.20 \cdot 10^{-3}$	$2.20 \cdot 10^{-3}$	$2.60 \cdot 10^{-3}$	$1.45 \cdot 10^{-3}$	$1.70 \cdot 10^{-3}$
Cl	$1.53 \cdot 10^{-1}$	$1.39 \cdot 10^{-1}$(2)	$1.38 \cdot 10^{-1}$	$1.38 \cdot 10^{-1}$	$1.38 \cdot 10^{-1}$
SO_4^{2-}	$6.80 \cdot 10^{-3}$	$6.80 \cdot 10^{-3}$	$3.44 \cdot 10^{-2}$	$2.20 \cdot 10^{-2}$	$2.60 \cdot 10^{-2}$
Ca	$2.33 \cdot 10^{-2}$	$2.33 \cdot 10^{-2}$	$1.83 \cdot 10^{-2}$	$3.34 \cdot 10^{-2}$	$2.97 \cdot 10^{-2}$
Na	$8.88 \cdot 10^{-2}$	$8.88 \cdot 10^{-2}$	$1.54 \cdot 10^{-1}$	$2.93 \cdot 10^{-2}$	$2.96 \cdot 10^{-2}$
K	$8.75 \cdot 10^{-4}$	$8.75 \cdot 10^{-4}$	$1.14 \cdot 10^{-3}$	$2.38 \cdot 10^{-3}$	$2.41 \cdot 10^{-3}$
Mg	$9.30 \cdot 10^{-3}$	$9.30 \cdot 10^{-3}$	$8.86 \cdot 10^{-3}$	$4.27 \cdot 10^{-2}$	$5.04 \cdot 10^{-2}$
Fe	$3.31 \cdot 10^{-5}$	$3.31 \cdot 10^{-5}$	$3.31 \cdot 10^{-5}$	$3.31 \cdot 10^{-5}$	$3.31 \cdot 10^{-5}$
Si	$1.85 \cdot 10^{-4}$	$1.85 \cdot 10^{-4}$	$1.26 \cdot 10^{-4}$	$1.27 \cdot 10^{-4}$	$1.26 \cdot 10^{-4}$

(1) pH and pe used in the models for Forsmark groundwater differ from the values actually measured (pH = 7.2; pe = –2.42, in the first column) because these parameters were defined by the equilibrium with calcite and pyrite, respectively; (2) Chloride concentration is different from the one actually measured due to charge balance calculation.

As previously mentioned, two types of bentonite are considered in the reactive transport simulations and the corresponding initial porewater is assumed to be in equilibrium with the reactive minerals and the cation exchanger of each bentonite type. In addition, it is expected that the bentonite blocks introduced in each deposition hole will be prepared with a mixture of bentonite powder and the groundwater available at the site which is the Forsmark groundwater. In this context, the initial porewater composition of each bentonite buffer has been set by equilibrating the Forsmark groundwater with calcite, pyrite, gypsum, quartz and the cation exchanger.

Although no calcite has been determined by XRD analysis in the MX-80 bentonite (Table 3-2), the initial porewater of this bentonite has been assumed to be in equilibrium with calcite. This mineral is likely to be present in trace amounts in bentonite which could not be detected by XRD analysis but are enough to control the pH of the corresponding porewater and for this reason calcite equilibrium was considered when defining the initial porewater composition of MX-80 bentonite.

For the Deponit CA-N bentonite, besides the minerals considered in the MX-80 bentonite, and according to its mineralogy (shown in Table 3-2) dolomite is also considered. The initial porewater composition of each bentonite type is shown in Table 4-7 (columns MX-80 and Deponit CA-N).

In Case II, the groundwater that enters through the vertical section of the backfilled tunnel is considered to have been flowing through the tunnel sections that are located upgradient of the modelled domain. In this context, the groundwater entering through the left border of the modelled domain (Figure 4-4) has been set by equilibrating the Forsmark groundwater with the backfill minerals and cation exchanger shown in Table 4-3 and Table 3-2, respectively. The initial backfill porewater composition is equal to the composition of the groundwater entering through the left border of the modelled domain that is shown in the last column of Table 4-7 (Backfill).

In Figure 4-4, the boundary conditions for Case II are shown. According to /SKB 2006, Hartley et al. 2006/, the equivalent flow rate through the backfill accounting for at least 50% of the deposition holes is $2 \cdot 10^{-3}$ m^3/yr. Taking into account this value and the equations in /Hartley et al. 2006, SKB 2006/, the flow through the backfill has been calculated to be $7.3 \cdot 10^{-4}$ m^3/yr. Finally, According to /SKB 2006/ the maximum flow entering into the deposition gallery through a fracture is 10^{-4} m^3/yr.

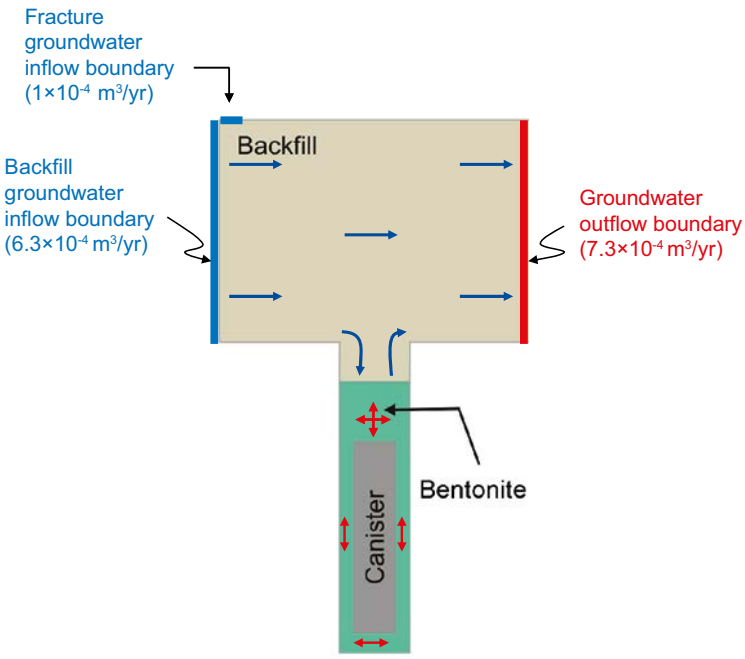

Figure 4-4. *Boundary conditions and expected groundwater flow directions for Case II. Blue arrows indicate expected directions of groundwater flow. Red arrows indicate predominance of diffusive flow (modified from /Arcos et al. 2006/).*

4.2.6 Sensitivity analysis

The sensitivity analysis exercise performed using PHAST is based on the numerical models developed by /Arcos et al. 2006/. In Case I a fracture of the granitic host rock is considered to reach a deposition hole, while in Case II the fracture is considered to reach the backfilled tunnel, so that the Forsmark groundwater circulating in the fracture may subsequently flow through the backfill and the bentonite, triggering geochemical changes in the near-field. In each case, two reference cases exist; one considering the MX-80 bentonite buffer and another considering the Deponit CA-N bentonite buffer.

In Case I, the two reference cases (each with one type of bentonite buffer) are set with a flow rate of 10^{-3} m^3/yr, and with the following initial and boundary waters (Table 4-7):

- In the bentonite buffer, the initial porewater is the MX-80 porewater or the Deponit CA-N porewater, depending on the buffer composition considered.
- The groundwater entering through the fracture is the Forsmark groundwater.

In Case II, the two reference cases (each with one type of bentonite buffer) are set with the hydrodynamic boundary conditions as shown in Figure 4-4, and the chemical composition of the initial and boundary waters as follows (Table 4-7):

- The initial porewater in the area occupied by the backfill material is the backfill porewater.
- The initial porewater in the area occupied by the bentonite buffer is the MX-80 porewater or the Deponit CA-N porewater, depending on the reference case considered.
- The groundwater entering through the left border of the modelled domain is the backfill porewater.
- The groundwater entering through the fracture is the Forsmark groundwater.

In order to assess the influence of certain parameters on the geochemical changes induced by the inflow of groundwater into the near-field, a sensitivity analysis has been performed on selected parameters:

- In Case I, besides the hydraulic conditions of the reference case (Figure 4-3), three additional cases have been performed regarding the flow rate of groundwater flowing through the fracture (Table 4-8). In addition, for the flow rates 10^{-3} and 0.1 m^3/yr, a sensitivity analysis on the chemical composition of the groundwater flowing through the fracture has also been performed.
- In Case II, a sensitivity analysis on the chemical composition of the groundwater entering through the fracture has been performed with the flow rates as shown in Figure 4-4.

The sensitivity analysis developed for the hydrodynamic conditions of Case I relies on four simulations where different groundwater flow rates are considered to circulate through the fracture that reaches the deposition hole. These flow rates vary from 10^{-5} to 10 m^3/yr (Table 4-8).

The sensitivity analysis for the chemical composition of the groundwater entering through the hypothetical fracture relies on a series of eighteen simulations (in addition to the reference case) which account for changes on key chemical parameters of the selected Forsmark groundwater sample (Table 4-9). The key chemical parameters that constitute the basis of this sensitivity analysis exercise are: pH, concentration of aqueous carbonate, calcium aqueous concentration and ratio between aqueous calcium and sodium, and concentration of aqueous sulphate.

In Table 4-10, a summary of all the sensitivity cases performed for Case I and Case II are listed. It should be noted that all the sensitivity cases have been performed for the two bentonite types under consideration: the MX-80 and the Deponit CA-N.

Table 4-8. Selected flow rates for the sensitivity analysis on the groundwater flow rate of the fracture intersecting a deposition hole, in Case I.

Q_f (m^3/yr)	10^{-5}	10^{-3}	0.1	10
Q_{eq} (m^3/yr)	10^{-5}	10^{-4}	10^{-3}	10^{-2}
Darcy velocity (m/yr)	$3.35 \cdot 10^{-6}$	$3.35 \cdot 10^{-4}$	$3.35 \cdot 10^{-2}$	3.35

Legend: Q_f – volumetric flux in the fracture adjacent to the deposition hole Q_{eq} – equivalent flow rate.

Table 4-9. Chemical compositions of the groundwater flowing through the hypothetical fracture for the sensitivity cases.

Parameter	pH	pH	pH	pH	pH	C(IV)	C(IV)	C(IV)	Ca/Na
pH	10	9	8	7	6	7.05	7.05	6.51	7.05
pe	–6.22(1)	–5.06(1)	–3.92(1)	–2.78(1)	–1.63(1)	–2.83(1)	–2.83(1)	–2.22(1)	–2.80(1)
HCO_3^-	1.12E–5(2)	3.04E–5(2)	3.35E–6(2)	3.35E–6	3.35E–6	1.00E–4	1.00E–3	1.00E–2	3.35E–6
Cl	1.41E–1(3)	1.41E–1(3)	1.41E–1(3)	1.39E–1(3)	1.41E–1(3)	1.41E–1(3)	1.40E–1(3)	1.35E–1(3)	9.30E–2(3)
SO_4^{2-}	6.80E–3	6.80E–3	6.80E–3	6.80E–3	6.80E–3	6.80E–3	6.80E–3	6.80E–3	6.80E–3
S(-II)	4.65E–10	2.68E–10	2.00E–10	2.35E–10	7.71E–10	2.19E–10	2.25E–10	4.07E–10	2.05E–10
Ca	2.33E–2	2.33E–2	2.33E–2	2.33E–2	2.33E–2	2.33E–2	2.33E–2	2.33E–2	1.00E–4
Na	8.88E–2	8.88E–2	8.88E–2	8.88E–2	8.88E–2	8.88E–2	8.88E–2	8.88E–2	8.88E–2
K	8.75E–4	8.75E–4	8.75E–4	8.75E–4	8.75E–4	8.75E–4	8.75E–4	8.75E–4	8.75E–4
Mg	9.30E–3	9.30E–3	9.30E–3	9.30E–3	9.30E–3	9.30E–3	9.30E–3	9.30E–3	9.30E–3
Fe	3.31E–5	3.31E–5	3.31E–5	3.31E–5	3.31E–5	3.31E–5	3.31E–5	3.31E–5	3.31E–5
Si	1.85E–4	1.85E–4	1.85E–4	1.85E–4	1.85E–4	1.85E–4	1.85E–4	1.85E–4	1.85E–4

Parameter	Ca/Na	Ca/Na	Ca/Na	Ca/Na	S(VI)	S(VI)	S(VI)	S(VI)	S(VI)
pH	7.05	7.05	7.05	7.05	7.02	7.02	7.03	7.06	7.49
pe	–2.81(1)	–2.82(1)	–2.87(1)	–3.00(1)	–3.21(1)	–3.07(1)	–2.93(1)	–2.82(1)	–3.20(1)
HCO_3^-	2.20E–3	2.20E–3	7.44E–4(2)	2.33E–4(2)	2.20E–3	2.20E–3	2.20E–3	2.20E–3	2.20E–3
Cl	9.48E–2(3)	1.13E–1(3)	2.94E–1(3)	2.10(3)	1.53E–1(3)	1.53E–1(3)	1.51E–1(3)	1.33E–1(3)	2.85E–2(3)
SO_4^{2-}	6.80E–3	6.80E–3	6.80E–3	3.78E–3(4)	1.00E–5	1.00E–4	1.00E–3	1.00E–2	5.00E–2
S(-II)	2.06E–10	2.16E–10	2.67E–10	2.18E–10	5.78E–10	4.16E–10	2.99E–10	2.18E–10	1.73E–10
Ca	1.00E–3	1.00E–2	1.00E–1	1.00	2.33E–2	2.33E–2	2.33E–2	2.33E–2	2.33E–2
Na	8.88E–2	8.88E–2	8.88E–2	8.88E–2	8.88E–2	8.88E–2	8.88E–2	8.88E–2	8.88E–2
K	8.75E–4	8.75E–4	8.75E–4	8.75E–4	8.75E–4	8.75E–4	8.75E–4	8.75E–4	8.75E–4
Mg	9.30E–3	9.30E–3	9.30E–3	9.30E–3	9.30E–3	9.30E–3	9.30E–3	9.30E–3	9.30E–3
Fe	3.31E–5	3.31E–5	3.31E–5	3.31E–5	3.31E–5	3.31E–5	3.31E–5	3.31E–5	3.31E–5
Si	1.85E–4	1.85E–4	1.85E–4	1.85E–4	1.85E–4	1.85E–4	1.85E–4	1.85E–4	1.85E–4

(1) Value defined by pyrite equilibrium; (2) Value defined by calcite equilibrium; (3) Value defined by charge balance; (4) Value defined by gypsum equilibrium.

In blue, the modified value of the chemical parameter is highlighted.

Table 4-10. Summary of the sensitivity cases considered for Case I and Case II.

	Case I				Case II
Flow rate (m^3/yr)	10^{-5}	10^{-3}	0.1	10	(Figure 4-4)
Forsmark GW (Table 4-7)	×	×	×	×	×
pH= 10		×	×		×
pH= 9		×	×		×
pH= 8		×	×		×
pH= 7		×	×		×
pH= 6		×	×		×
C(IV)= 10^{-4} mol/L		×	×		×
C(IV)= 10^{-3} mol/L		×	×		×
C(IV)= 10^{-2} mol/L		×	×		×
Ca/Na = 0.001		×	×		×
Ca/Na = 0.01		×	×		×
Ca/Na = 0.1		×	×		×
Ca/Na = 1		×	×		×
Ca/Na = 10		×	×		×
S(VI)= 10^{-5} mol/L		×	×		×
S(VI)= 10^{-4} mol/L		×	×		×
S(VI)= 10^{-3} mol/L		×	×		×
S(VI)= 10^{-2} mol/L		×	×		×
S(VI)= $5 \cdot 10^{-2}$ mol/L		×	×		×

5 Numerical results for the thermal period

The main objective of these models is to describe the transient evolution of the main thermal-hydraulic parameters during the thermal stage (temperatures, pressures and water saturation), and their influence on the mechanisms of solute transport and on the reactivity with the solid phases.

During the thermal period, the concentrations of the conservative solutes evolve according to the mixing mechanisms, under a scenario of water evaporation and condensation close to the canister boundary. On the other hand, the distribution of the reactive solutes is also influenced by changes of mineral solubilities and cation exchange capacities. All these mechanisms have been extensively explained in the framework of the models developed from the LOT-A2 experiments /Sena et al. 2010/. Therefore, in the present work, only specific aspects for the MX-80 and Deponit bentonites will be detailed.

5.1 Simulations with the MX-80 bentonite

5.1.1 Mechanisms of water saturation

With initial water saturation around 62%, the buffer is progressively saturated from its outer boundary located at the right side in Figure 5-1. The piston like flow is the key mechanism generating the humidity front. This front moves from the outer boundary of the buffer to the inner one, as a consequence of the pressure gradient imposed between the bentonite porewater and Forsmark groundwater that flows through a granitic fracture that intersects a deposition hole.

Regarding the time at which the bentonite is fully water saturated (from 10 to 2,000 years, according to /Åkesson et al. 2010/), four cases have been considered (Figure 5-1). The different time lags for fully water saturation of the bentonite buffer have been calibrated as a function of the pressure gradient between the bentonite buffer and the right border of the granite in the modelled domain. This results in a now flow through the fracture once the bentonite is fully saturated. An additional case were the composition in the groundwater of the fracture is fixed has been calculated in order to simulate the existence of a highly advective flow rate along the fracture (a fast renewal of the fracture groundwater). This sensitivity analysis has been performed for the cases where the bentonite saturation occurs at 10 and 100 years.

In the inner boundary of the buffer, the temperature increases from 45ºC to 80ºC during the first 10 years, with a thermal difference of 15–25ºC with respect to the outer boundary of the buffer (Figure 5-2). As a consequence of the temperature gradient that is established in the bentonite, the porewater evaporates close to the contact with the canister which induces the decrease of water saturation of the bentonite to values around 20%. Associated to the water evaporation in the vicinity of the canister, water condensation takes place where the temperature decreases, behind the evaporation front, increasing water saturation with respect to the initial value of 62% (Figure 5-3).

The evaporation front expands along a radius which is less than 0.55 m around the copper tube. The evaporation peak occurs during the first 50 years (Figure 5-3), when the temperature increases in the inner boundary of the buffer (Figure 5-2). In addition, the volume of porewater evaporated is higher in the cases where bentonite saturation occurs after longer time lags; 1,000 and 2,000 years. In these cases, the velocity of the wetting front (induced by the injection of the granitic groundwater through the outer boundary of the buffer) is slower than 10^{-3} m/yr.

In the cases where the wetting front moves slowly (saturation of the bentonite at 1,000 and 2,000 years), the capillary forces play a relevant role on the saturation of the porous adjacent to the humidity front (Figure 5-3). In these cases, the effect of suction (and the volume of water previously condensed) modifies the slope of the wetting front.

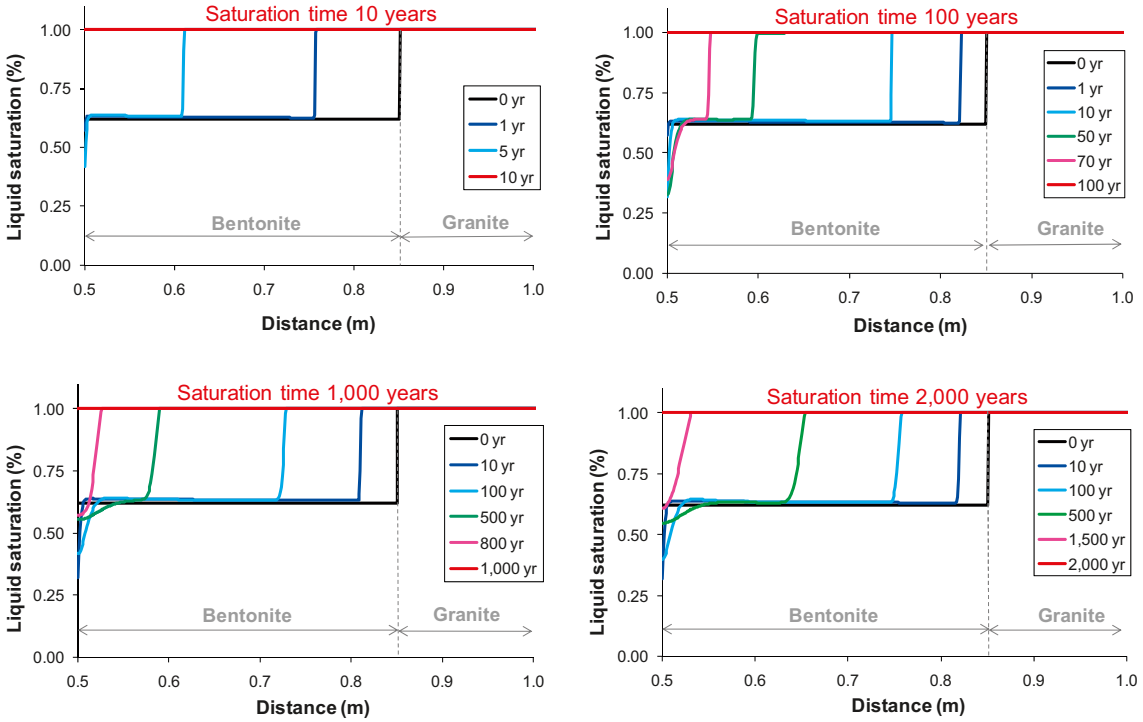

Figure 5-1. *Computed evolution of the water saturation in the modelled domain for the four cases analysed at 10, 100, 1,000 and 2,000 years.*

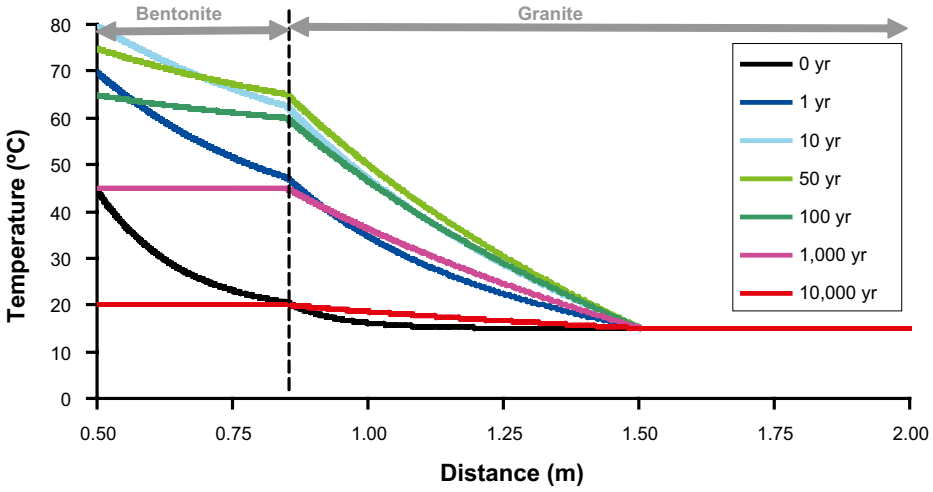

Figure 5-2. *Computed evolution of the temperature profile in the modelled domain for the case where saturation of the bentonite occurs at 1,000 years. It should be noted that the evolution of the temperature profile for the other cases under study is very similar to the evolution shown in the graph.*

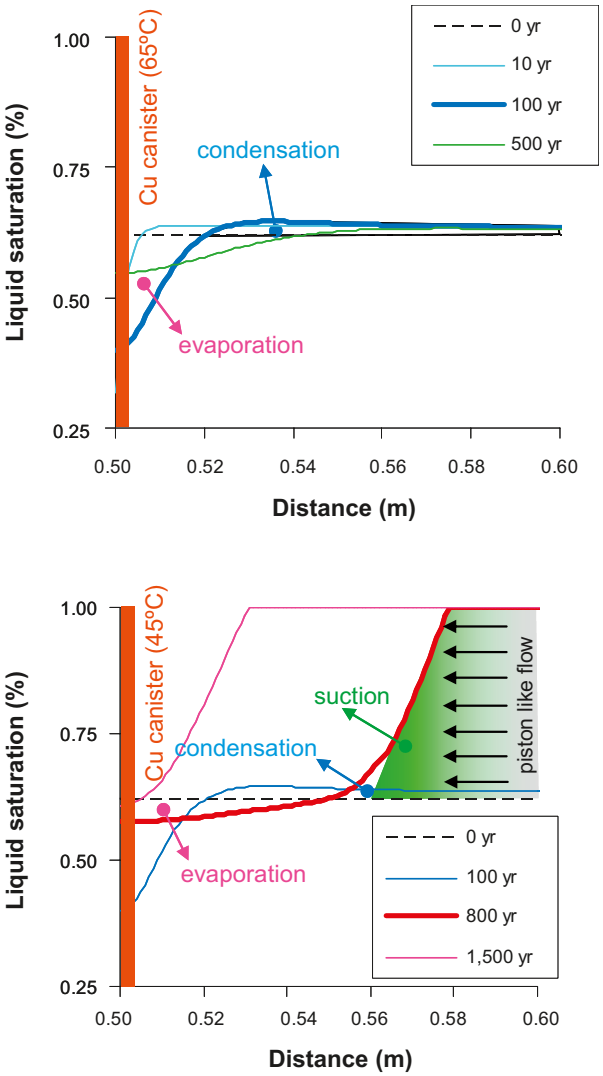

Figure 5-3. *Computed components of the wetting front for 100 and 800 years, during the bentonite saturation, in the 10 cm close to the copper canister, and for the cases where the velocity of the wetting front is relatively slow (saturation of the bentonite after 2,000 years).*

The effect of evaporation on the saturation profile is not completely developed in the cases where the wetting front moves relatively fast (saturation of the bentonite < 10 years), because the bentonite is fully water saturated before the establishment of the highest temperatures. In these cases the vapour pressures that develop as a consequence of heating are lower than the hydraulic pressure, and therefore evaporation of the bentonite porewater is not predicted.

The maximum temperature effect on the saturation process takes place in the case where the bentonite is fully water saturated after 100 years. For longer saturation times, the drying effect in the bentonite is similar to that computed for a saturation time of 100 years which is mainly due to the following processes:

1. The temperatures at the inner boundary of the bentonite decrease after 30 years so that after this time evaporation decreases substantially; and,
2. the capillary forces are more effective saturating the bentonite close to the copper tube.

Significant differences have not been observed in the cases where the advective flow along the fracture is high.

5.1.2 Conservative transport of chlorine

Chlorine has been considered as a conservative component in the aqueous solutions during the development of the geochemical processes simulated in this work. In this context, the temporary distribution of chlorine concentration reflects the role of the transport mechanisms (advection and diffusion) during the hydrological evolution of the near-field.

As previously mentioned, two advective scenarios have been modelled along the fracture zone (perpendicularly to the advance of the saturation front within the bentonite): (1) low advective flow rate (no flow as an extreme case), and (2) high advective flow rate (with an efficient transport of solutes beyond the outer boundary of the buffer).

Low flow rate along the fracture for the MX-80 bentonite

This hydrological scenario represents base case flow for the granitic groundwater along the fracture (see Section 4.2.2). In this scenario, during bentonite saturation, advective flow, induced by the existence of a pressure gradient between the regional groundwater and the bentonite porewater, is the main transport mechanism. After saturation of the bentonite, advection becomes negligible and diffusive transport prevails.

As previously mentioned, we have studied four full bentonite water saturation times: 10, 100, 1,000 and 2,000 years. For 10 and 100 years, the velocity of saturation and the advective flow in the bentonite is relatively high, while for 1,000 and 2,000 years the advective flow is considered relatively low.

With a high advective flow in the bentonite (saturation times of 10 and 100 years), the diffusive transport of chlorine starts to be effective only when the bentonite is completely water saturated. If the advective flow is lower (saturation times of 1,000 and 2,000 years) diffusive transport is effective from the first year.

The final chlorine concentration in the bentonite is slightly higher in the cases where saturation of the bentonite occurs faster (10 and 100 years, in Figure 5-4) compared to the slower saturation cases (>1,000 years).

When the bentonite reaches full saturation (10, 100 and 1,000 years, depending on the hydrological model), the bentonite porewater is more saline in the cases with higher advective flow. This is a consequence of the evolution of the salinity in the granitic groundwater close to the outer boundary of the buffer. In the models with low advective flow, the granitic groundwater flowing close to the bentonite boundary is characterized by a decrease in salinity as a consequence of the diffusive transport of chlorine to the bentonite porewater.

Due to the differences in porosity between the bentonite and the granite lithologies (bentonite porosity is much higher than granite porosity) the diffusion of chlorine from the granitic groundwater to the bentonite porewater induces a significant decrease of the chlorine concentration in the granitic groundwater, and a negligible increase of the salinity of the bentonite porewater (Figure 5-4). In the granite area close to the contact with the bentonite, chlorine concentration decreases until 1,000 years and then this tendency is reversed, so that from 1,000 to 10,000 years, the chlorine concentration increases in this area. This means that from 1,000 years, the dilution of chlorine concentration due to diffusion of chlorine from the granite to the bentonite porewater is compensated by the contribution of the transport of chlorine that comes from the distal area of the granite (> 3.3 m). Consequently, the concentration gradient between the bentonite porewater and the granitic groundwater is considerably reduced with respect to the initial value. The salinities of the bentonite porewater and the granitic groundwater become relatively homogenised after 10,000 years (Figure 5-5).

The evaporation induced by the increase of temperature in the inner boundary of the buffer during the first 10 years (Figure 5-3) does not substantially affect the concentration of chlorine in the bentonite porewater. Consequently, the main mechanism influencing the geochemical evolution of the conservative components should be mixing rather than evaporation. Diffusion efficiently homogenises the concentration fronts within the bentonite porewater.

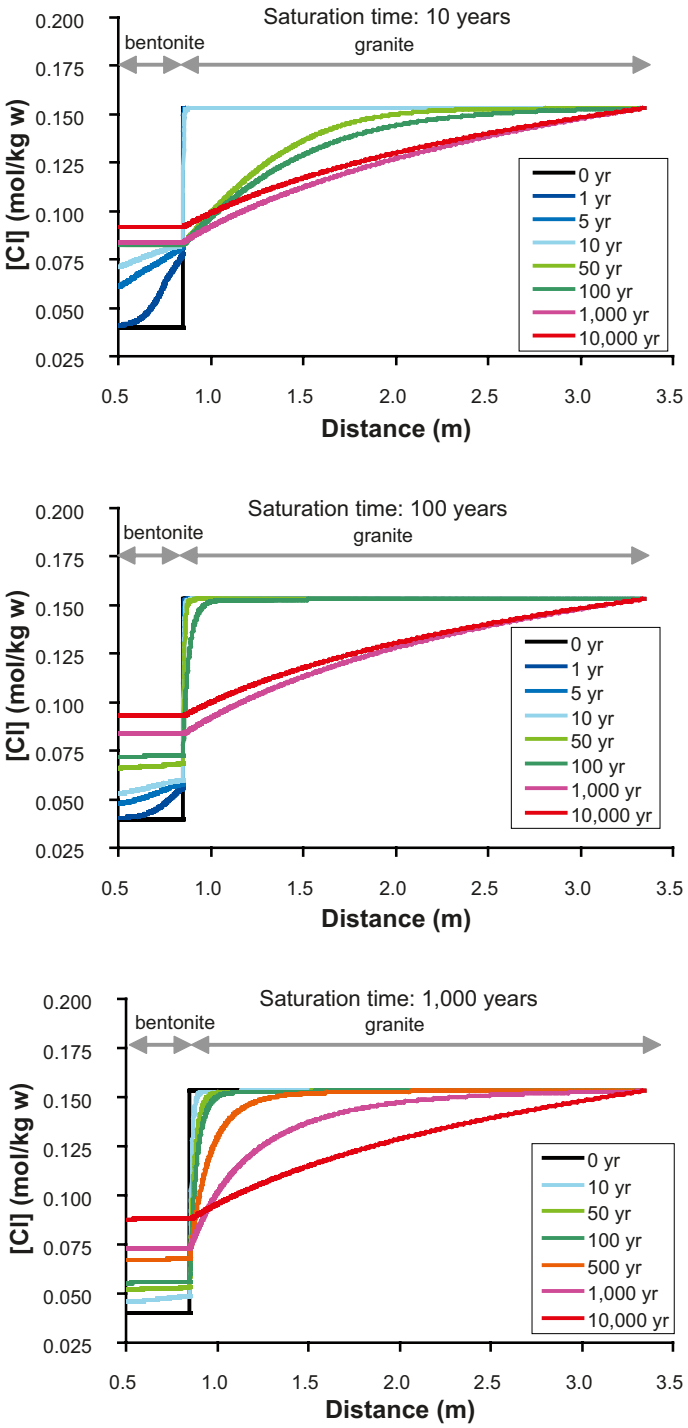

Figure 5-4. *Computed evolution of total chlorine concentration in the modelled domain for the scenario with a low advective flow in the fracture, and saturation of the MX-80 bentonite at 10 years, 100 years and 1,000 years.*

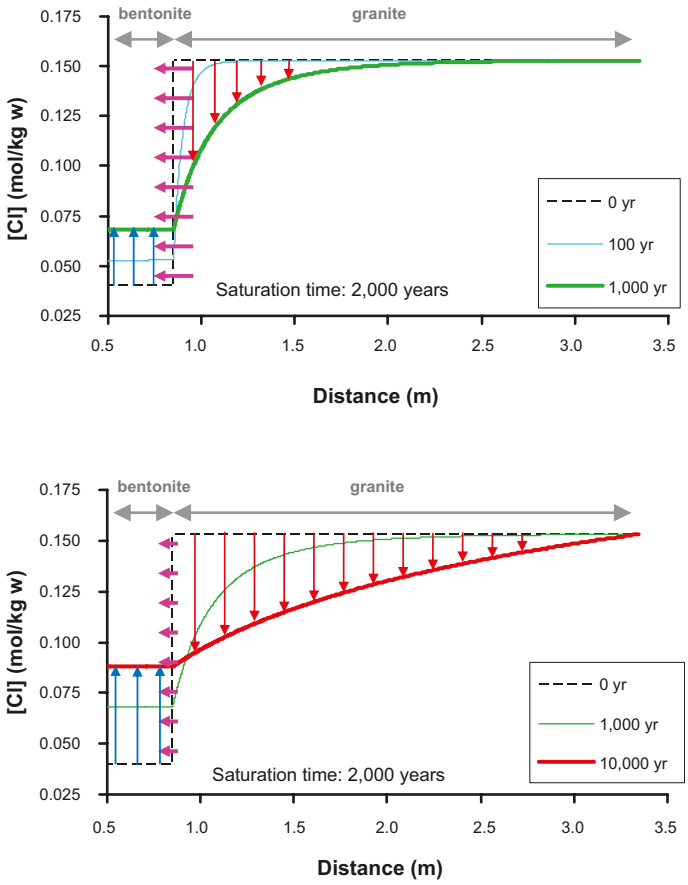

Figure 5-5. *Computed evolution of the Cl concentration in the modelled domain for (1) the scenario with a low advective flow in the fracture, and (2) a low velocity of the MX-80 bentonite water saturation (MX-80 bentonite is fully water saturated at 2,000 years). Purple arrows indicate the direction of solute transport by diffusion, induced by the existence of a gradient of concentrations between the granitic groundwater and the bentonite porewater. After 1,000 and 10,000 years, red arrows indicate the decrease of concentrations in the granitic groundwater in the vicinity of the buffer, and blue arrows show the corresponding increase of Cl concentration the in MX-80 bentonite porewater.*

High flow rate along the fracture for the MX-80 bentonite

In this hydrological scenario, the flow rate of the granitic groundwater is so high that it is able to maintain the concentration of solutes in the granite area close to the contact with the bentonite practically constant along time. In this context, the system is able to preserve a relatively high gradient of concentrations between the outer boundary of the buffer and the granite. Consequently, after 10,000 years the concentration of chlorine in the bentonite porewater is practically identical to the Forsmark groundwater (Figure 5-6).

In Figure 5-7, selected chlorine profiles in the bentonite buffer are shown for two cases: saturation of the bentonite after 10 and 100 years. The selected profiles show that the chlorine content is lower in the case with a higher saturation time (100 years) than for shorter saturation times (10 years). Nevertheless, the difference between both cases becomes less evident at longer simulation times, meaning that regardless the time of saturation, the chlorine concentration will become equal to that of the surrounding Forsmark groundwater.

The computed results indicate that, when the advective flow rate in the fracture is high, the homogenizing effect of diffusion within the buffer is not much efficient for the earlier stages of bentonite saturation. But, after saturation of the bentonite buffer, diffusion leads to a homogeneous distribution of chlorine in the buffer (Figure 5-7).

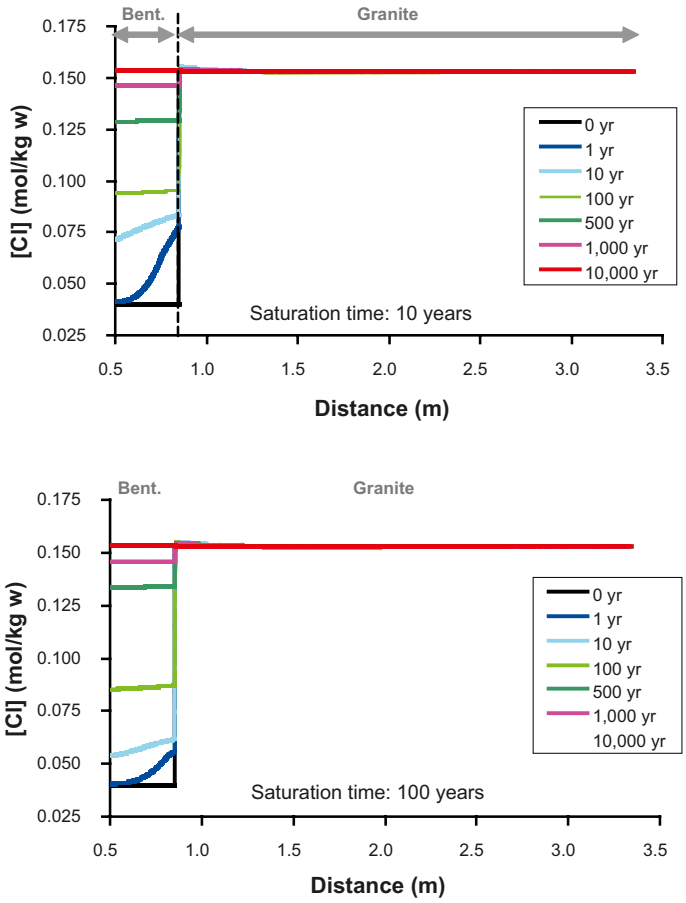

Figure 5-6. *Computed evolution of chlorine concentration for the scenario with a high advective flow in the fracture, and two cases: saturation at 10 years and at 100 years.*

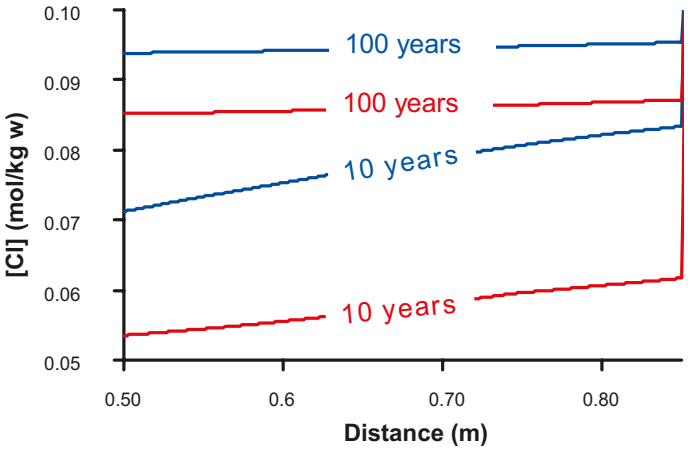

Figure 5-7. *Selected profiles of chlorine concentration in the MX-80 bentonite for the scenario with a high advective flow in the fracture. Blue lines: full water saturation after 10 years. Red lines: full water saturation after 100 years.*

5.1.3 Reactive transport of solutes and mineral reactions in the MX-80 bentonite

Ca-sulphates and aqueous sulphate concentration

Ca-sulphates are originally present in the MX-80 bentonite mineralogy. At the beginning of the thermal period, anhydrite precipitates in the bentonite pores due to the increase of temperature, except close to the outer boundary of the buffer where the granitic groundwater (which is unsaturated with respect to this mineral) flows into the buffer. The dissolution of the primary Ca-sulphate is more efficient for higher saturation velocities (10 and 100 years in Figure 5-8).

Close to the copper canister (left boundary of the modelled domain), where the higher temperatures are established, anhydrite accumulates forming a peak. The formation of this anhydrite peak was already observed in the LOT-A2 experiment /Karnland et al. 2009/ and also in the numerical models performed for this experiment /Sena et al. 2010/.

In the numerical models of the near-field, the anhydrite peak evolves with the evaporation front, i.e. the highest anhydrite peak is computed when the highest evaporation rate occurs which is around 50 years for the cases of bentonite saturation after 100, 1,000 and 2,000 years. After 50 years, the temperature close to the copper canister decreases and anhydrite is dissolved to maintain the mineral equilibrium with the bentonite porewater (Figure 5-8).

When temperatures are homogeneous within the buffer (after 500 years), anhydrite is progressively dissolved from the contact with the granite towards the canister, reaching exhaustion close to the granite and maintaining a small amount of this mineral close to the inner surface of the buffer where anhydrite had previously precipitated.

The amount of anhydrite dissolution depends on the velocity of bentonite saturation. Under a scenario of a relatively fast saturation time (10 years), at the end of the simulated period (10,000 years), only a small amount of anhydrite prevails, forming a thin ring of 2–3 cm near the copper canister. In the cases with a slower saturation time (2,000 years), more anhydrite remains around the copper canister (up to 13 cm from the copper canister as shown in Figure 5-8).

Gypsum remains unsaturated during the calculations. Only when the temperatures are lower than 30ºC (after 2,000 years of simulation), gypsum becomes oversaturated in the bentonite porewater.

When a high advective flow along the fracture is considered, anhydrite is exhausted quickly; between 600 and 1,000 years (Figure 5-9). This is a consequence of the faster transport of aqueous sulphate away from the near field.

Quartz and SiO_2(aq) aqueous concentration in the MX-80 bentonite

Quartz is also a primary mineral of the MX-80 bentonite. The primary quartz in the bentonite is preferentially dissolved close to the inner surface of the buffer (left side in Figure 5-10). In the case with a relatively fast saturation (10 years), a small amount of quartz is also dissolved during the saturation period, close to the contact with the granite. Until 10 years, the SiO_2(aq) concentration progressively increases, both in the bentonite and in the granite due to the solute supply by quartz dissolution close to the hot boundary of the system. After 10 years the aqueous SiO_2 concentration decreases due to dilution provided by the inflow of the granitic groundwater which is depleted in SiO_2(aq) compared to the initial bentonite porewater.

Solute diffusion homogenizes the SiO_2(aq) concentration in the bentonite and granite porewater and, from 100 years, quartz starts to precipitate in the "cold" part of the bentonite buffer, close to the contact with the granite (Figure 5-10).

In the previous case (saturation of the bentonite at 10 years), the increase of the SiO_2(aq) concentration in the granitic groundwater due to diffusion from the bentonite porewater to the granite is only effective after complete water saturation of the bentonite. However, in the cases with slower saturation velocities (1,000 and 2,000 years), diffusion as a mechanism of solute transport to the granitic groundwater is relevant also before bentonite saturation (Figure 5-11).

By comparing Figure 5-10 with Figure 5-11, it is possible to see that the amount of quartz dissolved and/or precipitated is not that sensitive to the velocity of bentonite water saturation. It seems that

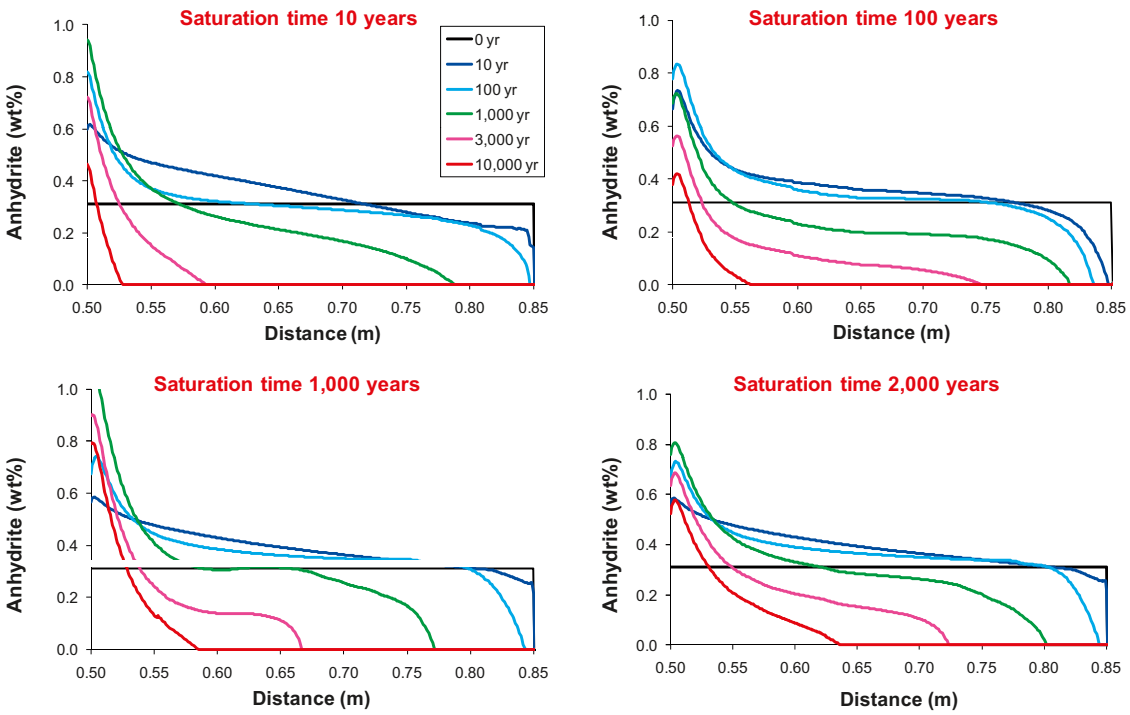

Figure 5-8. *Computed evolution of the amount of anhydrite in the MX-80 bentonite buffer for the scenario with a low advective flow rate in the fracture, and saturation of the bentonite at 10, 100, 1,000 and 2,000 years.*

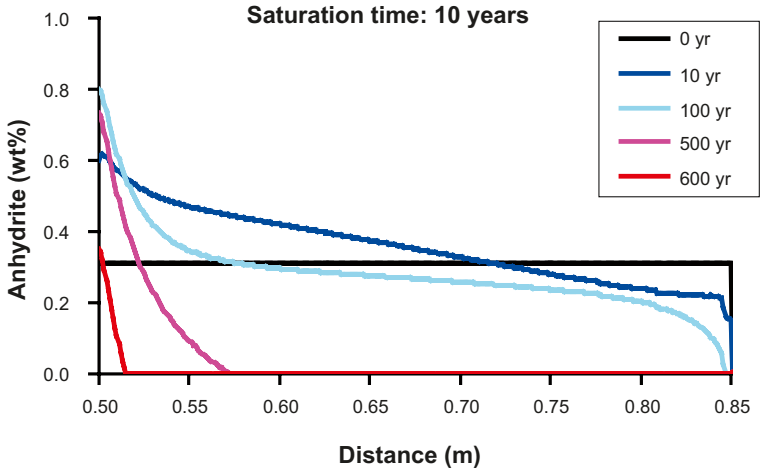

Figure 5-9. *Computed evolution of the amount of anhydrite in the MX-80 bentonite buffer, for the scenario with a high advective flow rate in the fracture, and saturation of the bentonite at 10 years.*

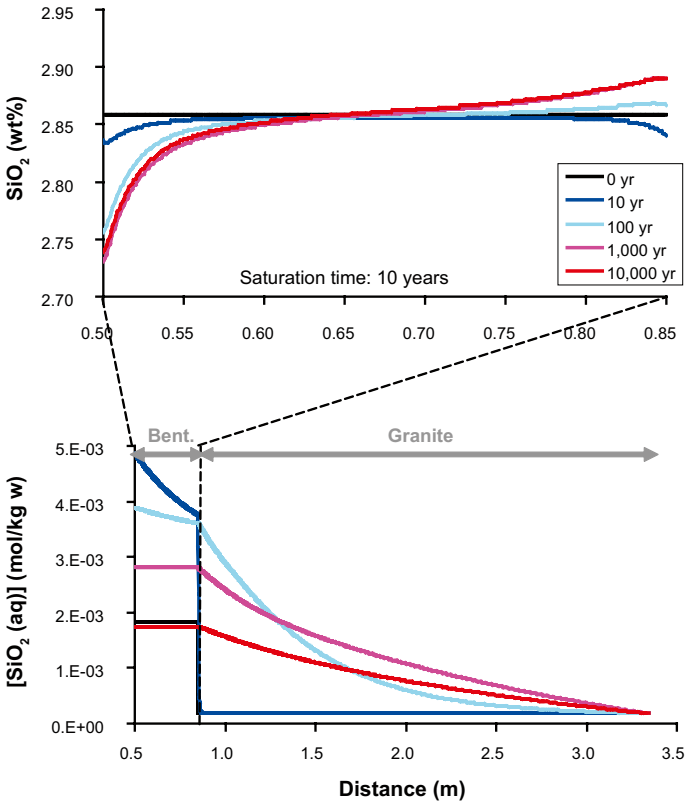

Figure 5-10. *Computed evolution of the amount of quartz in the modelled domain of MX-80 bentonite, for the scenario with a low advective flow rate in the fracture and saturation of the bentonite after 10 years.*

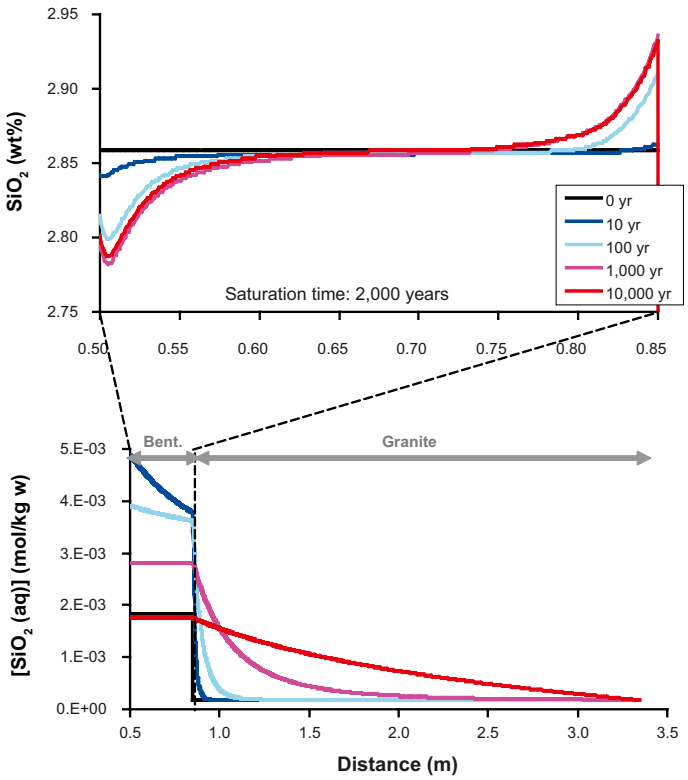

Figure 5-11. *Computed evolution of the amount of quartz in the modelled domain of MX-80 bentonite, for the scenario with a low advective flow rate in the fracture and saturation of the bentonite after 2,000 years.*

the evolution of the amount of quartz would be basically controlled by the thermal evolution of the system, which triggers the following processes:

1. Dissolution of quartz in the warm boundary of the model,
2. diffusion of the SiO_2(aq) released by quartz dissolution, from the inner boundary of the bentonite towards the granite; and,
3. precipitation of quartz in the coldest border of the bentonite.

In the case with a high flow along the fracture (Figure 5-12), the calculated evolution of the amount of quartz dissolved in the vicinity of the inner (hot) boundary of the buffer and also the evolution of the SiO_2(aq) concentration in the bentonite porewater are very similar to the previous cases (Figure 5-10 and Figure 5-11). When the advective flow in the fracture is high, the SiO_2(aq) concentration in the granitic groundwater remains constant during the calculations (as already seen for the case of chlorine). In this context, the rate of diffusion of SiO_2(aq) from the bentonite to the granite is higher than in the previous cases. In order to maintain the equilibrium with quartz, this mineral phase is dissolved in the area close to the contact with the granite where SiO_2(aq) is leaving the bentonite pores and diffusing into the surrounding granite (Figure 5-12). The diffusion of SiO_2(aq) to the granite is more efficient after complete water saturation of the bentonite pores.

Calcite equilibrium and distribution of aqueous calcium, carbonate species, and pH values

The MX-80 is depleted in carbonate minerals, and therefore, calcite is not considered a primary mineral in the conceptual model of this type of bentonite. However, if oversaturation is reached, calcite is allowed to form in the numerical calculations.

Numerical results indicate that, in general, the amount of calcite precipitated is negligible. In the hydrological scenario reproducing low flow rates along the granitic materials, calcite only precipitates in the bentonite during the first years and, exclusively, in the models with saturation times of 10

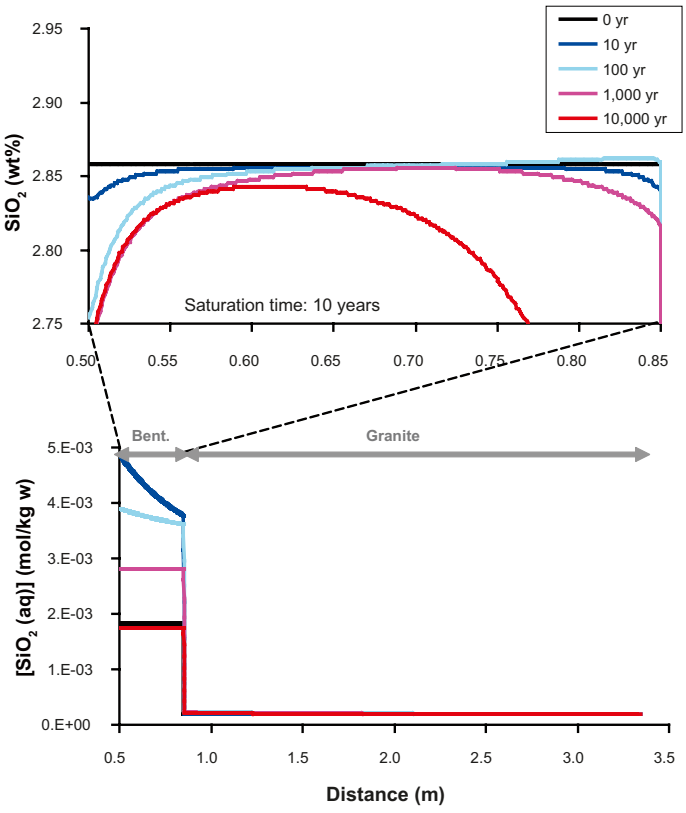

Figure 5-12. *Computed evolution of the amount of SiO_2 in the modelled domain of MX-80 bentonite for the scenario with a high advective flow rate in the fracture and saturation of the bentonite after 10 years.*

and 100 years. In any case, it is re-dissolved before 5 years, remaining unsaturated until the end of the simulation period. In the granite, calcite precipitates exclusively in the area affected by the high temperature that is emitted from the copper canister (i.e. between 0.85 and 1.5 m in Figure 5-13). However, after 3,000–5,000 years, secondary calcite is re-dissolved and exhausted (Figure 5-13). On the other hand, in the model reproducing high groundwater flow along the fracture zone, calcite preferently precipitates during the last stages of the modelization (cold period), as a consequence of the continuous supply of solutes from the granitic groundwater non affected by the presence of the buffer. In this way, the calculated Ca concentration is a key parameter controlling carbonate precipitation. In the bentonite porewater, it is basically controlled by (1) solute transport from the granite to the bentonite, (2) cation exchange reactions in the bentonite, and (3) mineral reactions (being the precipitation/dissolution of Ca-sulphate the main mineral reaction influencing calcium concentration). However, the Ca concentrations in the granitic porewater are mainly controlled by the diffusive transport of solutes. In the case with a high advective flow along the fracture, the aqueous Ca concentration remains practically constant in the granite domain close to the buffer (the dilution effect of the diffusion is negligible in front of the constant supply of solute by the advective transport along the fracture zone). In this context, Ca concentrations close to the outer boundary of the bentonite are higher than in the case with low advective flow along the fracture (Figure 5-13). The gradient of concentrations between the granitic groundwater and the bentonite porewaters is substantially different in both cases and, consequently, the amount of Ca transported by diffusion to the interstitial water of the buffer material. As a consequence, in this hydrological scenario the amount of secondary calcite precipitated close to the outer boundary of the buffer is two orders of magnitude higher than the previous one.

The computed precipitation of calcite triggers the decrease of the pH values and aqueous carbonate concentration with respect to the initial values in the granitic material (Figure 5-14). In the models considering a high advective flow rate along the fracture zone, differences with respect to the composition of the granitic groundwater are lesser than considering a low groundwater flow rate along the granitic materials. It is a consequence of the more effective supply of solutes. In consequence,

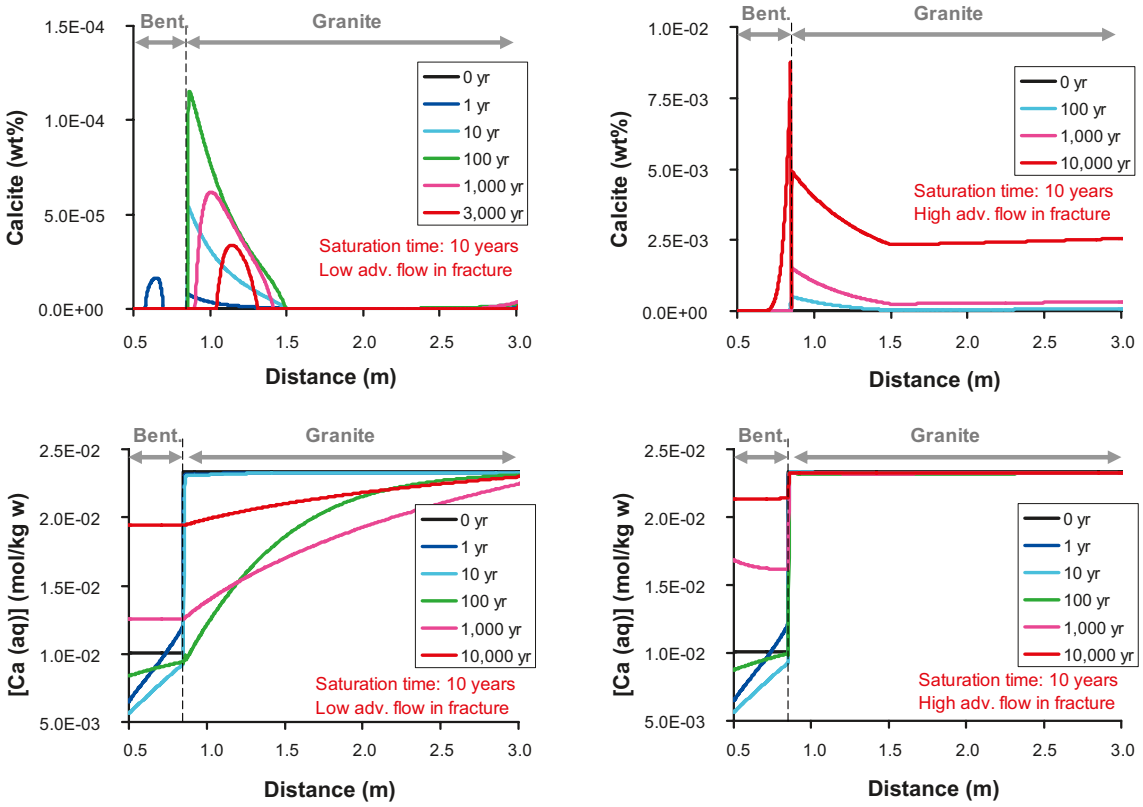

Figure 5-13. *Computed evolution of the amount of calcite and the concentration of aqueous calcium for the case where saturation of the MX-80 bentonite occurs after 10 years, and for the two scenarios of advective flow in the fracture (low and high).*

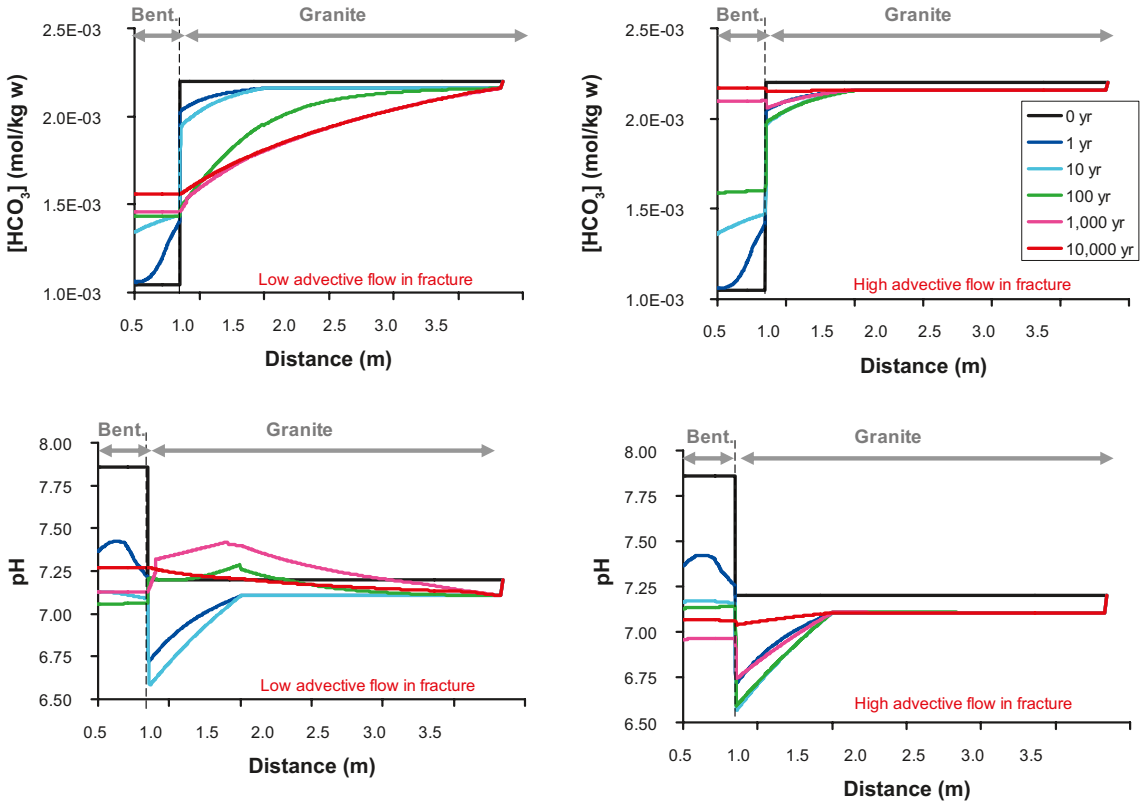

Figure 5-14. *Computed evolution of bicarbonate concentration and pH in the case with a low advective flow along the fracture and water saturation of the MX-80 bentonite at 10 years.*

the carbonate concentration and the pH values calculated at 10,000 years are similar in the bentonite porewater and in the fracture zone. With the resulting Ca concentrations, the calculated pH values and the concentration of aqueous carbonate species being controlled by calcite equilibrium.

When the imposed groundwater flow rate along the granitic materials is very low, initially, the pH values also decreases in the granitic groundwater due to calcite precipitation. Then, the calculated pH values increase due to the dissolution of the previously precipitated calcite just it is exhausted (after 3,000 years). The final pH values, as soon as the secondary calcite has been exhausted, are similar than those defined for the granitic groundwater (Figure 5-14).

The evolution of the montmorillonite exchanger composition

In general, the computed evolution of the composition montmorillonite exchanger in the bentonite indicates that the concentration of sodium decreases with time in favour of more calcium adsorbed. The concentration of potassium and magnesium also decreases in the montmorillonite exchanger. Within the same case of advective flow in the fracture, the computed evolution of the composition of the exchanger is very similar for the different scenarios of bentonite saturation.

The comparison between the cases with low and high advective flow in the fracture, for a saturation time of 10 years is shown in Figure 5-15. It is seen that for a high advective flow in the fracture, the final composition of the exchanger has suffered more profound changes than for the case with a low advective flow in the fracture. In the first case, from an initial content of 76% of NaX, the final concentration of sodium in the exchanger decreases to 41%, while in the second it decreases to 72%. The corresponding increase of the concentration of calcium leads to a final concentration of 39% of calcium in the case with a high advective flow in the fracture, and 17% when the advective flow in the fracture is low.

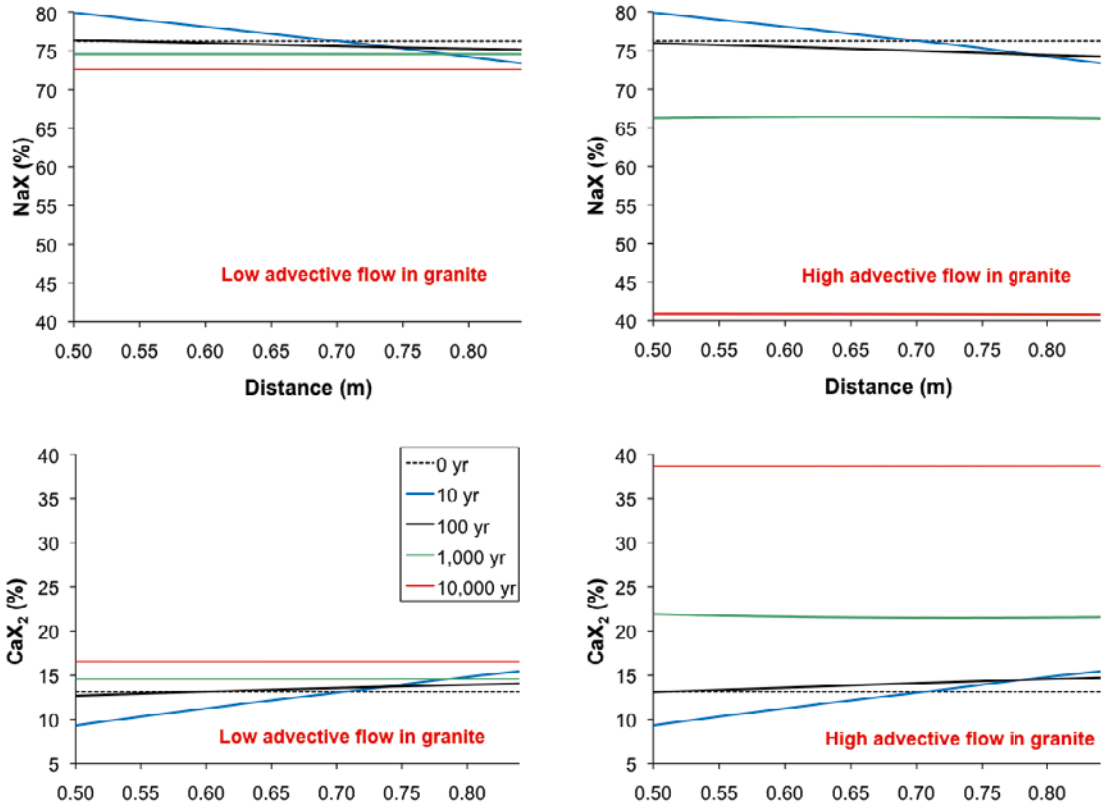

Figure 5-15. *Computed evolution of the concentration of sodium and calcium in the montmorillonite exchanger for the case where the MX-80 bentonite is fully water saturated at 10 years, and for the two scenarios of advective flow in the fracture (low and high).*

5.2 Numerical results for the Deponit CA-N bentonite

The hydrological results in the case of the Deponit CA-N bentonite are practically identical to those previously explained in the Section 5.1.3 for the MX-80 bentonite. Only the rates of the diffusive transport of solutes are different, because the initial porewater composition of the Deponit CA-N is substantially more saline (0.138 mol Cl/kg of porewater) than the MX-80 bentonite porewater (0.040 mol Cl/kg of porewater) (Table 3-4). However, it is slightly less saline (Figure 5-16) than the granitic groundwater (0.153 mol Cl/kg of porewater). In spite of these differences, the trends of the evolution of chlorine concentrations computed for both bentonite types are similar. At 10,000 years, the salinity of the Deponit CA-N bentonite porewater is around 0.146 mol Cl/kg of porewater which is substantially more saline than the concentration of the MX-80 bentonite porewater after 10,000 years (around 0.090 mol Cl/kg porewater, Figure 5-4).

The initial mineral composition of the Deponit CA-N bentonite implemented in our models is shown in Table 3-2. The main difference with respect to the case described for the MX-80 bentonite is the presence of calcite and dolomite as primary mineral phases.

As it has been previously indicated, anhydrite precipitates close to the copper canister during the period of relatively high temperatures (< 100 years), and dissolves from the outer boundary of the buffer. Its solubility is controlled by the thermal evolution of the bentonite porewater, and by the mechanism of solute transport (sulphate dilution as a consequence of the inflow of the granitic groundwater during the period of bentonite saturation, and by solute diffusion as soon as the bentonite is fully water saturated).

As it has been described in the case of the MX-80 bentonite, anhydrite is completely exhausted in the long term. The amount of secondary mineral precipitated and the time for its complete depletion are very sensitive with respect to the hydrological initial and boundary conditions implemented. If the groundwater flow is very low along the fracture in the granite, anhydrite is completely exhausted

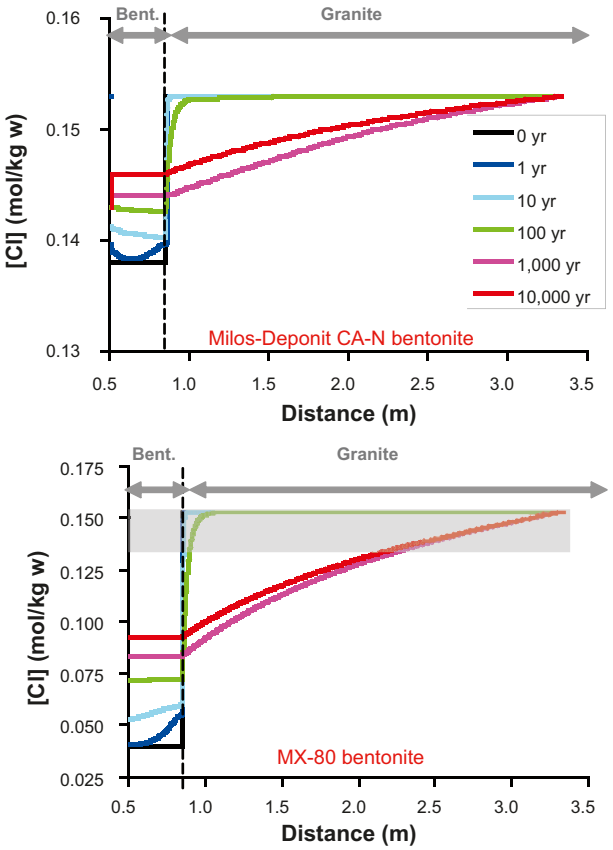

Figure 5-16. *Computed evolution of the total chlorine concentration for the scenario with a low advective flow in the fracture, for the Deponit CA-N and the MX-80 bentonites, and saturation of bentonite at 10 years. In the plot of the MX-80 bentonite, the range of the computed Cl concentrations in the case the Deponit CA-N bentonite has been emphasized in a grey square.*

after 1,000 years (Figure 5-17). The characteristic time for anhydrite depletion is slightly sensitive to the velocity of the bentonite water saturation. Considering high flow rates along the fracture zone, anhydrite is exhausted from the bentonite before 1,000 years.

The trend of the amount of quartz dissolved and/or precipitated has been explained for the MX-80 bentonite in the Section 0. It is remarkable that if high flow rates are considered along the fracture zone, quartz could be completely exhausted in the bentonite in a long term (> 10,000 years, Figure 5-17). This is the most pessimistic scenario: thermal period (increase of quartz solubility) and high advective fluid flow along the fracture zone during, at least, 10,000 years.

The primary dolomite is initially dissolved, being completely exhausted close to the outer boundary of the buffer after 1,000 years (Figure 5-18). However, in the vicinity of the copper canister, dolomite precipitates during the warming period, being re-dissolved during the cooling stage. The amount of dolomite dissolved and/or precipitated is not very sensitive to the velocity of bentonite water saturation. However, if we consider high flow rates along the fracture zone, dolomite could be exhausted in the bentonite domain before 10,000 years (Figure 5-18).

Similarly to a process of dedolomitization, secondary calcite precipitates in the Deponit CA-N bentonite (Figure 5-18). Calcite precipitation is controlled by the supply of solutes from dolomite dissolution. As a result, the aqueous Mg concentration in the bentonite porewater reaches values around 0.08 mol of Mg/kg of porewater at 10,000 years (Figure 5-19), one order of magnitude higher than that calculated in the case of the MX-80 bentonite. However, if we consider a model with a high flow rate along the fracture, the calculated Mg concentration at 10,000 years in the bentonite is around 0.022 mol of Mg/kg porewater, substantially lower than the reference case, as consequence of the higher efficiency of solute diffusion through the bentonite-granite interface.

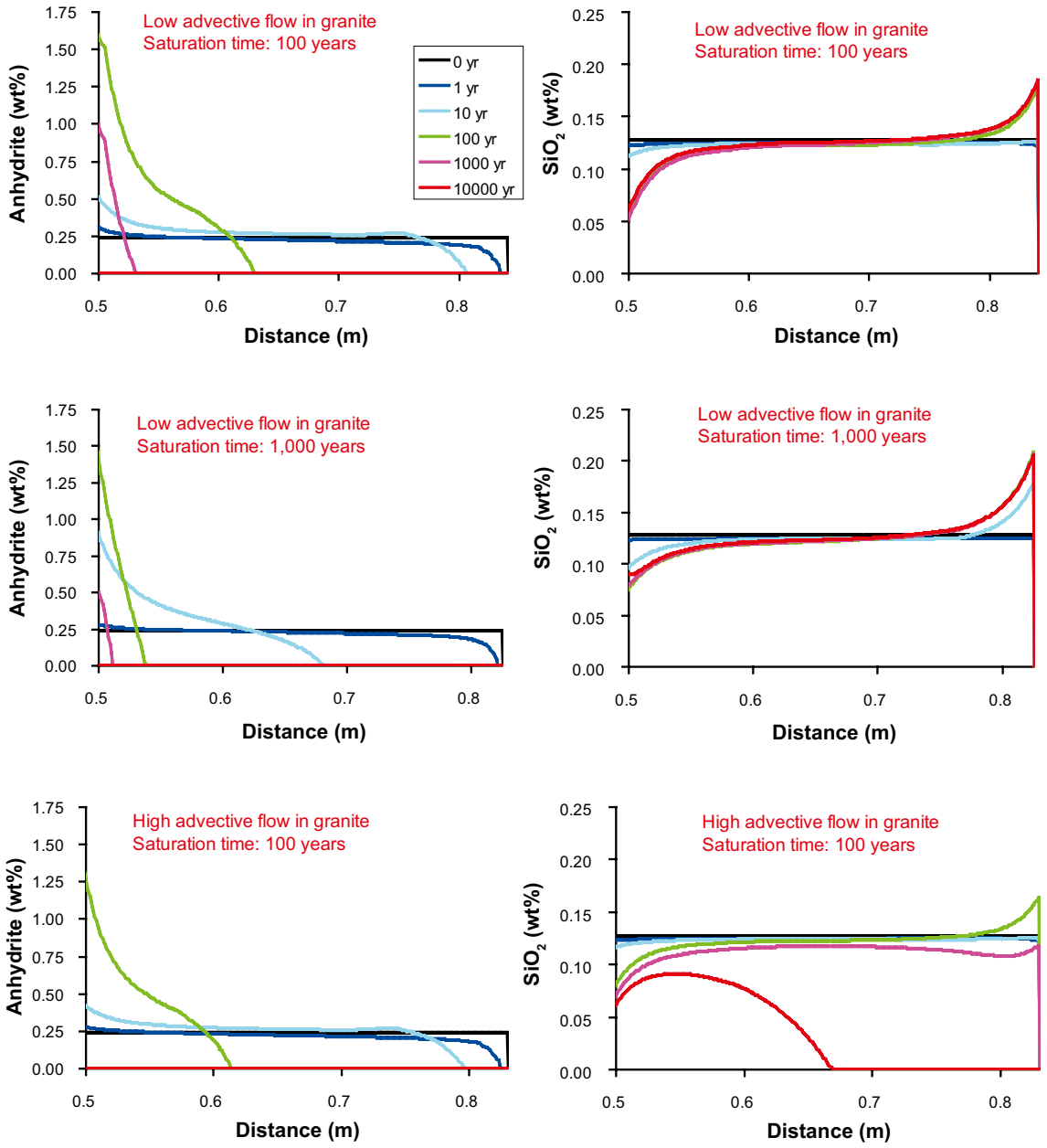

Figure 5-17. *Computed evolution of the amount of anhydrite and quartz in the Deponit CA-N bentonite, for the case where saturation of the bentonite occurs after 100 and 1,000 years, and for the scenarios of low and high advective flow in the fracture.*

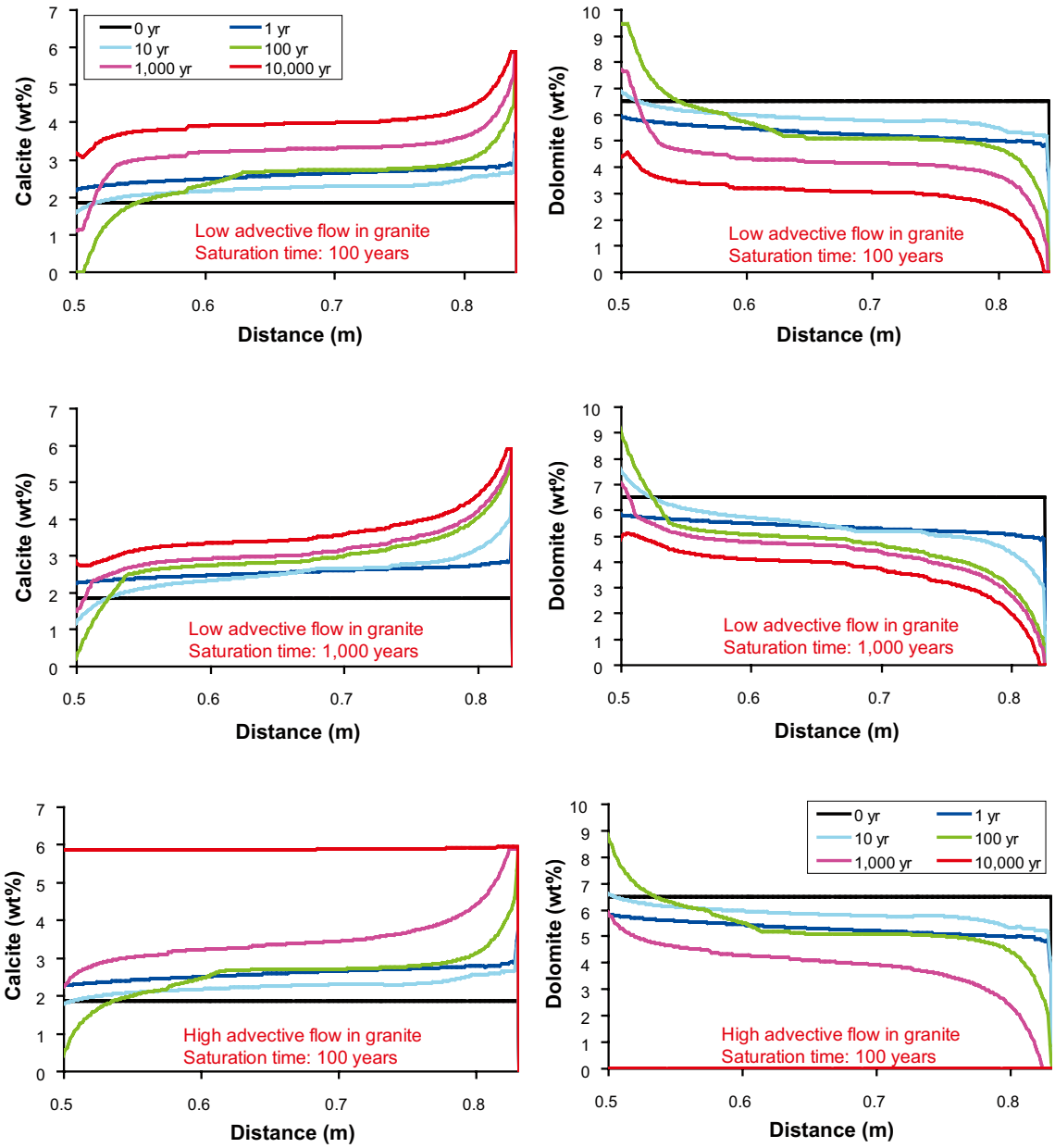

Figure 5-18. *Computed evolution of the amount of calcite and dolomite in the Deponit CA-N bentonite, for the case where saturation of the bentonite occurs after 100 and 1,000 years, and for the scenarios of low and high advective flow in the fracture.*

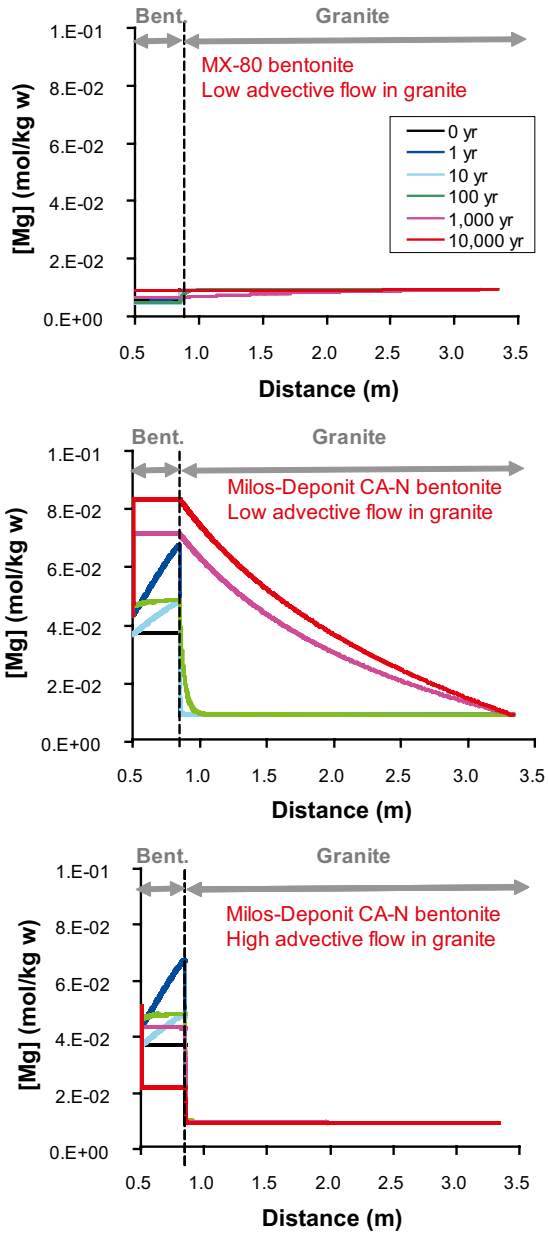

Figure 5-19. *Computed evolution of the total magnesium concentration for the scenarios with low and high advective flow rates along the fracture zone, for a time of 100 years of bentonite water saturation.*

The differences in the porewater composition of the Deponit CA-N bentonite with respect to the MX-80 bentonite are also reflected in the exchanger composition. The computed evolution of the composition of the exchanger is very similar for the different scenarios of bentonite saturation. As it was expected, calcium decreases in the exchanger with time in favour of more magnesium adsorbed (Figure 5-20). On the other hand, the concentration of potassium slightly decreases, while that of sodium increases. The comparison between the cases with low and high advective flow along the fracture, for a saturation time of 100 years is also shown in Figure 5-20 and in Figure 5-21. With high advective fluid flow along the fracture, the sodium concentration at 10,000 years in the montmorillonite exchanger increases from an initial content of 10% of NaX to a content of 35% (in contrast to 12.5% if we consider a low flow rate in the fracture). This enrichment in sodium is a consequence of the diffusive transport from the groundwater flowing along the fracture. This sodium mainly replaces magnesium, resulting in a final content of MgX_2 around 48% (in contrast to the values around of 78% of MgX_2, obtained with the models with low flow rate along the fracture). The excess of aqueous Mg in the bentonite porewater is transported by diffusion to the granitic materials, where it is efficiently transported by advection out of the modelled domain. As a consequence, the Mg concentration in the bentonite porewater decreases with respect to the cases where a low advective fluid flow is simulated along the fracture.

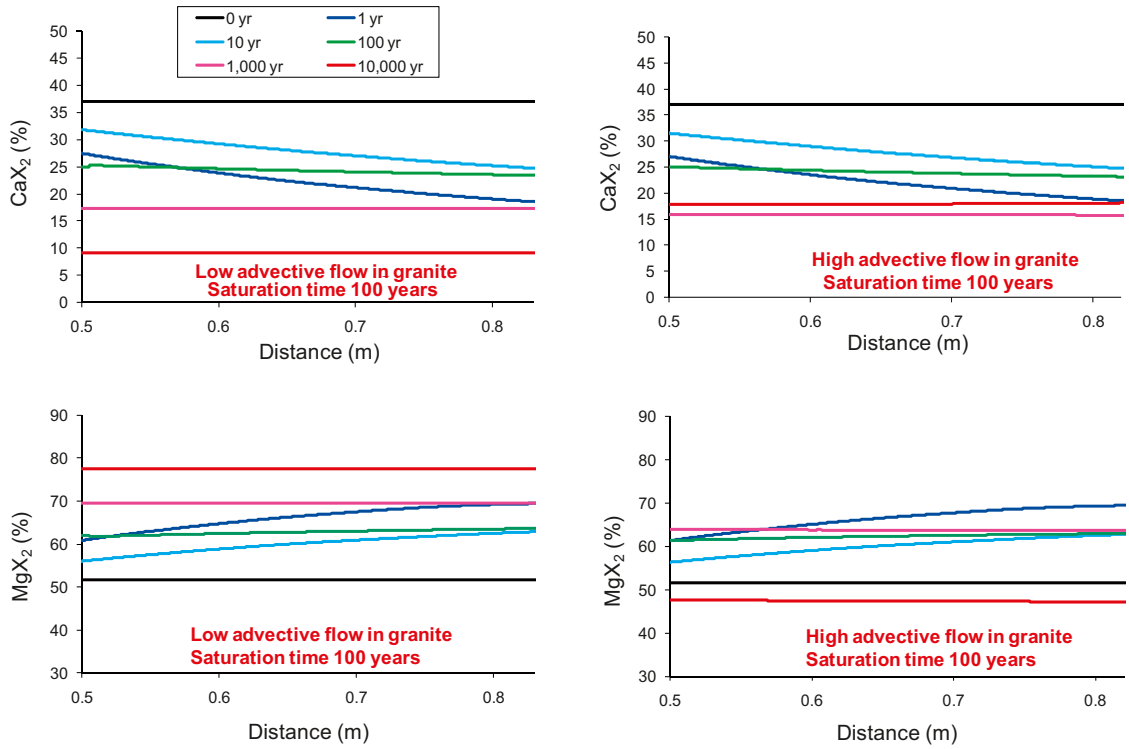

Figure 5-20. *Computed evolution of the concentration of calcium and magnesium in the montmorillonite exchanger for the case where the bentonite is fully water saturated at 100 years, and for the two scenarios of advective flow in the fracture (low and high).*

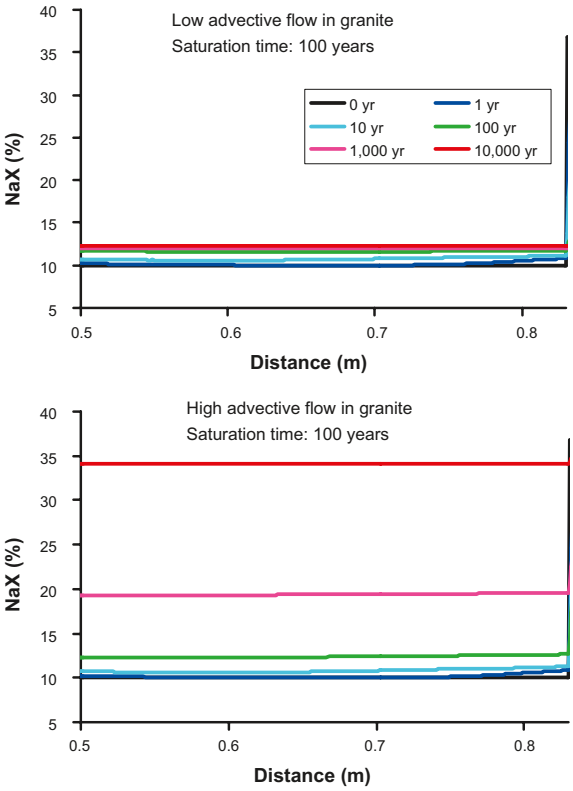

Figure 5-21. *Computed evolution of the concentration of sodium in the montmorillonite exchanger for the case where the bentonite is fully water saturated at 100 years, and for the two scenarios of advective flow in the fracture (low and high).*

5.3 Summary of the results attained for the thermal period

As a result of the numerical simulations, we can conclude that the main mechanisms controlling the mineralogical changes of the bentonite during the thermal period are related to (1) the dependence of the mineral solubilities on the evolution of the temperature in the near-field, and (2) the solute transport and mass transfer between the groundwater flowing along the fracture and the bentonite porewater.

The advection of solutes to the bentonite porewater is the main mechanism of transport during the period of bentonite saturation (before 10, 100, 1,000 and 2,000 years, depending on the hydrological model). The effect of solute diffusion between the inflowing groundwater and the bentonite porewater is negligible in the cases with a high velocity of water saturation (10 and 100 years). In the models with low velocities of saturation (1,000 and 2,000 years), the effects of the diffusion on the calculated concentrations during the period of saturation are also significant. In any case, when the bentonite buffer becomes fully saturated, diffusion is the exclusive mechanism of solute transport. Consequently, for each hydrological scenario, the evolution of the gradients of concentrations is the key factor controlling the development of the geochemical processes.

The evolution of the concentrations obtained for the bentonite porewater is a result of mixing with the local groundwater during the period of bentonite water saturation, whereas thereafter, diffusion of solutes is the dominant mechanism. Simultaneously, mineral reactions (anhydrite and carbonate dissolution and/or precipitation) and cation exchange reactions are the key mechanisms controlling the long term geochemical evolution of the buffer and its porewater. As it has been previously indicated, the evolution of the compositions of the bentonite porewater is strongly dependant on the hydrogeochemical evolution of the surrounding groundwater.

The distribution of the concentration of solutes in the granitic groundwater is a consequence of the ratio between (a) the diffusion rate through the granite-bentonite interface, and (b) the fluid flow rate along the fracture. In this way, the results obtained considering the two hydrological regimes of the groundwater flow rates along the hypothetical fracture are substantially different.

- With low flow rates along the fracture, the final composition of the bentonite porewater is significantly different from the Forsmark groundwater. The composition of the buffer porewater is able to modify, by diffusion, the composition of the surrounding granitic groundwater. In this way, the gradient of concentrations on the bentonite-granite interface can be only maintained during the period of bentonite water saturation. After bentonite saturation, diffusion scavenges solutes from granitic groundwater, decreasing the rate of solute transport through the interface. This hydrodynamic regime is strictly applicable to the case of high velocities in bentonite water saturation (10 and 100 years). However, in the case of low velocities of bentonite saturation (1,000 and 2,000 years), diffusion is effective diluting the gradients of concentrations even before full water saturation of the bentonite.
- With high flow rates along the fracture, the groundwater composition is practically constant during the modelled period, maintaining the gradients of concentrations and the rates of solutes transport by diffusion. Consequently, the final composition of the bentonite porewater is similar to the composition of the Forsmark groundwater.

The thermal evolution in the buffer modifies mineral solubilities (Ca-sulphates, carbonates and silica). The silica precipitation and/or dissolution in the bentonite is basically controlled by the changes of solubilities associated to the thermal evolution of the system, modifying slightly the mineralogical composition of the bentonite. Quartz dissolution is only significant when a continuous high flow rate is imposed along the fracture. In this case, quartz could be exhausted in the long term. However, the main processes simulated here that are able to modify the mineralogical composition of the bentonite are (1) precipitation of secondary Ca-sulphate during the warming period, (2) dissolution of the primary and the secondary Ca-sulphate during the cooling period, and (3) dolomite dissolution and calcite precipitation in the case of the Deponit CA-N bentonite.

The efficiency of the reactions of Ca-sulphate dissolution and/or precipitation is strongly sensitive with respect to the hydrological scenario considered in the hypothetical fracture. When high flow rates are imposed along the fracture zone, Ca-sulphates are exhausted from the bentonite in hundreds of years. However, when low flow rates are implemented in the granitic materials, Ca-sulphates are almost exhausted after 10,000 years.

The stability of the carbonate phases is the main geochemical difference between the two types of bentonite simulated.

- In the case of the MX-80 bentonite (without primary carbonate minerals), the precipitation of secondary calcite within the buffer porosity is practically negligible. In any case, it is re-dissolved in the long term. The precipitation of secondary carbonates in the granitic materials surrounding the buffer is related to the decrease of solubility during the thermal period. However, during the cooling period, it is also re-dissolved. Only when a high flow rate along the fracture is considered, carbonate precipitation is slightly significant. In this case, the solute diffusion to the bentonite porewater triggers the precipitation of a small amount of carbonate minerals within the buffer, mainly close to the outer boundary of the buffer.
- In the case of the Deponit CA-N bentonite (with calcite and dolomite as primary mineral phases), the primary dolomite is depleted at the outer boundary of the buffer after 1,000 years. Secondary dolomite precipitates during the warming period, preferentially close to the copper canister, being re-dissolved during the cooling stages. It could be completely exhausted in a scenario of high fluid flow along the fracture before 10,000 years. As a consequence of the increase of calcite saturation when dolomite dissolves, secondary calcite precipitates replacing dolomite.

Concluding, the mechanisms of solute transport (advection and diffusion), the mixing processes and the thermal evolution of the buffer will control (1) the mineralogical changes of the bentonite, and (2) the evolution of the montmorillonite composition. As soon as the bentonite becomes (1) fully water saturated and (2) with temperatures similar to the surrounding granite, the diffusive transport of solutes will homogenize, in the long term, the porewater and the groundwater composition.
As a result of all these processes, anhydrite, quartz and dolomite will be depleted in the bentonite (depending on the hydrological regime along the fracture zone), precipitating calcite which may fill the fracture in the granitic material, and in the Deponit CA-N bentonite.

6 Numerical results for the water-saturated period

As previously mentioned, the numerical simulations performed for the water-saturated period, using the code PHAST, comprise two cases; Case I where a hypothetical fracture of the granitic host rock contacts directly with the bentonite buffer in a deposition hole, and Case II where a hypothetical fracture of the host rock contacts the backfilled tunnel. Within each case, two types of bentonite buffer were considered: the MX-80 bentonite and the Deponit CA-N bentonite, so that each case comprises two reference cases, one for each bentonite type.

Numerical results for the two cases under study indicate that none of the three iron phases considered, pyrite, ferrihydrite and siderite, dissolve or precipitate. Pyrite is the primary iron phase considered both in the bentonite and the backfill. Computed results do not predict pyrite dissolution or precipitation during the simulation period. In addition, the secondary iron phases allowed to precipitate which are ferrihydrite and siderite do not reach oversaturation, and therefore, their precipitation in the modelled domain is not computed. For this reason, the discussion of the numerical results is focused on the following parameters:

- pH,
- amount of calcite, gypsum, dolomite,
- concentration of calcium in the aqueous phase and in the montmorillonite interlayer.

6.1 Case I

6.1.1 MX-80 bentonite buffer

In the case where the bentonite buffer is composed of MX-80 bentonite, the results computed for Case I show that the continuous flow of Forsmark groundwater in the near-field leads to almost no change of the pH of the bentonite, from 7.19 to 7.18 (Figure 6-1). This is mainly due to the fact that calcite is predicted to precipitate in the bentonite (Figure 6-2) buffering the pH of the system, due to diffusion of both calcium and carbonate, and also to gypsum dissolution. Gypsum dissolution in the buffer is mainly caused by the out-diffusion of sulphate. After the end of the simulation period, gypsum is already exhausted in the bentonite buffer (Figure 6-3).

The computed results lead to a progressive enrichment of the montmorillonite interlayer in calcium (Figure 6-4). Gypsum dissolution (Figure 6-3) releases calcium into solution which, in turn, favours the enrichment of the montmorillonite interlayer in this cation.

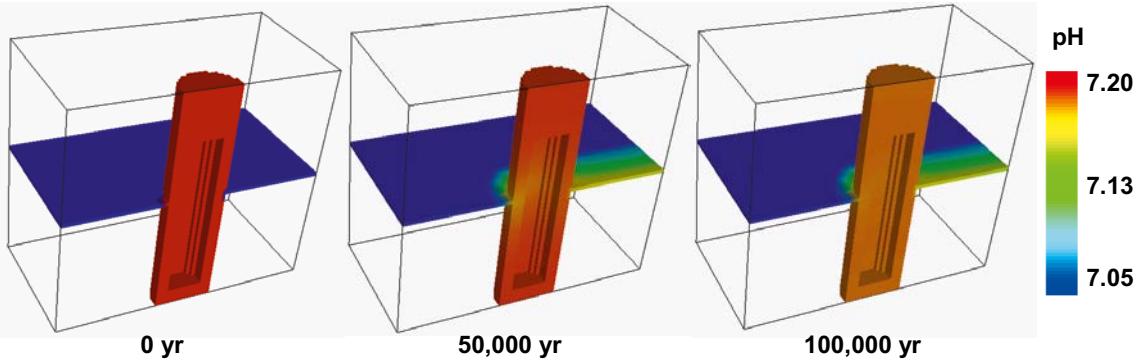

Figure 6-1. *Computed evolution of pH in the modelled domain of Reference Case I, MX-80 bentonite. Initial groundwater compositions are listed in Table 4-7.*

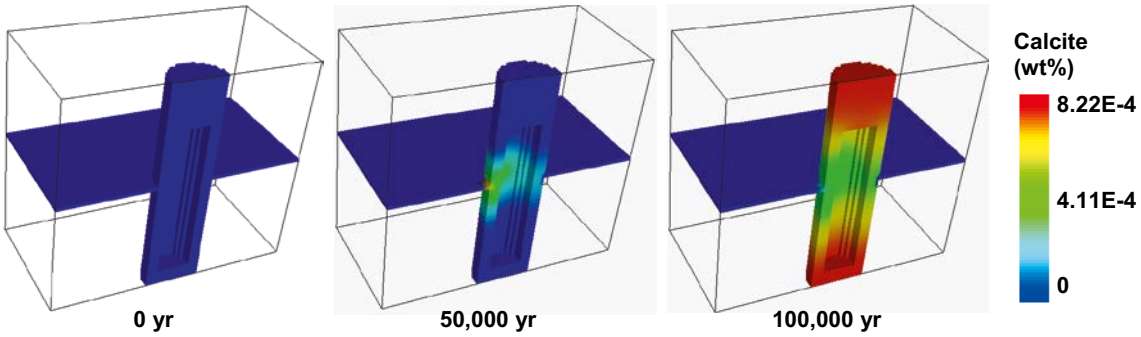

Figure 6-2. *Computed evolution of calcite content in the modelled domain of Reference Case I, MX-80 bentonite (initial contents are listed in Table 3-2 and Table 4-3).*

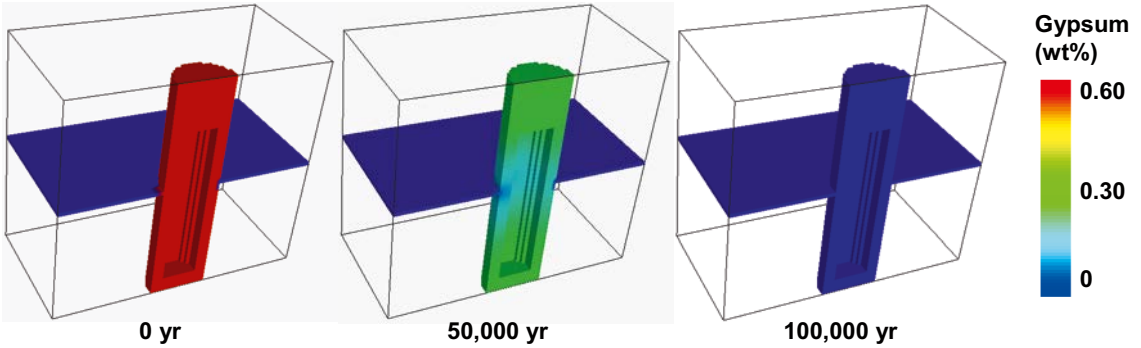

Figure 6-3. *Computed evolution of gypsum content in the modelled domain of Reference Case I, MX-80 bentonite (initial contents are listed in Table 3-2 and Table 4-3).*

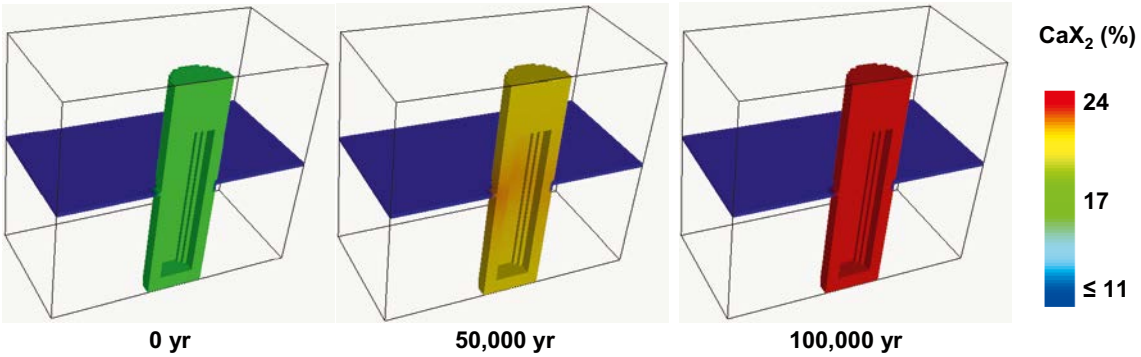

Figure 6-4. *Computed evolution of calcium in the montmorillonite interlayer in the modelled domain of Reference Case I, MX-80 bentonite.*

The numerical results attained in /Arcos et al. 2006, 2008/ are relatively similar to the ones attained here. The main difference is that in /Arcos et al. 2006, 2008/, the geochemical reactions computed within the buffer are predicted to undergo faster than in the present work. This is mainly due to the fact that /Arcos et al. 2006, 2008/ have considered a higher flow rate through the fracture ($5.44 \cdot 10^{-3}$ m^3/yr) than the flow rate considered here for the reference case (10^{-3} m^3/yr).

6.1.2 Sensitivity analysis, Case I, MX-80 bentonite

A sensitivity analysis on the flow rate of the groundwater that flows through the hypothetical fracture of Case I has been performed. As previously mentioned in Section 4.2.6, besides the "Reference Case" flow rate (10^{-3} m^3/yr), three additional flow rates have been considered (a lower flow rate of

10^{-5} m^3/yr and two higher flow rates of 0.1 and 10 m^3/yr). The location of the observation point for the analysis of computed results of all the sensitivity cases developed for Case I is shown in Figure 6-5.

Computed results show that higher flow rates lead to lower pH values in the MX-80 bentonite (Figure 6-6). This means that for higher flow rates a higher amount of calcite is precipitated (Figure 6-7) which in turn leads to a more pronounced pH decrease. The case with a flow rate of 10^{-5} m^3/yr leads to apparently negligible changes of pH, while the two cases with the highest flow rates lead to a small decrease of pH from 7.19 to 7.05.

Computed results for calcite content show that when the flow rates are higher, a higher amount of calcite is predicted to precipitate in the MX-80 bentonite buffer (Figure 6-7). The two cases with a higher flow rate lead to a remarkable precipitation of calcite in the MX-80 bentonite. In the case with a groundwater flow rate of 10^{-5} m^3/yr, a relatively small and temporary precipitation of calcite is predicted, while for the reference case (flow rate of 10^{-3} m^3/yr) calcite precipitation occurs between 50,000 and 75,000 years, after which calcite begins to dissolve. The change of tendency, from calcite precipitation to calcite dissolution computed for the case with a flow rate of 10^{-3} m^3/yr, is due to the fact the gypsum is exhausted (Figure 6-8).

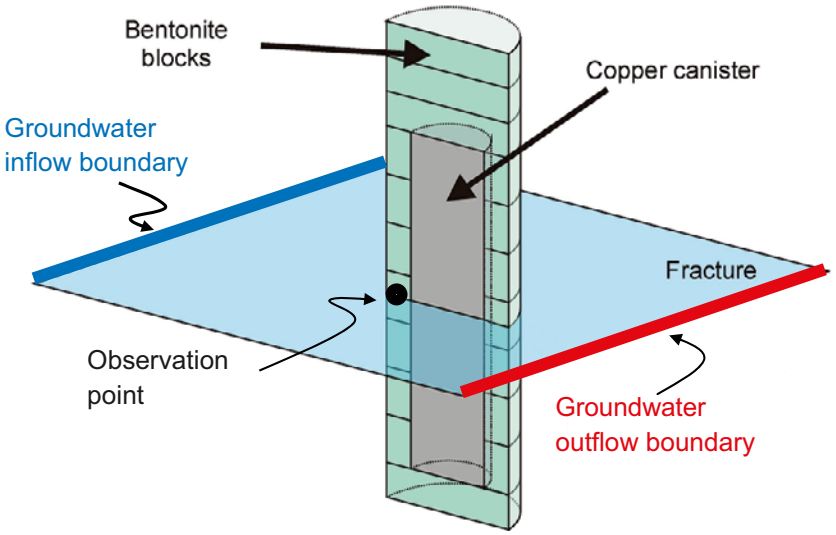

Figure 6-5. *Location of the observation point where the computed time evolution of selected chemical parameters has been analysed for the sensitivity cases considered in Case I. The coordinates of this point are: X= 4.508 m; Y= 0.116 m; Z= 6.480 m.*

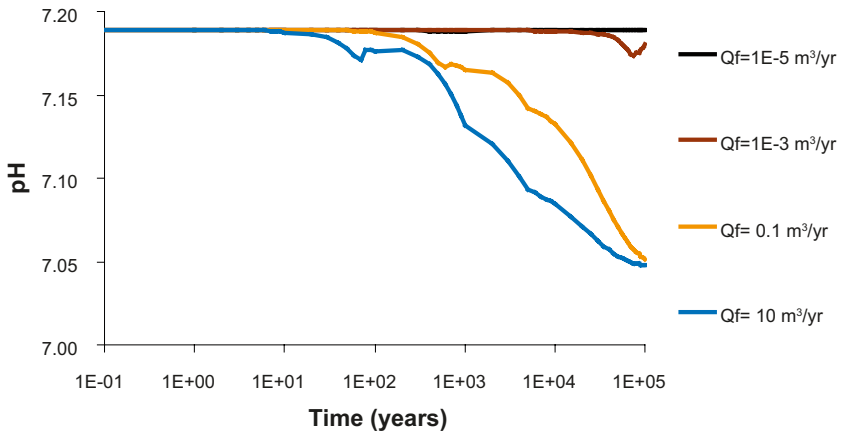

Figure 6-6. *Computed time evolution of pH in observation point located in the bentonite (see Figure 6-5), for the four flow rates analysed in Case I, MX-80 bentonite (Table 4-8). Initial groundwater compositions are listed in Table 4-7.*

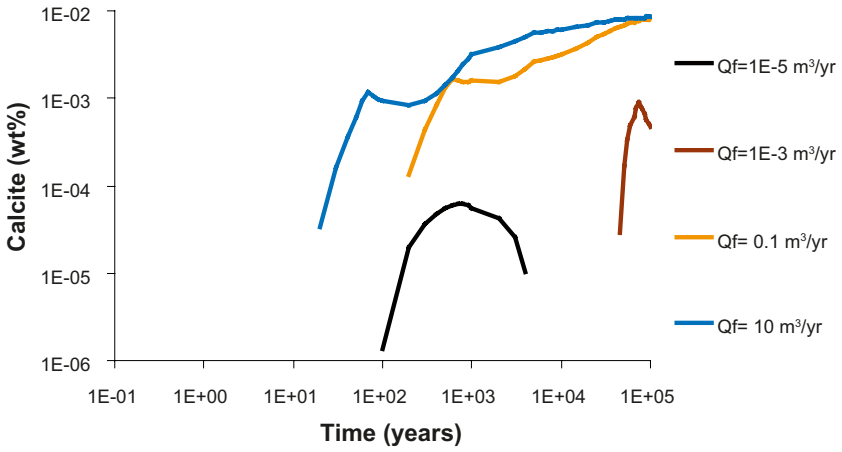

Figure 6-7. *Computed time evolution of calcite content in the observation point located in the bentonite (see Figure 6-5) for the four flow rates analysed in Case I, MX-80 bentonite (Table 4-8). Initial contents are listed in Table 3-2.*

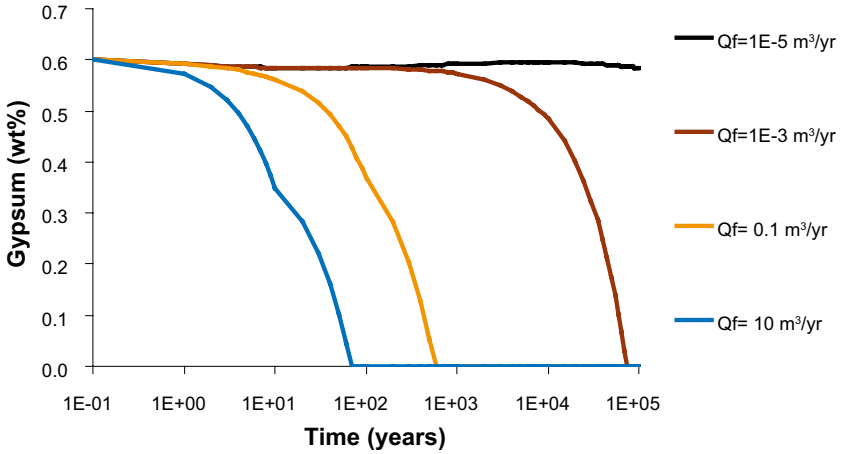

Figure 6-8. *Computed time evolution of gypsum content in the observation point located in the bentonite (see Figure 6-5) for the four flow rates analysed in Case I, MX-80 bentonite (Table 4-8). Initial contents are listed in Table 3-2.*

If the flow rate in the fracture is higher than 10^{-3} m³/yr, gypsum is computed to be exhausted within the first 500 years. When the flow rate in the fracture is 10^{-5} m³/yr, the computed evolution of gypsum content shows a very slow dissolution of gypsum. Finally, in the reference case (10^{-3} m³/yr), gypsum is dissolved until its exhaustion at 75,000 years (Figure 6-8).

Computed time evolution of aqueous calcium concentration in the MX-80 bentonite buffer shows that higher groundwater flow rates lead to a higher concentration of aqueous calcium at the end of the simulation (Figure 6-9). Although calcite precipitation and the enrichment of the montmorillonite interlayer in calcium (Figure 6-10) consume aqueous calcium, gypsum dissolution is able to speed-up the increase of aqueous calcium concentration.

As previously mentioned, computed dissolution of gypsum leads to an increase of the concentration of aqueous calcium which in turn triggers the increase of the concentration of calcium in the montmorillonite interlayer. When the groundwater flow rate is higher, gypsum is exhausted earlier which leads to a faster enrichment of the montmorillonite interlayer in calcium (Figure 6-10).

In addition to the sensitivity cases developed for the groundwater flow rate, sensitivity cases accounting for the chemical composition of the groundwater flowing through the fracture have also been developed (Table 4-10). As previously seen, when the flow rate is lower than the reference case, the geochemical changes computed for the MX-80 bentonite buffer are very small. In addition,

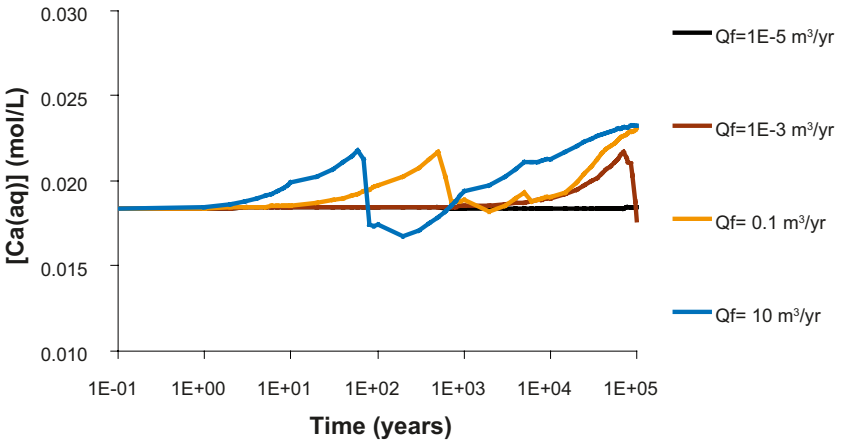

Figure 6-9. *Computed time evolution of aqueous calcium concentration in the observation point located in the bentonite (see Figure 6-5) for the four flow rates analysed in Case I, MX-80 bentonite (Table 4-8). Initial groundwater compositions are listed in Table 4-7.*

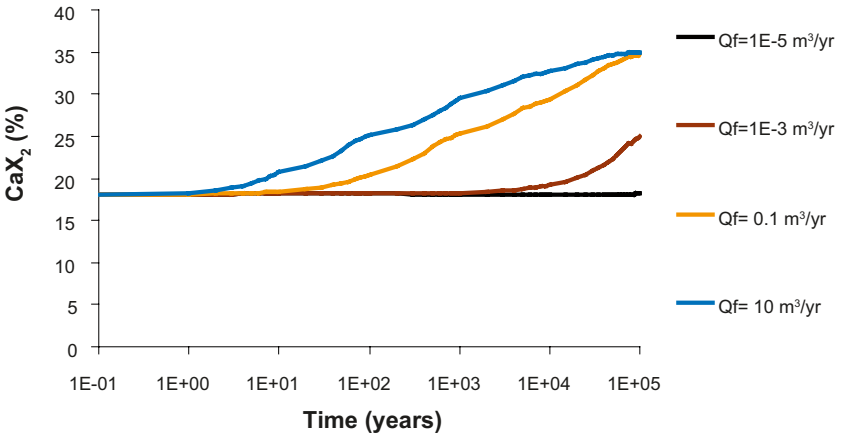

Figure 6-10. *Computed time evolution of calcium content in the exchanger of montmorillonite in the observation point located in the bentonite (see Figure 6-5) for the four flow rates analysed in Case I, MX-80 bentonite (Table 4-8).*

for higher flow rates it is seen that the computed geochemical changes are visibly more pronounced than for the reference case. In this context, the sensitivity analysis developed for the chemical composition of the groundwater flowing through the fracture has been performed for two flow rates: 10^{-3} and 10^{-1} m^3/yr.

The sensitivity analysis on the chemical composition of the inflowing water, performed for the flow rate of 10^{-3} m^3/yr, shows that when the concentration of aqueous carbonate of the inflowing groundwater is 10^{-2} mol/L ($2.2 \cdot 10^{-3}$ mol/L in the reference case), computed pH decreases from 7.19 to 6.63 (Figure 6-11). The computed pH decrease is mostly due to the fact that a higher amount of calcite is predicted to precipitate in this case (Figure 6-13).

When the pH of the inflowing groundwater is 10, computed pH for porewater increases from 7.2 to 7.3, which reflects a relatively efficient pH buffering capacity of the MX-80 bentonite due to calcite precipitation (Figure 6-13).

When the Ca/Na is 10, computed pH evolution shows an initial and fast decrease to 7.05 pH units which is followed by a very slow increasing tendency towards the end of the simulation period. This is mainly due to the fact that calcite is predicted to precipitate at the beginning of the simulation period, and then, calcite progressively dissolves (Figure 6-13).

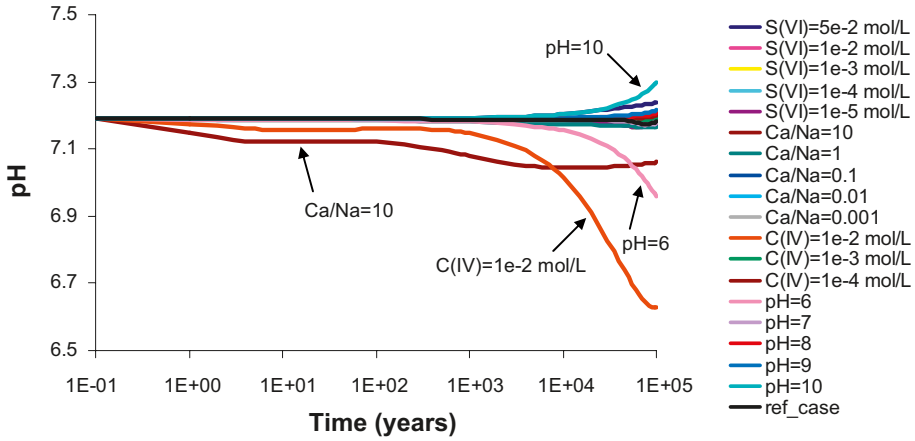

Figure 6-11. *Computed time evolution of pH in the observation point located in the bentonite (see Figure 6-5) for the nineteen inflow water compositions analysed in Case I (Table 4-9), flow rate 10^{-3} m^3/yr, MX-80 bentonite. Initial groundwater compositions are listed in Table 4-7.*

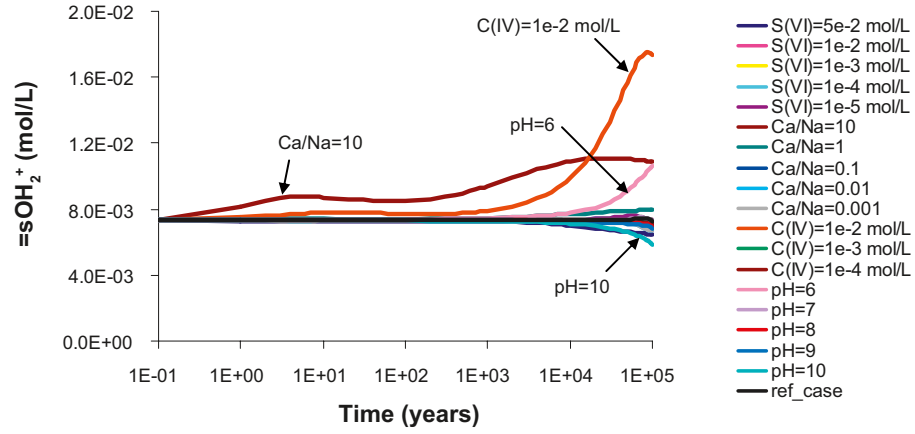

Figure 6-12. *Computed time evolution of the protonated surface site of montmorillonite ($=sOH_2^+$) in the observation point located in the bentonite (see Figure 6-5) for the nineteen inflow water compositions analysed in Case I (Table 4-9), flow rate 10^{-3} m^3/yr, MX-80 bentonite.*

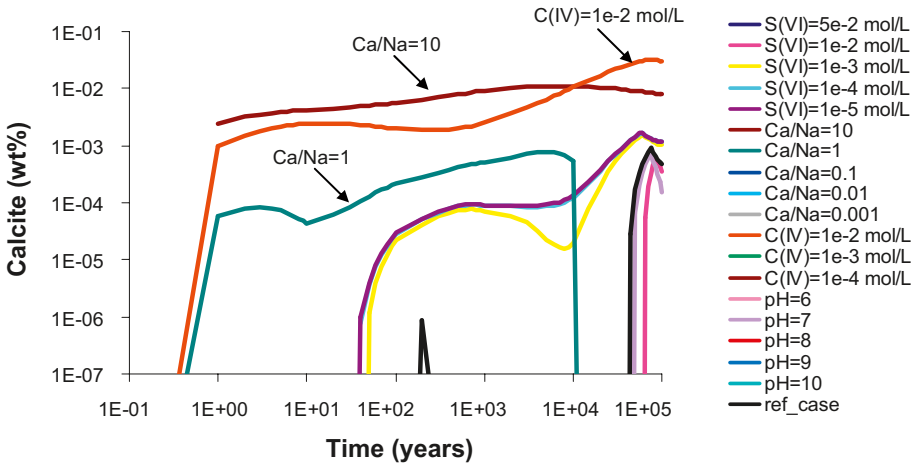

Figure 6-13. *Computed time evolution of calcite content in the observation point located in the bentonite (see Figure 6-5) for the nineteen inflow water compositions analysed in Case I (Table 4-9), flow rate 10^{-3} m^3/yr, MX-80 bentonite. Initial contents are listed in Table 3-2.*

In the case where the inflowing water has a pH of 6, the pH of the bentonite buffer decreases from 7.2 to 6.9. Since the MX-80 is depleted in carbonate minerals, the decrease of pH induced by the inflowing groundwater lacks the buffering effect that calcite dissolution could provide which is reflected on the protonation of the montmorillonite sites (Figure 6-12).

Computed results for the evolution of the calcite amount in the MX-80 bentonite buffer show that most of the cases analysed for the flow rate of 10^{-3} m^3/yr lead to results which are relatively similar to the ones attained in the reference case (Figure 6-13). Exceptions are made for the cases where the aqueous carbonate concentration of the inflowing water is 10^{-2} mol/L, when the Ca/Na is 10 and when the aqueous sulphate concentration is lower than 10^{-3} mol/L. When the aqueous carbonate concentration of the inflowing water is 10^{-2} mol/L computed calcite content reaches a maximum of $3.2 \cdot 10^{-2}$ wt% between 70,000 and 90,000 years, after which calcite starts to dissolve. In this case, the maximum of calcite precipitated occurs after the exhaustion of gypsum (Figure 6-14), which is the main contributor of aqueous calcium that is needed for calcite precipitation. In the cases with a Ca/Na of 10 and 1, the excess of calcium in the system triggers the precipitation of a more important amount of calcite. Finally, in the cases with a lower concentration of aqueous calcium, gypsum dissolution provides the calcium needed for calcite precipitation.

When the Ca/Na of the inflowing water is 10 it means that there is ten times more aqueous calcium than sodium in the inflowing water. In this case, computed results show an initial and relatively fast precipitation of calcite (Figure 6-13) and gypsum (Figure 6-14). Afterwards, calcite progressively dissolves while the gypsum content increases to near 1 wt% (Figure 6-14).

Computed time evolution of gypsum amount in the MX-80 bentonite buffer shows a wide range of results for the nineteen sensitivity cases developed here (Figure 6-14). As in the reference case, in all the analysed cases except three, gypsum is predicted to dissolve until its exhaustion. In one of the three exceptional cases, gypsum also dissolves, but at such a slow trend that within the simulated time length gypsum exhaustion is not reached. This is the case where the Ca/Na of the inflowing water is 1. In this case, there is an excess of calcium with respect to sodium in the inflowing water, which disturbs gypsum equilibrium by inducing its dissolution in favour of calcite precipitation. Gypsum dissolution becomes faster at the end of the simulation, which coincides with the fast dissolution of calcite (see case Ca/Na= 1 in Figure 6-13). This is mainly due to the fact that the excess calcium provided by the inflowing water is being preferentially retained in the montmorillonite exchanger (Figure 6-16).

The other two exceptional cases where gypsum is not exhausted, gypsum is predicted to precipitate. In the case where the Ca/Na is 10, gypsum precipitates at a relatively slow rate until 500 years, after which the gypsum amount rapidly reaches a more or less stable value around 1 wt%. In the case where the concentration of aqueous sulphate is $5 \cdot 10^{-2}$ mol/L, gypsum is predicted to precipitate throughout the whole simulation period.

Among the cases where gypsum exhaustion is reached, the cases:

- C(IV)= 10^{-2} mol/L,
- S(VI)= 10^{-3} mol/L, S(VI)= 10^{-4} mol/L,
- Ca/Na= 0.1, Ca/Na= 0.01, Ca/Na= 0.001.

lead to a faster exhaustion of gypsum than the reference case (Figure 6-14).

Computed evolution of the concentration of aqueous calcium reflects the precipitation/dissolution reactions of calcite and gypsum which were previously described. In the case where Ca/Na is 10, a remarkable increase of aqueous calcium is computed (Figure 6-15). This is mainly due to the high concentration of aqueous calcium (1 mol/L) in the inflowing water. When the Ca/Na is 1, predicted aqueous calcium concentration also shows a visible increase.

If the aqueous sulphate concentration of the inflowing water is $5 \cdot 10^{-2}$ mol/L, computed aqueous calcium concentration shows a progressive decrease, which is mainly due to the continuous precipitation of gypsum (see Figure 6-14). The remaining sensitivity cases show a relatively slow increase of aqueous calcium concentration in the MX-80 bentonite, and after 60,000 years of simulation, computed evolution of the concentration of aqueous calcium decreases for most of the cases,

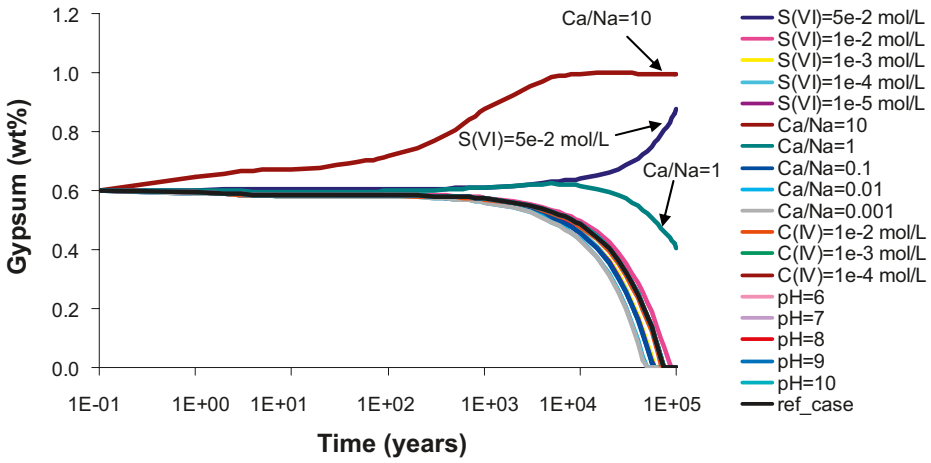

Figure 6-14. *Computed time evolution of gypsum content in the observation point located in the bentonite (see Figure 6-5) for the nineteen inflow water compositions analysed in Case I (Table 4-9), flow rate 10^{-3} m^3/yr, MX-80 bentonite. Initial contents are listed in Table 3-2.*

including the reference case. The final decrease computed for the concentration of aqueous calcium in the MX-80 bentonite buffer is related to the fact that gypsum is already exhausted (Figure 6-14) but calcite is still precipitating (Figure 6-13).

All the analysed cases lead to an enrichment of the montmorillonite interlayer in calcium. The highest content of calcium in the montmorillonite interlayer is computed in the case where Ca/Na is 10. This case leads to the highest excess of calcium in the MX-80 bentonite buffer, which is subsequently partitioned through all the Ca-containing phases: calcite (Figure 6-13), gypsum (Figure 6-14), aqueous phase (Figure 6-15) and the exchanger (Figure 6-16). Computed evolution of the concentration of the other cations in the montmorillonite interlayer indicates that the concentration of sodium and potassium decreases along the simulated period, while the concentration of magnesium slightly increases. The case with Ca/Na of 1 has a similar evolution to the previous one, although the changes in the system are not as relevant and it reaches a lower occupancy of Ca in the exchanger.

When the flow rate of the water flowing through the fracture is two orders of magnitude higher (10^{-1} m^3/yr) than in the previous cases (10^{-3} m^3/yr), the geochemical reactions that occur in the MX-80 bentonite buffer lead to more pronounced modifications of the geochemistry of the MX-80 bentonite (Figure 6-17 to Figure 6-21).

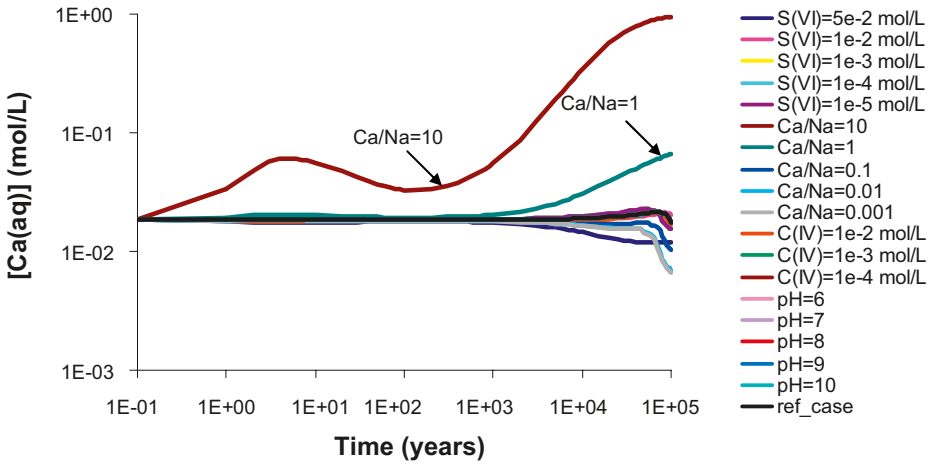

Figure 6-15. *Computed time evolution of aqueous calcium concentration in the observation point located in the bentonite (Figure 6-5) for the nineteen inflow water compositions analysed in Case I (Table 4-9),flow rate 10^{-3} m^3/yr, MX-80 bentonite. Initial groundwater compositions are listed in Table 4-7.*

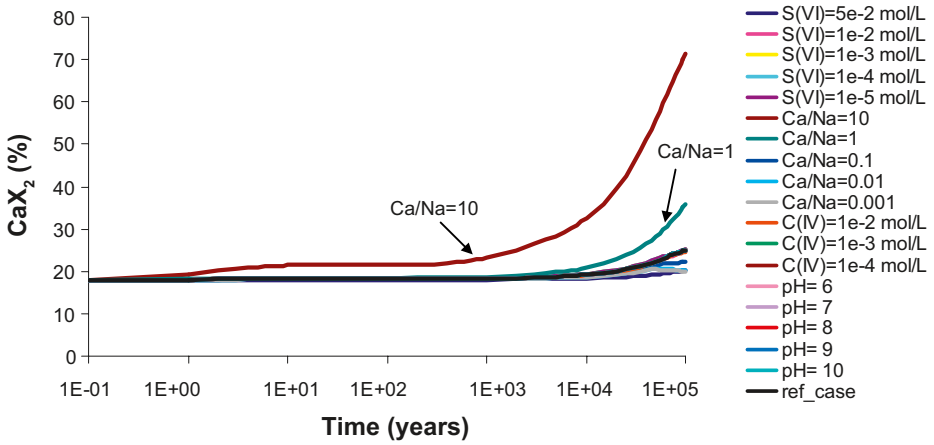

Figure 6-16. *Computed time evolution of Ca content in the exchanger of montmorillonite in the observation point (Figure 6-5) for the nineteen inflow water compositions analysed in Case I (Table 4-9), flow rate 10^{-3} m^3/yr, MX-80 bentonite.*

The maximum pH reached when the flow rate in the fracture is 10^{-1} m^3/yr is 8.22, and it corresponds to the case where the pH of the groundwater flowing in the fracture is 10 (Figure 6-17). The maximum pH reached in this case is higher than that attained when the flow rate is 10^{-3} m^3/yr (7.30).

In the set of cases with a flow rate of 10^{-1} m^3/yr, the minimum pH reached at the end of the simulation is 6.09 and it is computed for the case where the pH of the inflowing water is 6.

When the aqueous carbonate concentration of the inflowing groundwater is of the order of 10^{-2} mol/L, calcite is predicted to precipitate at the beginning of the simulation, and then it gradually dissolves until the end of the simulation period (Figure 6-18). It should be noted that the maximum amount of calcite precipitated for the higher flow rate ($2.79 \cdot 10^{-2}$ wt%, in Figure 6-18) is slightly lower than the amount of calcite precipitated when the flow rate is 10^{-3} m^3/yr ($3.19 \cdot 10^{-2}$ wt%, in Figure 6-7).

There are seven cases where calcite is not predicted to precipitate. These are the cases where Ca/Na is 0.1, 0.01 and 0.001, and also where the pH is equal to 6, 8, 9 and 10. Conceptually, calcite will buffer pH if it is present. It follows that a very wide range of pH is only possible if it is absent.

When the flow rate is higher, computed results indicate that gypsum is exhausted relatively quickly for most of the cases. Exception is made for three cases (Figure 6-19):

- In the case where Ca/Na of the inflowing water is 1, gypsum is exhausted in 20,000 years.
- In the case where Ca/Na of the inflowing water is 10, the amount of gypsum in the MX-80 bentonite is relatively stable during the whole simulated period.
- Where the sulphate concentration of the inflowing water is $5 \cdot 10^{-2}$ mol/L, gypsum is continuously precipitating until the end of the simulation period.

Computed results for the higher flow rate indicate that the concentration of aqueous calcium reaches a maximum of 1 mol/L in the case where Ca/Na is 10, and the corresponding increase of calcium concentration occurs in a very short time lag (Figure 6-20). The predicted concentration of aqueous calcium in the MX-80 bentonite reaches that of the inflowing water. The same is also seen for the case where Ca/Na of the inflowing water is 1.

For the cases where Ca/Na is 0.01 and 0.001, the concentration of aqueous calcium in the MX-80 bentonite progressively decreases along the simulation time which is also reflected in the concentration of this cation in the montmorillonite interlayer (Figure 6-21).

The evolution of calcium content in the montmorillonite interlayer mimics that of aqueous calcium (Figure 6-21).

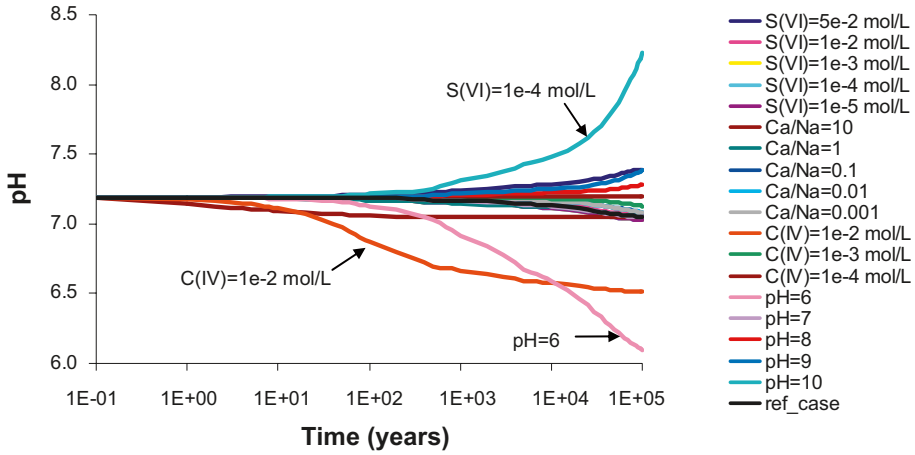

Figure 6-17. *Computed time evolution of pH in the observation point located in the bentonite (see Figure 6-5) for the nineteen inflow water compositions analysed in Case I (Table 4-9), flow rate 0.1 m³/yr, MX-80 bentonite. Initial groundwater compositions are listed in Table 4-7.*

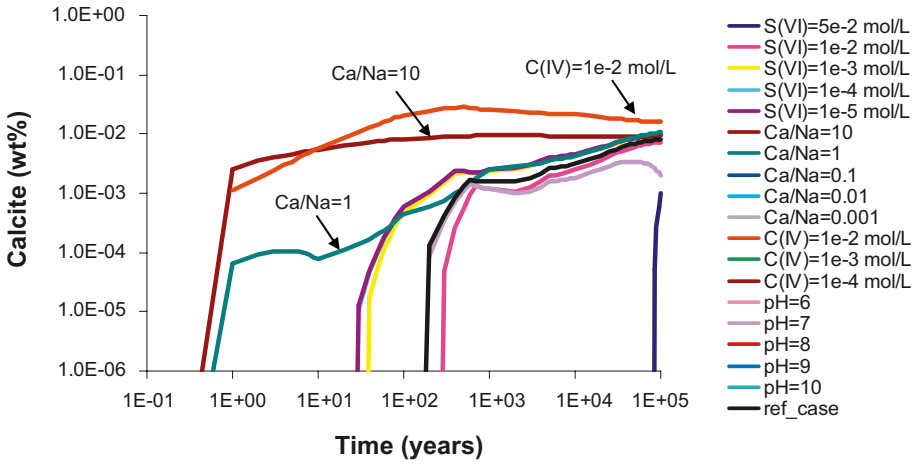

Figure 6-18. *Computed time evolution of calcite content in the observation point located in the bentonite (see Figure 6-5) for the nineteen inflow water compositions analysed in Case I (Table 4-9), flow rate 0.1 m³/yr, MX-80 bentonite. Initial contents are listed in Table 3-2.*

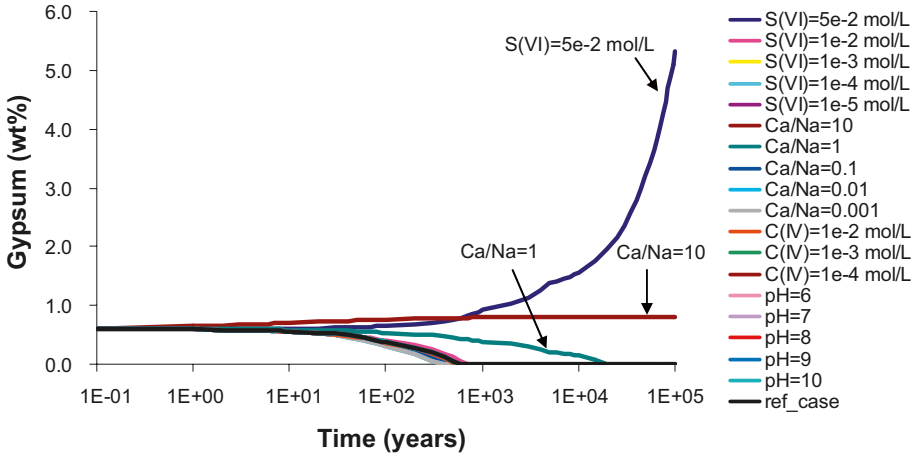

Figure 6-19. *Computed time evolution of gypsum content in the observation point located in the bentonite (see Figure 6-5) for the nineteen inflow water compositions analysed in Case I (Table 4-9), flow rate 0.1 m³/yr, MX-80 bentonite. Initial contents are listed in Table 3-2.*

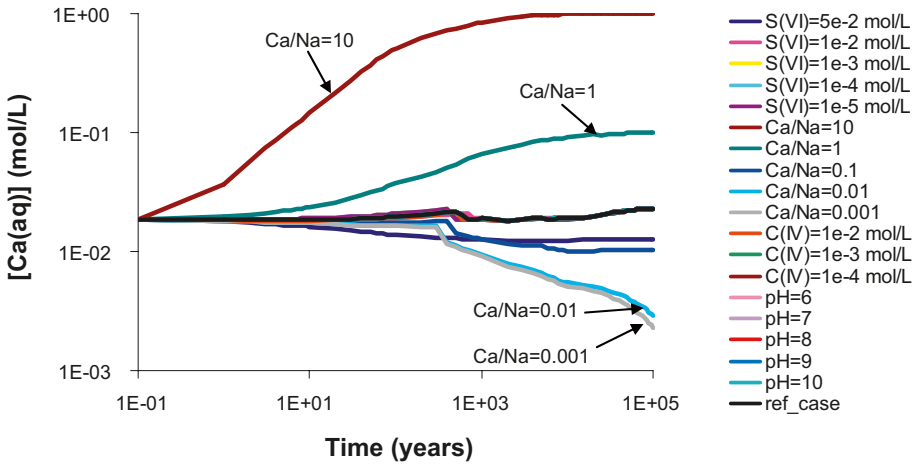

Figure 6-20. *Computed time evolution of aqueous calcium concentration in the observation point located in the bentonite (see Figure 6-5) for the nineteen inflow water compositions analysed in Case I (Table 4-9), flow rate 0.1 m³/yr, MX-80 bentonite. Initial groundwater compositions are listed in Table 4-7.*

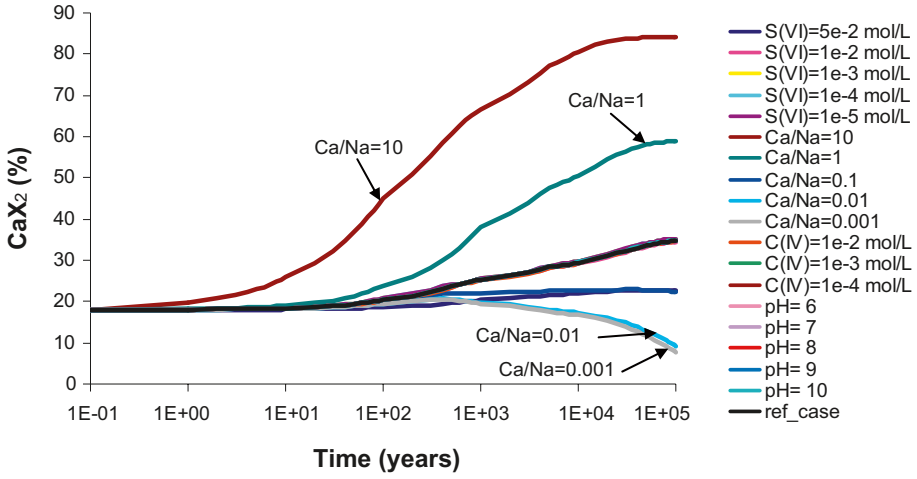

Figure 6-21. *Computed time evolution of calcium content in the exchanger of montmorillonite in the observation point located in the bentonite (see Figure 6-5) for the nineteen inflow water compositions analysed in Case I (Table 4-9), flow rate 0.1 m³/yr, MX-80 bentonite.*

6.1.3 Deponit CA-N bentonite buffer

As previously mentioned, the main differences between the two bentonite types analysed here are the content of carbonate minerals and the dominant cation of the montmorillonite interlayer. In this context, besides the parameters that were analysed for the MX-80 bentonite, computed evolution of the amount of dolomite is also analysed in the numerical results attained with the Deponit CA-N bentonite.

In Figure 6-22, it is seen that the pH of Deponit CA-N bentonite slightly decreases due the inflow of Forsmark groundwater through the engineered barrier. The same was already seen for the case of MX-80 bentonite (Figure 6-1). The computed pH decrease from 7.17 to 7.09 is mainly due to calcite precipitation (Figure 6-23).

As already seen for the case with the MX-80 bentonite, calcite is predicted to precipitate (Figure 6-23) and gypsum is predicted to dissolve (Figure 6-24) in the Reference Case I with Deponit CA-N bentonite due to the inflow of Forsmark groundwater.

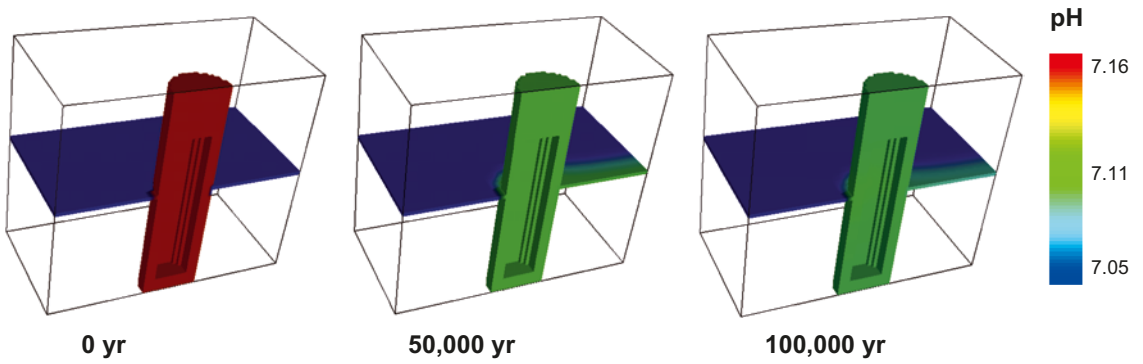

Figure 6-22. *Computed evolution of pH in the modelled domain of Reference Case I, Deponit CA-N bentonite. Initial groundwater compositions are listed in Table 4-7.*

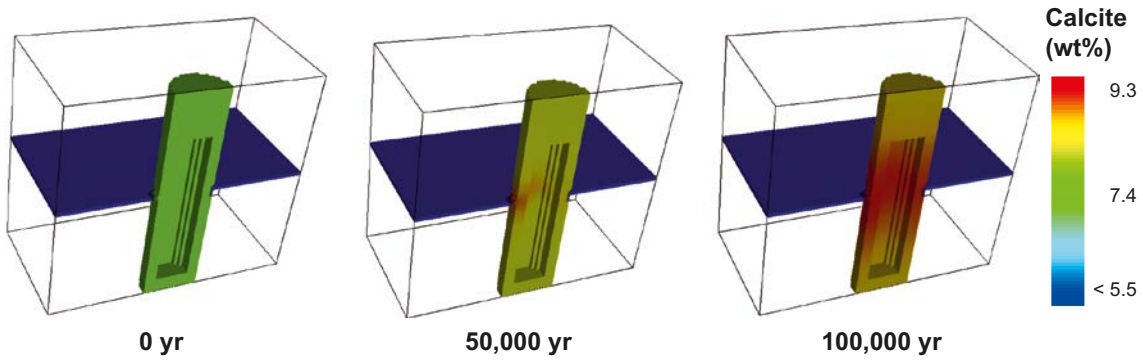

Figure 6-23. *Computed evolution of calcite content in the modelled domain of Reference Case I, Deponit CA-N bentonite. Initial contents are listed in Table 3-2.*

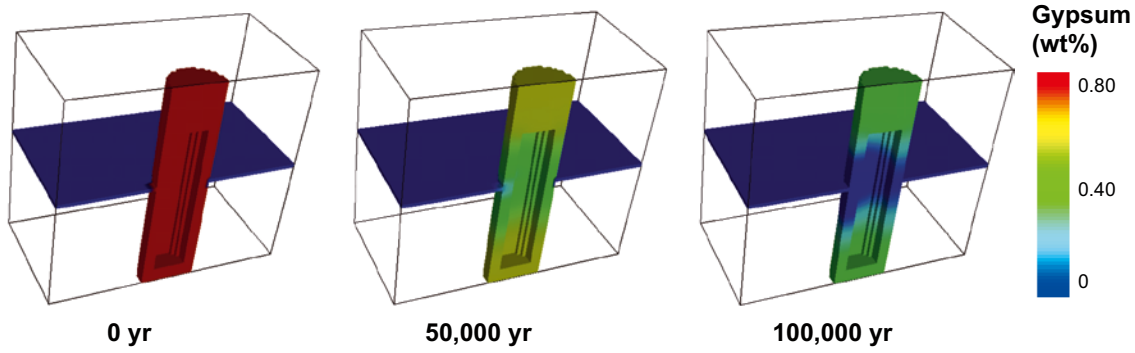

Figure 6-24. *Computed evolution of gypsum content in the modelled domain of Reference Case I, Deponit CA-N bentonite. Initial contents are listed in Table 3-2.*

While calcite is predicted to precipitate, dolomite is predicted to dissolve due to the inflow of Forsmark groundwater (Figure 6-25). The interaction between Forsmark groundwater and the minerals of Deponit CA-N bentonite, leads to a gradual depletion of gypsum and dolomite in favour of more calcite precipitated.

Although two Ca-bearing minerals are predicted to dissolve gradually throughout the simulation period (gypsum and dolomite) supplying calcium to the aqueous phase, the montmorillonite interlayer becomes slightly depleted in calcium (Figure 6-26).

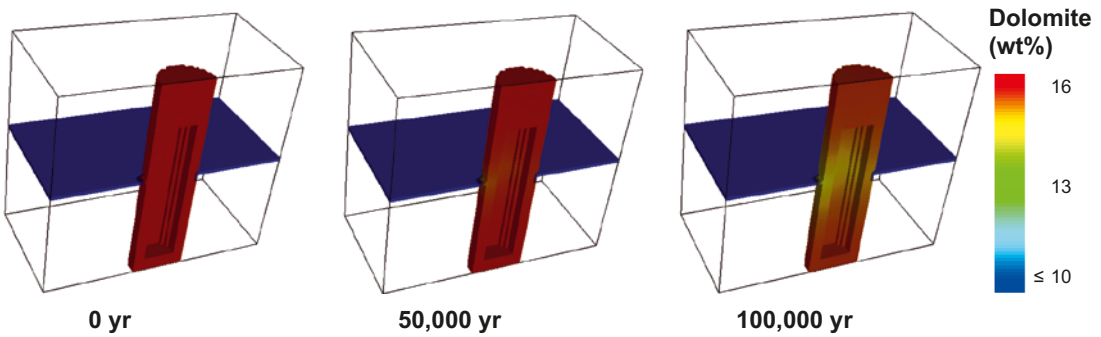

Figure 6-25. *Computed evolution of dolomite content in the modelled domain of Reference Case I, Deponit CA-N bentonite. Initial contents are listed in Table 3-2.*

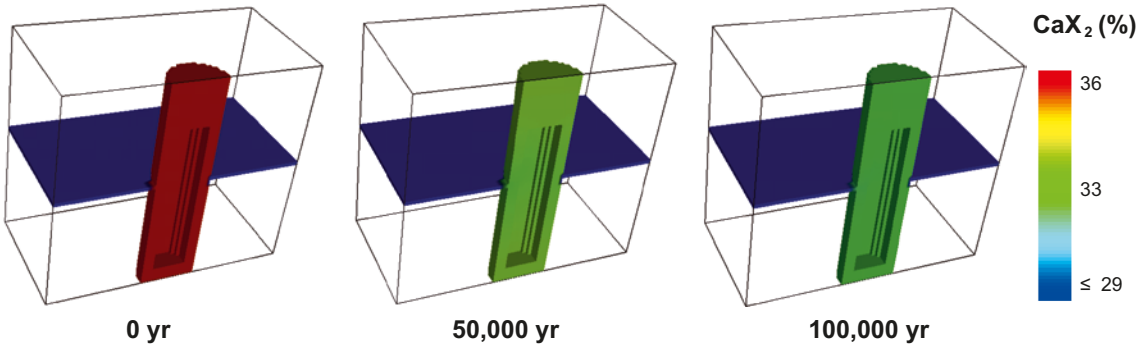

Figure 6-26. *Computed evolution of calcium content in the montmorillonite interlayer in the modelled domain of Reference Case I, Deponit CA-N bentonite.*

6.1.4 Sensitivity analysis, Case I, Deponit CA-N bentonite

The sensitivity analysis performed for the flow rate of the groundwater in the fracture, considering a buffer composed of Deponit CA-N bentonite, leads to computed results different from the ones previously attained when the MX-80 was considered.

Computed pH in the Deponit CA-N bentonite buffer shows that for the reference case pH slightly drops from 7.17 to 7.09 (Figure 6-27), while for higher flow rates (0.1 and 10 m^3/yr) pH initially decreases (within the first 1,000 years), and then progressively increases to 7.23. This means that although calcite precipitates throughout the simulation period for these higher flow rate cases (Figure 6-28), dissolution of dolomite (Figure 6-30) has a larger effect on pH than calcite precipitation. This pH controlling effect was not seen for the case with MX-80 bentonite (Figure 6-6), since there were no other carbonate minerals available to counteract the pH drop induced by calcite precipitation.

Calcite precipitation is computed for the reference case (10^{-3} m^3/yr) and the two cases with higher flow rate (Figure 6-28). Computed calcite precipitation reaches a maximum of 15 wt% for the case with the highest flow rate (10 m^3/yr).

Computed gypsum evolution in the Deponit CA-N bentonite buffer indicates that this mineral dissolves throughout the simulation period for the four flow rates analysed (Figure 6-29). In the two cases with the higher flow rates, gypsum is exhausted within the first 1,000 years, while for the reference case (10^{-3} m^3/yr) gypsum exhaustion is reached at 100,000 years. In the case with the lowest flow rate, gypsum dissolves at a very slow rate, so its exhaustion is not reached even at the end of the simulated period.

Computed evolution of the amount of dolomite in the Deponit CA-N bentonite buffer indicates that this mineral dissolves throughout the simulation period. Forsmark groundwater is undersaturated in dolomite (SI= –0.51), and therefore, its interaction with the Deponit CA-N bentonite buffer leads to the dissolution of dolomite. In addition, for higher flow rates the amount of dolomite dissolved at the end of the simulation is higher than for lower flow rates (Figure 6-30).

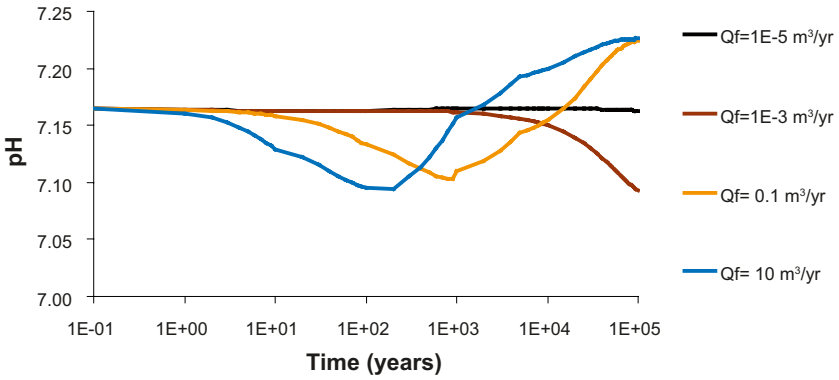

Figure 6-27. *Computed time evolution of pH in the observation point located in the bentonite (Figure 6-5), for the four flow rates analysed in Case I, Deponit CA-N bentonite (Table 4-8). Initial groundwater compositions are listed in Table 4-7.*

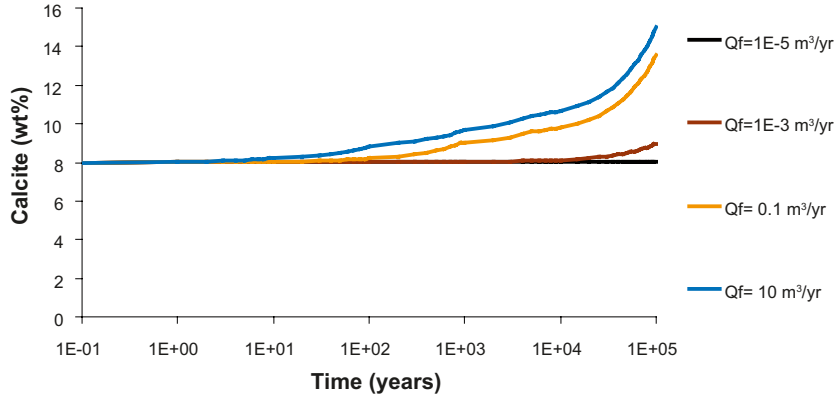

Figure 6-28. *Computed time evolution of calcite content in the observation point located in the bentonite (see Figure 6-5), for the four flow rates analysed in Case I, Deponit CA-N bentonite (Table 4-8). Initial contents are listed in Table 3-2.*

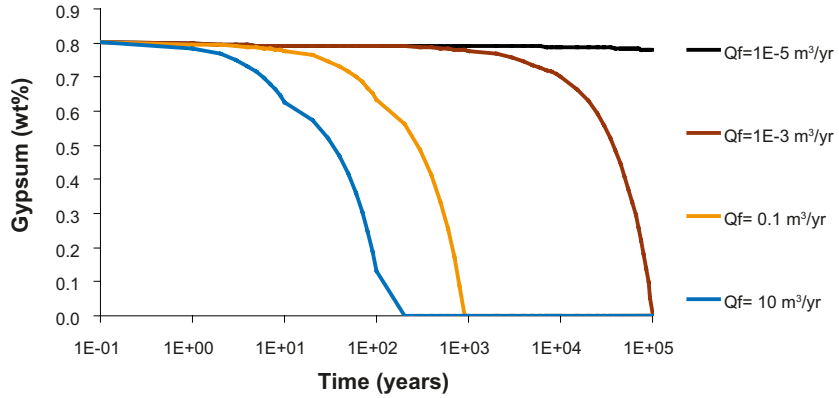

Figure 6-29. *Computed time evolution of gypsum content in the observation point located in the bentonite (see Figure 6-5), for the four flow rates analysed in Case I, Deponit CA-N bentonite (Table 4-8). Initial contents are listed in Table 3-2.*

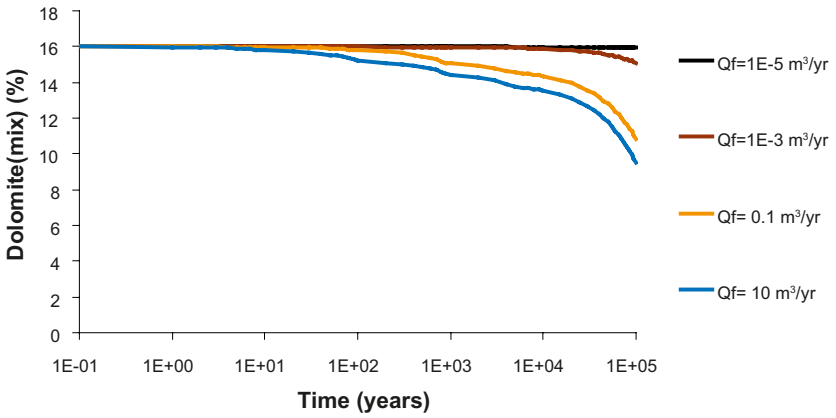

Figure 6-30. *Computed time evolution of dolomite content in the observation point located in the bentonite (see Figure 6-5), for the four flow rates analysed in Case I, Deponit CA-N bentonite (Table 4-8). Initial contents are listed in Table 3-2.*

As previously observed for the pH evolution, the evolution of aqueous calcium reflects the hypothesis that the precipitation of calcite overlaps the effect of gypsum and dolomite dissolution because calcium concentration in the aqueous phase decreases throughout the simulation period (Figure 6-31). The depletion of aqueous calcium, induced by calcite precipitation, is also reflected in the montmorillonite interlayer which shows a gradual decrease of the amount of calcium adsorbed (Figure 6-32). In addition, it is seen that the depletion of calcium both in the aqueous phase and in the exchanger is more pronounced in the cases with higher groundwater flow rates.

In the sensitivity analysis performed for the chemical composition of the inflowing water, and with a flow rate of 10^{-3} m^3/yr, computed pH evolution shows a relatively wide range of results (Figure 6-33).

When the concentration of aqueous carbonate of the inflowing water is high (10^{-2} mol/L), pH gradually decreases to 6.53 which is close to the value of the pH of the inflowing water (6.51, C(IV)=10^{-2} mol/L, Table 4-10), while in the case that the inflowing water has a pH of 10, the pH in the Deponit CA-N bentonite buffer increases to 7.45. The remaining cases lead to a final pH of the Deponit CA-N bentonite buffer that is within these values.

Computed results indicate that the highest amount of calcite precipitated in the Deponit CA-N bentonite buffer occurs when the inflowing water has a Ca/Na of 10 (Figure 6-34). The rest of the sensitivity cases leads to less calcite precipitated in the Deponit CA-N bentonite buffer.

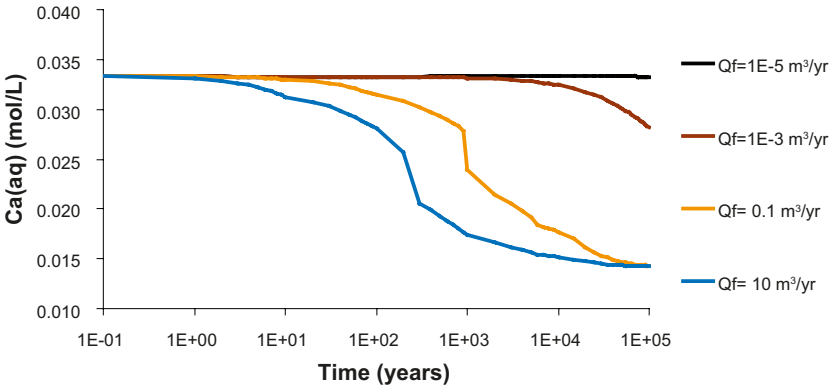

Figure 6-31. *Computed time evolution of aqueous calcium concentration in the observation point located in the bentonite (see Figure 6-5), for the four flow rates analysed in Case I, Deponit CA-N bentonite (Table 4-8). Initial groundwater compositions are listed in Table 4-7.*

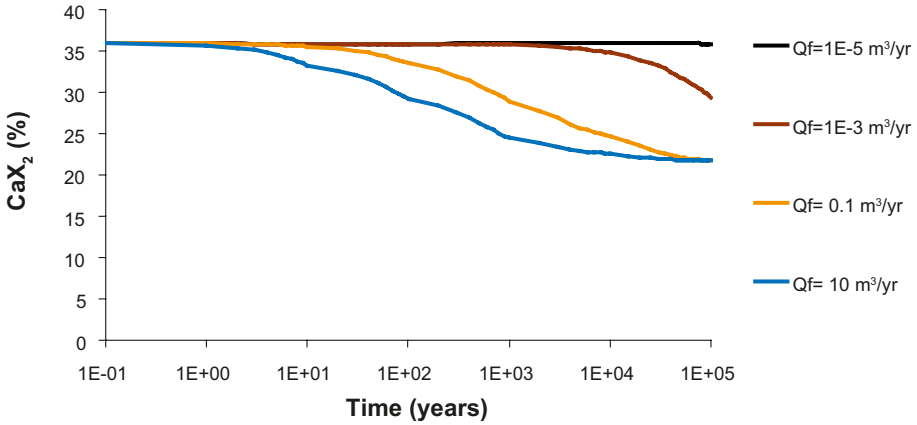

Figure 6-32. *Computed time evolution of calcium content in the montmorillonite interlayer in the observation point located in the bentonite (see Figure 6-5), for the four flow rates analysed in Case I, Deponit CA-N bentonite (Table 4-8).*

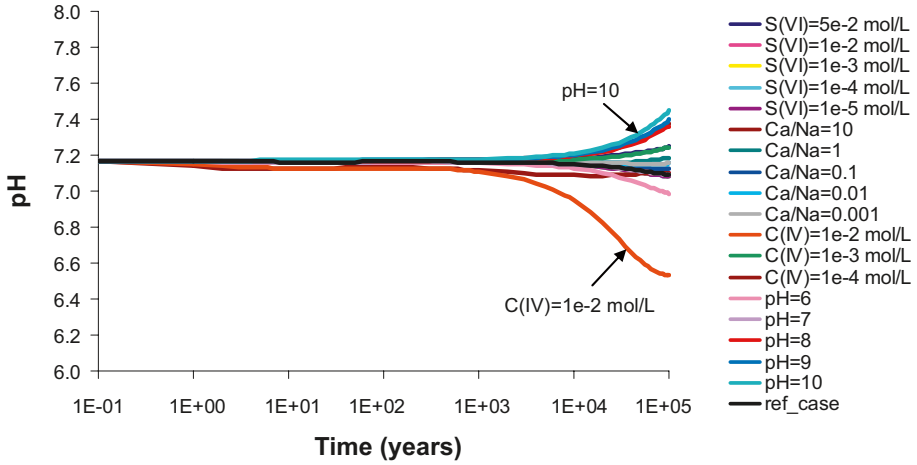

Figure 6-33. *Computed time evolution of pH in the observation point located in the bentonite (see Figure 6-5) for the nineteen inflow water compositions analysed in Case I (Table 4-9), flow rate 10^{-3} m^3/yr, Deponit CA-N bentonite. Initial groundwater compositions are listed in Table 4-7.*

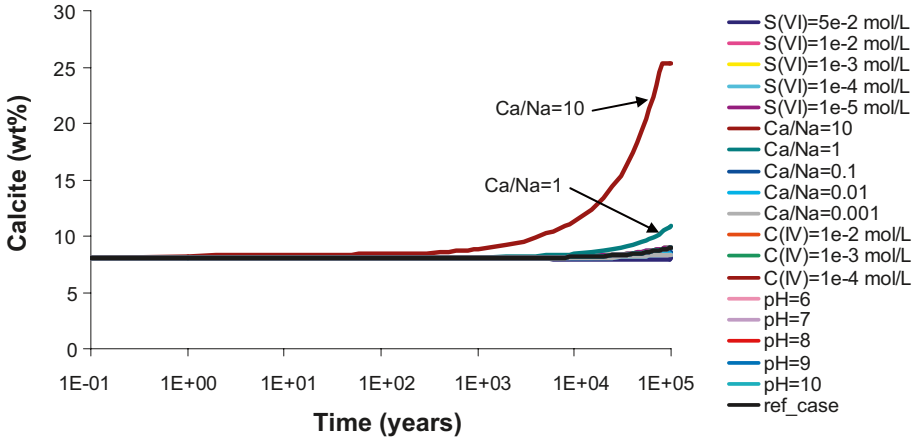

Figure 6-34. *Computed time evolution of calcite content in the observation point located in the bentonite (see Figure 6-5) for the nineteen inflow water compositions analysed in Case I (Table 4-9), flow rate 10^{-3} m^3/yr, Deponit CA-N bentonite. Initial contents are listed in Table 3-2.*

Computed results indicate that gypsum dissolves in all the cases analysed, except for the case where the concentration of aqueous sulphate in the inflowing water is high ($5 \cdot 10^{-2}$ mol/L). In this case, gypsum is predicted to precipitate throughout the simulation period, reaching a maximum of 1.56 wt% at the end of the simulation period. The cases where the inflowing groundwater has lower concentration of aqueous sulphate (10^{-3}, 10^{-4} and 10^{-5} mol/L), and also those cases where the Ca/Na is low (0.1, 0.01 and 0.001) lead to an exhaustion of gypsum that occurs before that computed for the reference case (100,000 years).

Dolomite is computed to dissolve in most of the simulated cases. Nevertheless, this dissolution is much more pronounced in the case where Ca/Na is 10 than for all the other cases (Figure 6-36). In fact, this case leads to dolomite exhaustion in the Deponit CA-N bentonite buffer at 80,000 years.

When the Ca/Na of the inflowing water is 10, gypsum dissolves until 85,000 years, after which it slowly precipitates (Figure 6-35). Although there is an excess of calcium, the lack of aqueous carbonate hinders calcite precipitation, and when the dolomite is exhausted, calcite precipitation ceases (Figure 6-34).

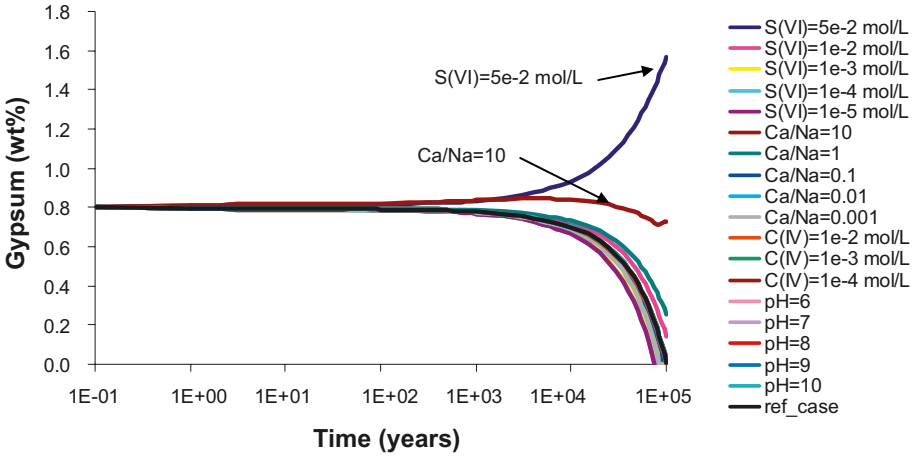

Figure 6-35. *Computed time evolution of gypsum content in the observation point located in the bentonite (see Figure 6-5) for the nineteen inflow water compositions analysed in Case I (Table 4-9), flow rate 10^{-3} m³/yr, Deponit CA-N bentonite. Initial contents are listed in Table 3-2.*

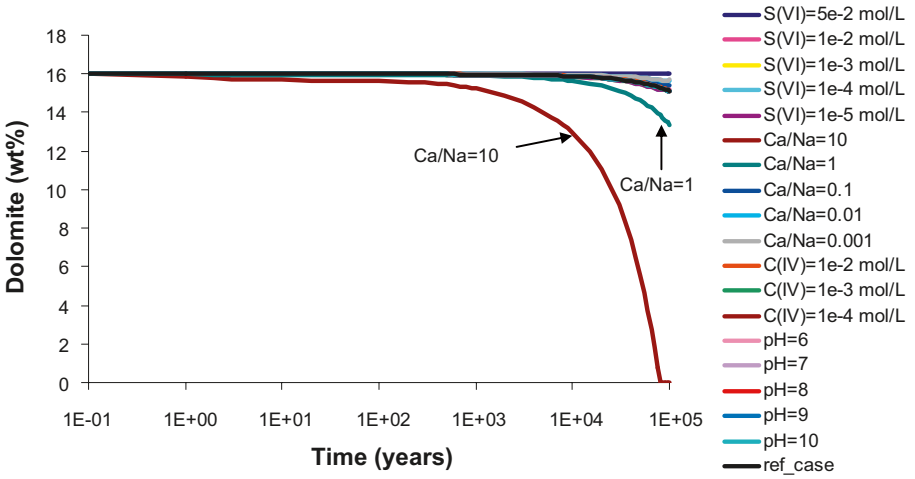

Figure 6-36. *Computed time evolution of dolomite content in the observation point located in the bentonite (see Figure 6-5) for the nineteen inflow water compositions analysed in Case I (Table 4-9), flow rate 10^{-3} m³/yr, Deponit CA-N bentonite. Initial contents are listed in Table 3-2.*

The inflow of a calcium-rich groundwater (with a Ca/Na > 1) leads to a visible increase of the concentration of aqueous calcium in the Deponit CA-N bentonite porewater, while in the rest of the simulation cases the concentration of calcium in the aqueous phase of the Deponit CA-N bentonite decreases along the simulated period (Figure 6-37). Computed evolution of calcium in the exchanger (Figure 6-38) reflects the behaviour of aqueous calcium in the Deponit CA-N bentonite porewater previously described (Figure 6-37).

When the inflowing water has a Ca/Na of 10, the calcium content in the montmorillonite interlayer increases at different rates. Until 75,000 years it increases at a relatively low rate because calcite is precipitating. Afterwards, calcium content in the exchanger increases at a higher rate. At this moment, dolomite is exhausted, calcite is not precipitating anymore and gypsum is still dissolving. Finally, from 85,000 years to the end of the simulation, the calcium content in the exchanger increases again at a relatively slow trend, because gypsum is not being dissolved, and therefore less calcium is available in the Deponit CA-N bentonite porewater. The remaining sensitivity cases lead to a progressive depletion of the exchanger in calcium, which is compensated by the increase of sodium concentration in the exchanger.

As previously observed for the cases with the MX-80 bentonite, when the flow rate of the inflowing water is high (0.1 m^3/yr), the geochemical changes in the bentonite buffer are more pronounced.

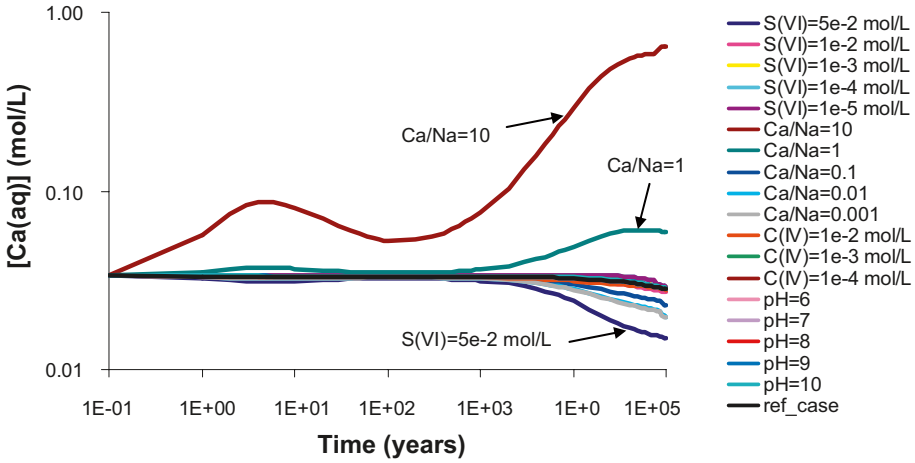

Figure 6-37. *Computed time evolution of aqueous Ca concentration in the observation point (Figure 6-5) for the nineteen inflow water compositions analysed in Case I (Table 4-9), flow rate 10^{-3} m^3/yr, Deponit CA-N bentonite. Initial groundwater compositions are listed in Table 4-7.*

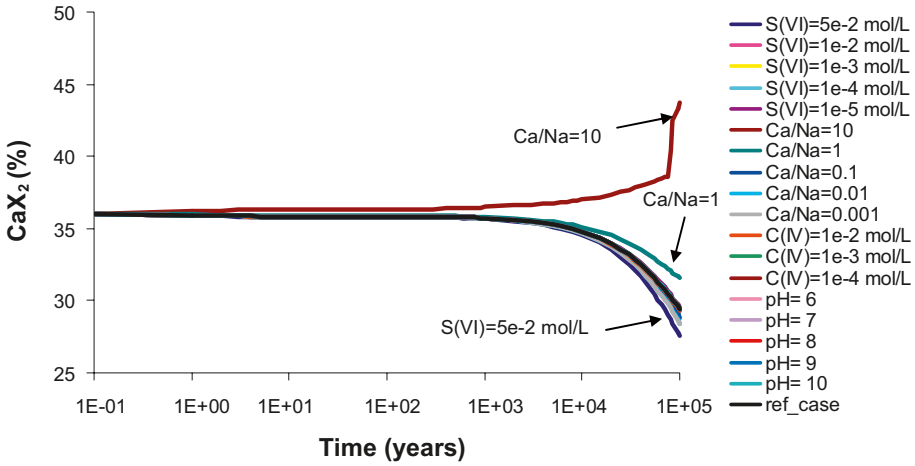

Figure 6-38. *Computed time evolution of Ca content in the montmorillonite interlayer in the observation point located in the bentonite (Figure 6-5) for the nineteen inflow water compositions analysed in Case I (Table 4-9), flow rate 10^{-3} m^3/yr, Deponit CA-N bentonite.*

Computed results for the sensitivity analyses with a higher flow rate indicate that the maximum pH reached is 8.70, in the case where the inflowing water has a pH of 10, and the minimum pH reached is 6.65, in the case where the concentration of aqueous carbonate of the inflowing water is high (10^{-2} mol/L). The remaining sensitivity cases lead to pH values, which are between these values (Figure 6-39).

Computed evolution of the amount of dolomite in the Deponit CA-N bentonite buffer indicates that this mineral dissolves in most of the analysed cases (Figure 6-42). When the Ca/Na of the inflowing water is 10, dolomite is exhausted relatively quickly (within the first 700 years), while if the Ca/Na of the inflowing water is 1 dolomite is exhausted after 55,000 years. When the Ca/Na of the inflowing water is 0.01 and 0.001, the lack of calcium in the system leads to the dissolution of calcite and the corresponding precipitation of dolomite.

Calcite is predicted to precipitate throughout the simulation period in all the sensitivity cases, except for two cases where the Ca/Na of the inflowing water is 0.01 and 0.001 (Figure 6-40).

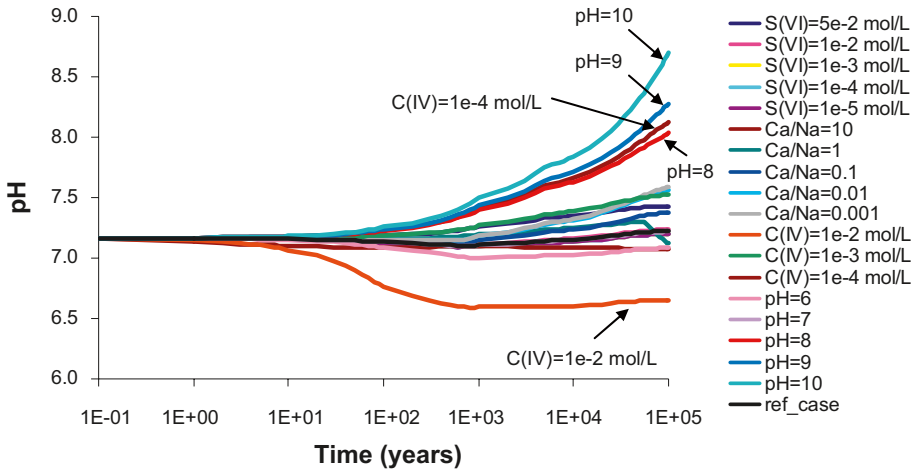

Figure 6-39. *Computed time evolution of pH in the observation point located in the bentonite (see Figure 6-5) for the nineteen inflow water compositions analysed in Case I (Table 4-9), flow rate 0.1 m³/yr, Deponit CA-N bentonite. Initial groundwater compositions are listed in Table 4-7.*

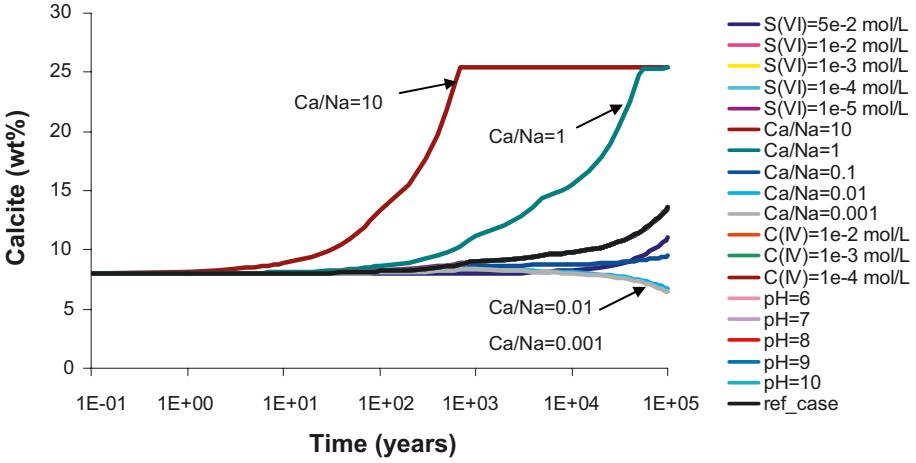

Figure 6-40. *Computed time evolution of calcite content in the observation point located in the bentonite (see Figure 6-5) for the nineteen inflow water compositions analysed in Case I (Table 4-9), flow rate 0.1 m³/yr, Deponit CA-N bentonite. Initial contents are listed in Table 3-2.*

When the Ca/Na of the inflowing water is 10, calcite precipitates within the first 700 years, reaching a maximum of 25.4 wt%, which is maintained until the end of the simulation. This maximum amount of calcite precipitated is also reached in the case where the Ca/Na of the inflowing water is 1, but it is reached latter than in the previous case (at 55,000 years). In general, the cease of calcite precipitation coincides with the exhaustion of dolomite, which indicates that dolomite is being replaced by calcite due to the inflow of a Ca-rich groundwater.

Gypsum is predicted to dissolve, in the Deponit CA-N bentonite buffer, in all the sensitivity cases analysed for the higher flow rate except for two cases. When the concentration of aqueous sulphate of the inflowing water is high ($5 \cdot 10^{-2}$ mol/L), gypsum precipitates gradually along the simulated period, while in the case where the Ca/Na of the inflowing water is 10, the amount of gypsum in the Deponit CA-N bentonite is relatively stable throughout the simulated period (Figure 6-41).

In most of the sensitivity cases analysed here, the concentration of calcium in the Deponit CA-N bentonite porewater decreases along the simulation period. Exception is made for those cases where the Ca/Na of the inflowing water is 1 and 10 (Figure 6-43). In these cases, calcium transported by the inflowing water is partitioned through the aqueous phase (Figure 6-43), calcite (Figure 6-40) and the montmorillonite interlayer (Figure 6-44).

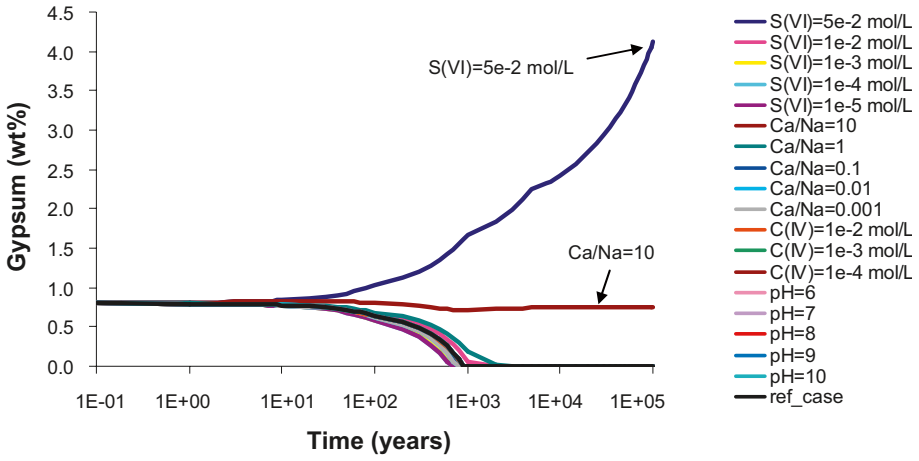

Figure 6-41. *Computed time evolution of gypsum content in the observation point located in the bentonite (see Figure 6-5) for the nineteen inflow water compositions analysed in Case I (Table 4-9), flow rate 0.1 m^3/yr, Deponit CA-N bentonite. Initial contents are listed in Table 3-2.*

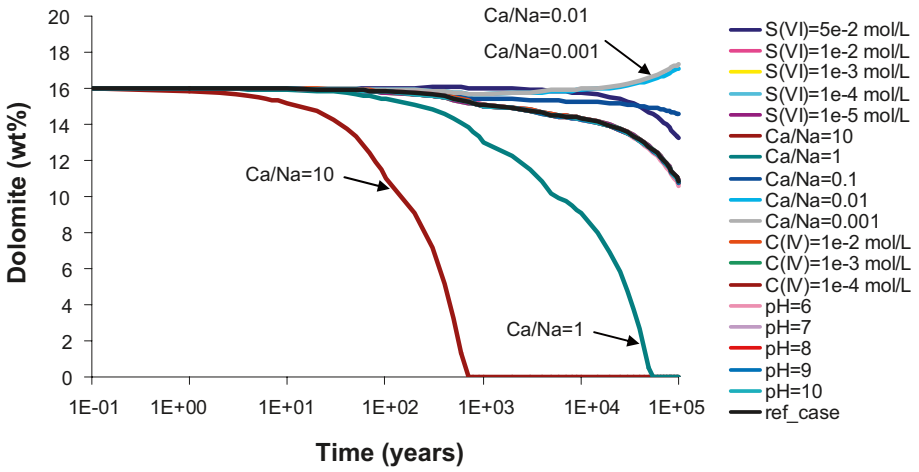

Figure 6-42. *Computed time evolution of dolomite content in the observation point located in the bentonite (see Figure 6-5) for the nineteen inflow water compositions analysed in Case I (Table 4-9), flow rate 0.1 m^3/yr, Deponit CA-N bentonite. Initial contents are listed in Table 3-2.*

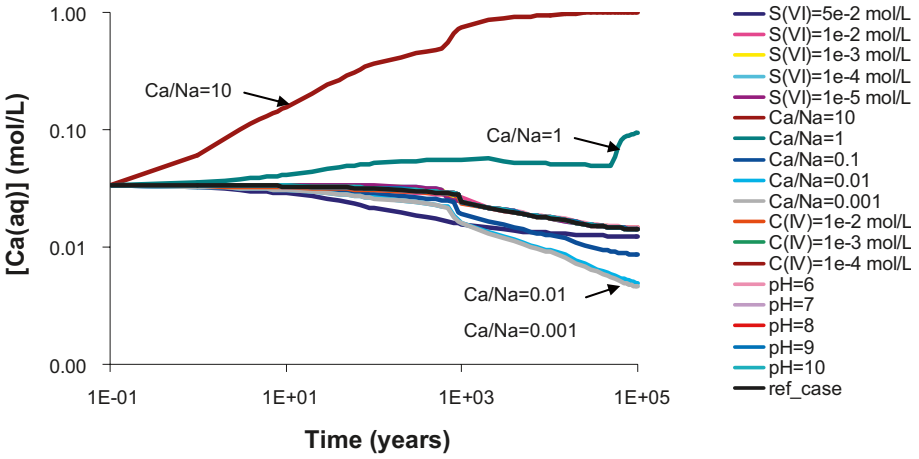

Figure 6-43. *Computed time evolution of aqueous calcium concentration in the observation point located in the bentonite (see Figure 6-5) for the nineteen inflow water compositions analysed in Case I (Table 4-9), flow rate 0.1 m³/yr, Deponit CA-N bentonite. Initial groundwater compositions are listed in Table 4-7.*

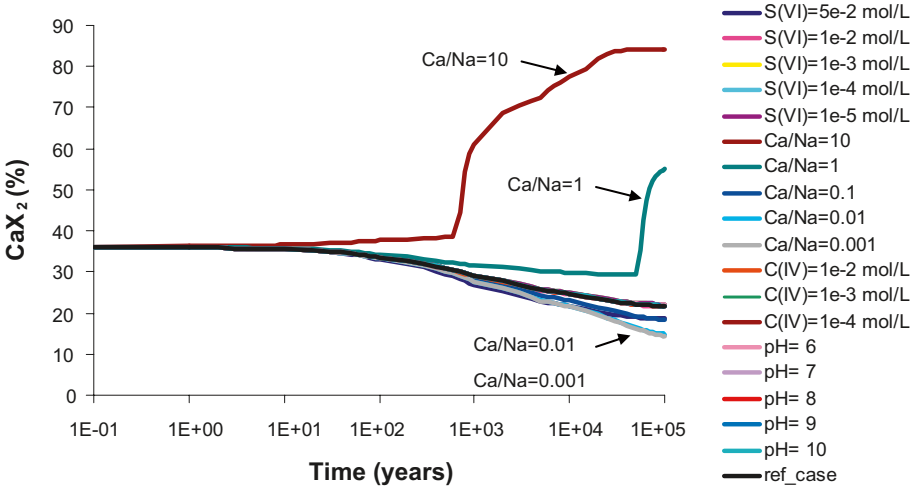

Figure 6-44. *Computed time evolution of calcium content in the montmorillonite interlayer in the observation point located in the bentonite (see Figure 6-5) for the nineteen inflow water compositions analysed in Case I (Table 4-9), flow rate 0.1 m³/yr, Deponit CA-N bentonite.*

In the cases where computed aqueous calcium concentration decreases (all except the cases with a Ca/Na of 1 and 10), the amount of calcite that precipitates in the Deponit CA-N bentonite is higher than the amount of calcium released into the aqueous phase by gypsum and dolomite dissolution. Therefore, the concentration of calcium in the aqueous phase (Figure 6-43) and in the montmorillonite interlayer (Figure 6-44) decreases along time. It is worth noting that in the case with a Ca/Na of 1, the content of calcium both in the aqueous phase and in the exchanger is computed to decrease until dolomite exhaustion (which is accompanied by calcite precipitation). When dolomite is exhausted and calcite precipitation ceases, the content of calcium in the aqueous phase and in the exchanger starts to increase.

Table 6-1. Summary of the main results achieved in the sensitivity analysis performed for the chemical composition of the groundwater flowing in the hypothetical fracture of the granite in Case I.

Bentonite	Flow rate (m^3/yr)	Variable	Value	Sensitivity Case
MX-80	10^{-3}	Maximum pH	7.30	pH= 10
		Minimum pH	6.63	C(IV)=1E–2 mol/L
		Maximum amount of calcite	3.19E–2 wt%	C(IV)=1E–2 mol/L
		Fastest gypsum exhaustion	At 50,000 yr	Ca/Na= 0.001
		Maximum amount of gypsum	1 wt%	Ca/Na= 10
		Maximum [Ca(aq)]	1 mol/L	Ca/Na= 10
		Maximum [CaX_2]	71.2%	Ca/Na= 10
		Minimum [CaX_2]	20.0%	Ca/Na= 0.001
	10^{-1}	Maximum pH	8.22	pH= 10
		Minimum pH	6.09	pH= 6
		Maximum amount of calcite	2.79E–2 wt%	C(IV)=1E–2 mol/L
		Fastest gypsum exhaustion	At 400 yr	Ca/Na= 0.001
		Maximum amount of gypsum	5.32 wt%	S(VI)= 5E–2 mol/L
		Maximum [Ca(aq)]	1 mol/L	Ca/Na= 10
		Maximum [CaX_2]	84.0%	Ca/Na= 10
		Minimum [CaX_2]	7.6%	Ca/Na= 0.001
Deponit CA-N	10^{-3}	Maximum pH	7.45	pH= 10
		Minimum pH	6.53	C(IV)=1E–2 mol/L
		Maximum amount of calcite	25.4 wt%	Ca/Na=10
		Fastest gypsum exhaustion	At 80,000 yr	S(VI)= 1E–5 mol/L
		Maximum amount of gypsum	1.56 wt%	S(VI)= 5E–2 mol/L
		Maximum [Ca(aq)]	6.45E–1 mol/L	Ca/Na= 10
		Maximum [CaX_2]	43.8%	Ca/Na= 10
		Minimum [CaX_2]	27.5%	S(VI)= 5E–2 mol/L
		Fastest dolomite exhaustion	At 80,000 yr	Ca/Na= 10
		Maximum amount of dolomite	16 wt%	S(VI)= 5E–2 mol/L
	10^{-1}	Maximum pH	8.70	pH=10
		Minimum pH	6.65	C(IV)=1E–2 mol/L
		Maximum amount of calcite	25.4 wt%	Ca/Na=10; Ca/Na= 1
		Fastest gypsum exhaustion	At 700 yr	S(VI)= 1E–5 mol/L
		Maximum amount of gypsum	4.13 wt%	S(VI)= 5E–2 mol/L
		Maximum [Ca(aq)]	1 mol/L	Ca/Na= 10
		Maximum [CaX_2]	84.0%	Ca/Na= 10
		Minimum [CaX_2]	14.4%	Ca/Na= 0.001
		Fastest dolomite exhaustion	At 700 yr	Ca/Na= 10
		Maximum amount of dolomite	17.4 wt%	Ca/Na= 0.001

6.1.5 Summary of Case I for the water-saturated period

In Table 6-1, a summary of the main results attained in the sensitivity analysis performed for the Case I is presented. It is seen that the higher pH reached in all the cases is 8.7 which is computed for the case with Deponit CA-N bentonite and an inflowing water that has a pH of 10 (flow rate of 10^{-1} m^3/yr). The case leading to the lowest pH (6.09) occurs in the MX-80 bentonite buffer, with a flow rate of 10^{-1} m^3/yr, in which the pH of the inflowing water is 6.

The highest concentration of aqueous calcium reached in the bentonite buffer is 1 mol/L, and it is computed for the two bentonite types under study, in the case where the Ca/Na of the inflowing water is 10. Gypsum is exhausted faster in the case where the inflowing water has a Ca/Na of 0.001, with a groundwater flow rate of 10^{-1} m^3/yr and in a buffer composed of MX-80 bentonite.

In all cases thermodynamic equilibria has been considered. However, the relative influence of kinetics of gypsum dissolution (and calcite precipitation and ion-exchange) could be a subject for future sensitivity studies, specially when very high flow rates are considered.

The system is buffered by pCO_2 and mineral reactions, involving carbonate phases and ion-exchange. Essentially, the key outcome is the choice between the higher swelling capacity of Na-bentonite and the better pH buffering capacity of the Ca-bentonite.

6.2 Case II

As previously mentioned, the modelled domain for Case II is a 2D domain (Figure 4-2). In the following paragraphs, the discussion on the results computed for the sensitivity cases developed for Case II is presented.

6.2.1 MX-80 bentonite buffer

In the case that the bentonite buffer is composed of the MX-80 bentonite, there are no primary carbonates in the buffer, but since the backfill is composed of 69% of Deponit CA-N bentonite, it has primary carbonate minerals: calcite and dolomite (see Section 4.2.3, for more details).

No sensitivity analysis on the flow rate of the groundwater entering through the fracture and the hydraulic conductivity of the backfill has been performed for Case II. In this context, the sensitivity analysis for this case is focused on the chemical composition of the inflowing water (Table 4-10).

Computed results for the reference Case II with the MX-80 bentonite indicate that the pH of the MX-80 bentonite porewater slightly decreases during the simulated period (Figure 6-45). The initial pH of MX-80 bentonite porewater (pH = 7.19) is higher than the pH of the Forsmark groundwater (pH = 7.05) and very similar to the pH of the backfill porewater (pH = 7.16). In addition, a small amount of calcite precipitates in the MX-80 bentonite buffer, which contributes to the computed pH decrease. The pH of the porewater in the backfilled tunnel is almost invariable during the 100,000 yr simulated.

Besides precipitating in the MX-80 bentonite buffer, calcite is also predicted to precipitate in the backfilled tunnel close to the contact with the simulated fracture where Forsmark groundwater enters the modelled domain (Figure 6-46).

The inflow of Forsmark groundwater through the backfilled tunnel leads to the exhaustion of gypsum in the backfill, while in the MX-80 bentonite buffer gypsum dissolves but it is not exhausted at the end of the simulation (Figure 6-47).

Dolomite, which is present in the portion of Deponit CA-N bentonite that constitutes the backfill material, is predicted to dissolve in the vicinity of the contact with the hypothetical fracture (yellowish coloured area) where Forsmark groundwater enters the modelled domain. In addition, immediately above the deposition hole where the MX-80 bentonite porewater is in contact with the backfill, dolomite is also predicted to dissolve (yellowish coloured area, in Figure 6-48). In addition, no dolomite precipitation is computed within the MX-80 bentonite buffer.

As previously observed for Case I, the amount of calcium in the montmorillonite interlayer increases along the simulation period in the MX-80 bentonite buffer (Figure 6-49). The calcium being adsorbed is mainly provided by gypsum dissolution (Figure 6-47).

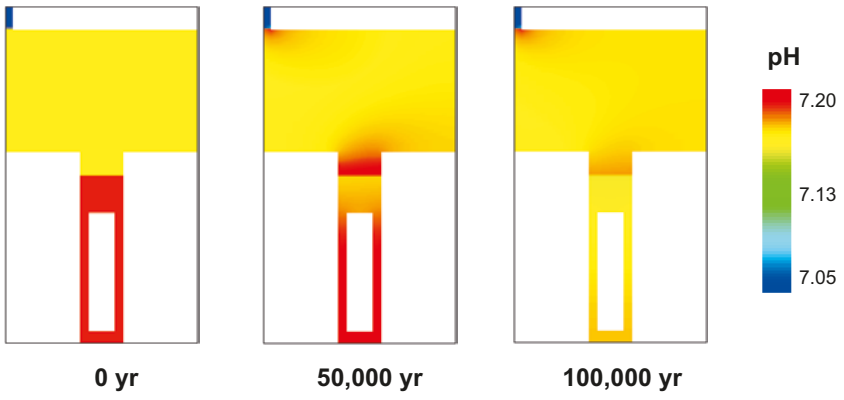

Figure 6-45. *Computed evolution of pH in the modelled domain of Reference Case II, MX-80 bentonite buffer. Initial groundwater compositions are listed in Table 4-7.*

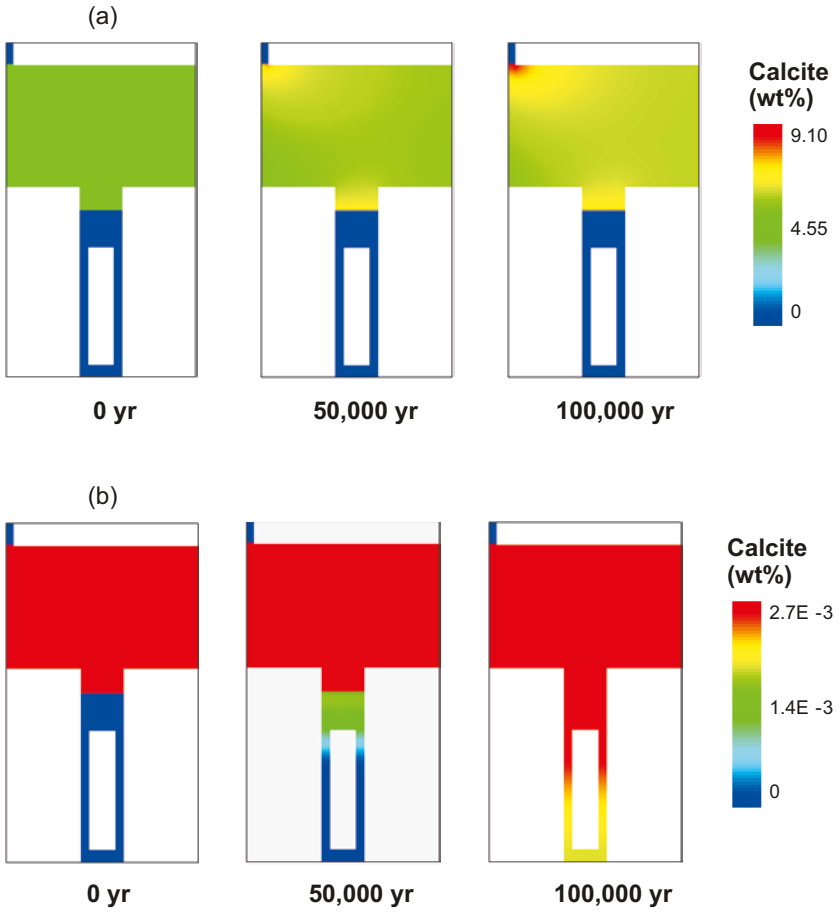

Figure 6-46. *Computed evolution of calcite content in the modelled domain of Reference Case II, MX-80 bentonite buffer. Graphics (a) and (b) are made with different scales for the amount of calcite. Initial contents are listed in Table 3-2 and in Table 4-3.*

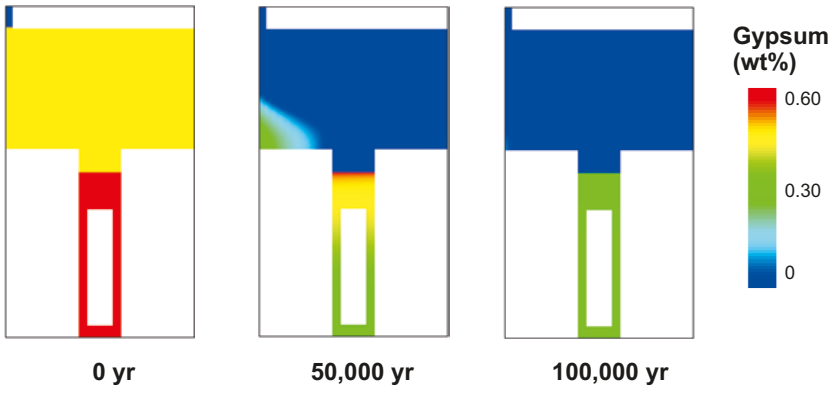

Figure 6-47. *Computed evolution of gypsum content in the modelled domain of Reference Case II, MX-80 bentonite buffer. Initial contents are listed in Table 3-2 and in Table 4-3.*

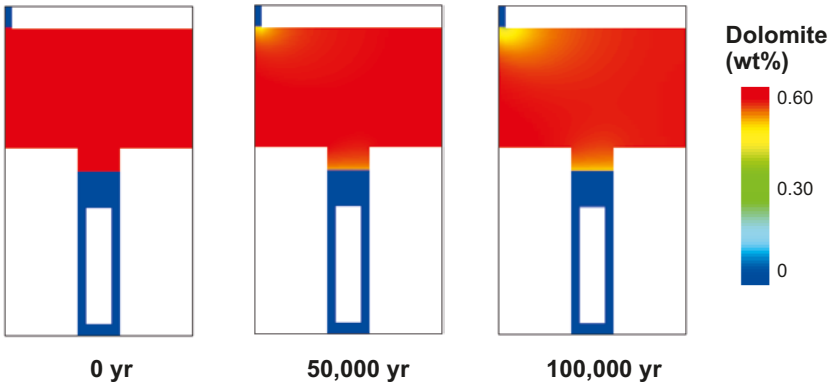

Figure 6-48. *Computed evolution of dolomite content in the modelled domain of Reference Case II, MX-80 bentonite buffer. Initial contents are listed in Table 3-2 and in Table 4-3.*

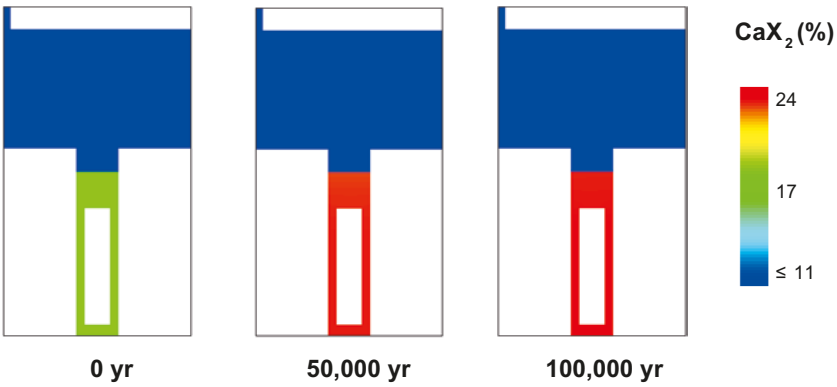

Figure 6-49. *Computed evolution of calcium content in the montmorillonite interlayer in the modelled domain of Reference Case II, MX-80 bentonite buffer.*

6.2.2 Sensitivity analysis, Case II, MX-80 bentonite

In order to compare the results computed in the sensitivity cases (see Table 4-10) performed for Case II, two sections of the modelled domain were selected for the analysis of the results computed at the end of the simulation period (Figure 6-50). Section 1 intersects solely the backfilled tunnel, along a horizontal line, which is located at the mid height of the tunnel, while Section 2 intersects the bentonite buffer and the backfilled tunnel along a vertical line that is on the left side of the canister, closer to the point where Forsmark groundwater enters the modelled domain.

The results computed along Section 1 are very similar for the two reference cases (with the MX-80 bentonite buffer and the Deponit CA-N bentonite buffer). Therefore, the results computed for Section 1, at the end of the simulation period, are only analysed for the reference case with the MX-80 bentonite buffer.

The initial pH of the backfill porewater is 7.16. At the end of the simulation period, almost all the cases lead to a pH profile equal or slightly higher than the initial value. Exception is made for two cases (Figure 6-51):

- [C(IV)] of the groundwater entering through the fracture is 10^{-2} mol/L,
- Ca/Na of the groundwater entering through the fracture is 10.

When the carbonate content of the groundwater entering through the fracture is10^{-2} mol/L, the final pH in the mid-height of the tunnel is around 7. The computed pH decrease with respect to the initial value of 7.16 is mainly due to the fact that the pH of the inflowing water is relatively low (6.51, or C(IV)=10^{-2} mol/L,in Table 4-9 and Table 4-10).

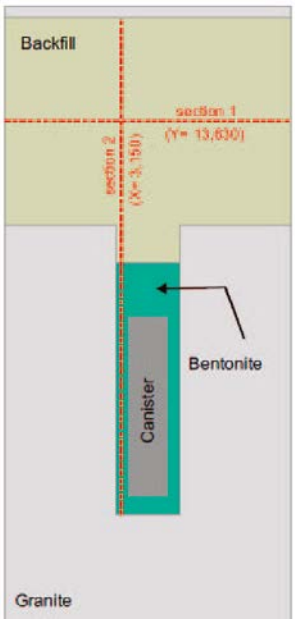

Figure 6-50. *Location of the two sections of Case II where computed outputs have been analysed for the sensitivity cases developed.*

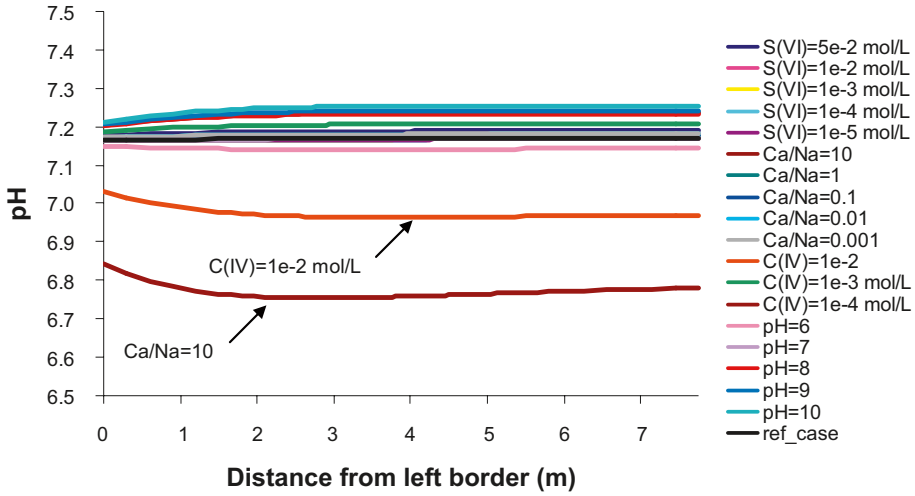

Figure 6-51. *Computed pH profiles along Section 1 (see Figure 6-50) for the sensitivity cases (Table 4-9), at the end of the simulation period. Case II, MX-80 bentonite buffer. Initial groundwater compositions are listed in Table 4-7.*

When the Ca/Na of the groundwater entering through the fracture is 10, a considerable amount of calcite is predicted to precipitate in the backfilled tunnel (Figure 6-52), and therefore, the pH of the backfill porewater decreases to 6.7 (Figure 6-51), at the end of the simulation period.

The initial amount of calcite in the backfill is 5.56 wt% (Table 4-3). After 100,000 years of simulation, most of the sensitivity cases lead to a slight increase of the amount of calcite in the backfill. Two cases lead to a more remarkable amount of calcite precipitated (Figure 6-52). These are the cases where the Ca/Na of the groundwater entering through the fracture is 10 and 1. In the first case, the final amount of calcite in the backfill is near 18 wt%, while in the second case it is around 8 wt%.

Computed results indicate that in most of the cases, including the reference case, gypsum is exhausted at the end of the 100,000 years of simulation (Figure 6-53). The initial amount of gypsum in the backfill is 0.56 wt% (Table 4-3).

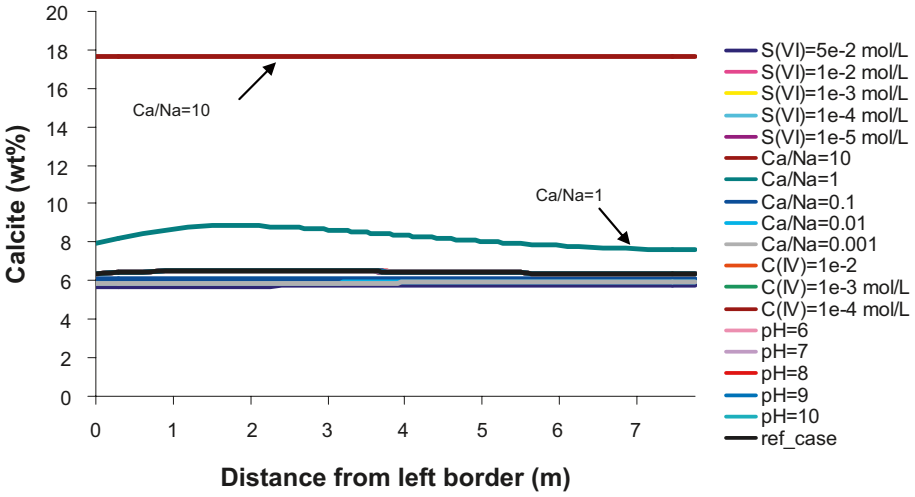

Figure 6-52. *Computed profiles for the amount of calcite along Section 1 (see Figure 6-50) for the sensitivity cases (Table 4-9), at the end of the simulation period. Case II, MX-80 bentonite buffer. Initial contents are listed in Table 3-2 and in Table 4-3.*

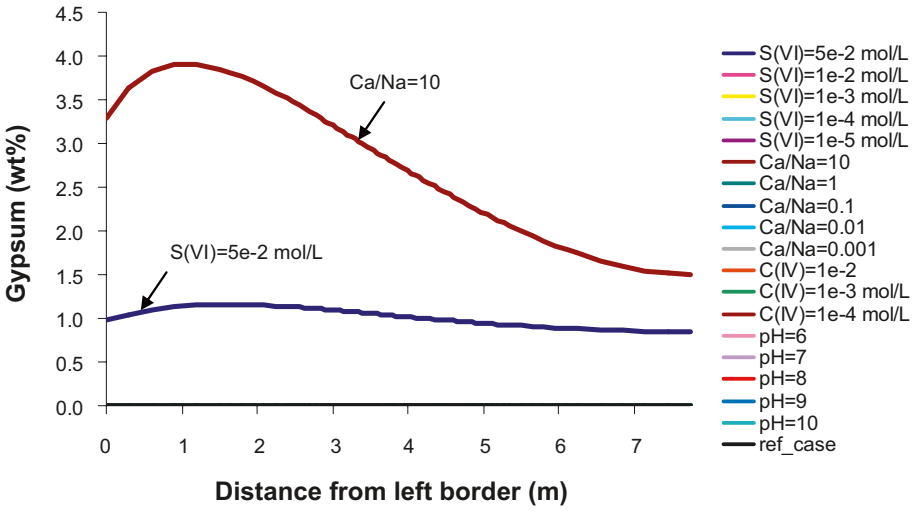

Figure 6-53. *Computed profiles for the amount of gypsum along Section 1 (see Figure 6-50) for the sensitivity cases (Table 4-9), at the end of the simulation period. Case II, MX-80 bentonite buffer. Initial contents are listed in Table 3-2 and in Table 4-3.*

When the Ca/Na of the inflowing water is 10, a remarkable increment of the amount of gypsum in the backfill is computed. In addition, if the concentration of sulphate in the groundwater entering through the fracture is $5 \cdot 10^{-2}$ mol/L, gypsum is also predicted to precipitate in the backfilled tunnel.

The initial amount of dolomite in the backfill is 11.11 wt% (Table 4-3). Most of the sensitivity cases developed here lead to an almost invariable amount of dolomite in the backfill (Figure 6-54).

In the two cases where a higher amount of calcite is predicted to precipitate (Ca/Na equal to 10 and to 1) dolomite dissolution is more pronounced (Figure 6-54). When the Ca/Na of the groundwater entering through the fracture is 10, a complete exhaustion of dolomite is predicted for the backfilled tunnel, and, when the Ca/Na of the groundwater is 1 the amount of dolomite decreases to around 9 wt%, mirroring the increase of calcite precipitated.

The concentration of calcium in the backfill porewater is controlled by the equilibrium with three Ca-bearing minerals (calcite, dolomite and gypsum) and the montmorillonite interlayer. The only

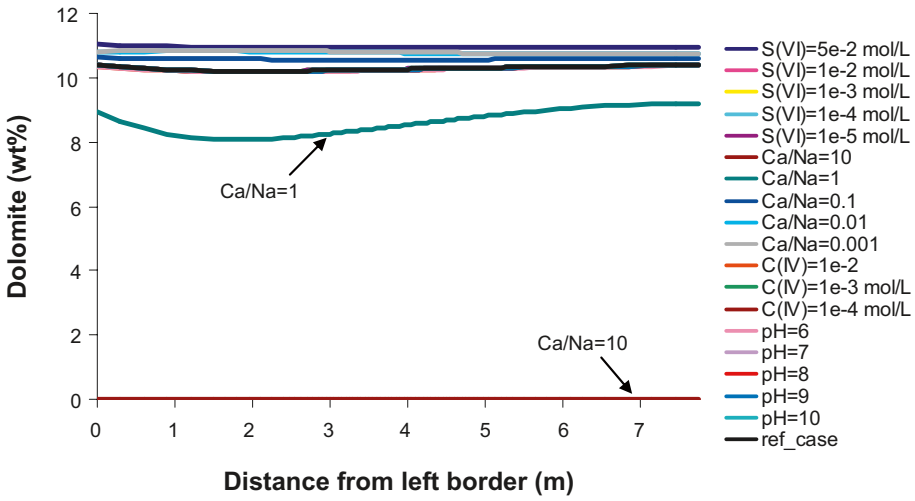

Figure 6-54. *Computed profiles for the amount of dolomite along Section 1 (see Figure 6-50) for the sensitivity cases (Table 4-9), at the end of the simulation period. Case II, MX-80 bentonite buffer. Initial contents are listed in Table 3-2 and in Table 4-3.*

case where the final amount of aqueous calcium is remarkably different from the initial concentration of calcium in the backfill porewater is that where the Ca/Na of the inflowing water is 10 (Figure 6-55). Although calcite precipitation is relatively important in this case, the capacity of the system to buffer the increment of aqueous calcium concentration is limited. Nevertheless, mixing between the backfill porewater and the fracture groundwater is able to provide some dilution of the added calcium. In the rest of the sensitivity cases, the concentration of calcium in the backfill porewater varies relatively little.

The initial amount of calcium in the montmorillonite interlayer of the backfill material is 40% (Table 3-2). Figure 6-56 shows that when the Ca/Na of the groundwater entering through the fracture is 10, the montmorillonite interlayer becomes relatively rich in calcium which occupies near 60% of the sites at the end of the simulation period. The rest of the sensitivity cases, including the reference case, lead to a slight depletion of calcium in the montmorillonite interlayer in favour of more sodium.

In the following paragraphs, the results computed for Case II with the MX-80 bentonite, along Section 2 of the modelled domain (Figure 6-50) are discussed.

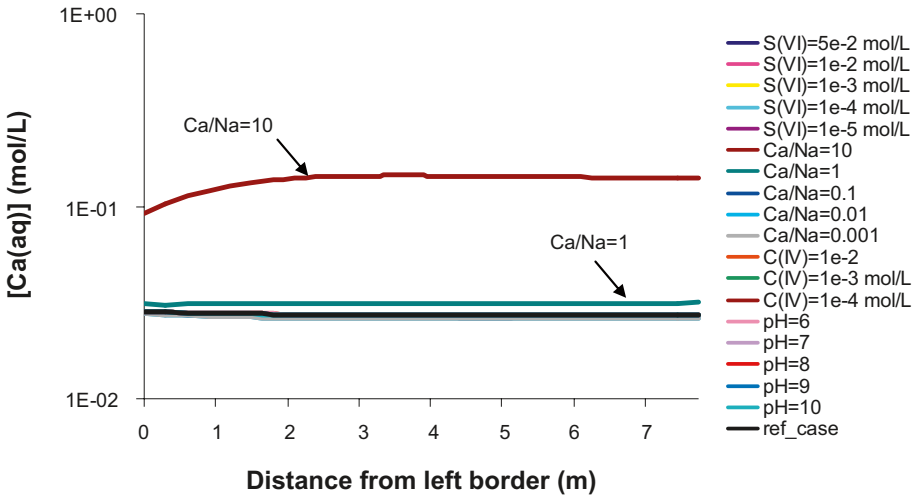

Figure 6-55. *Computed profiles for the concentration of aqueous calcium along Section 1 (see Figure 6-50) for the sensitivity cases (Table 4-9), at the end of the simulation period. Case II, MX-80 bentonite buffer. Initial groundwater compositions are listed in Table 4-7.*

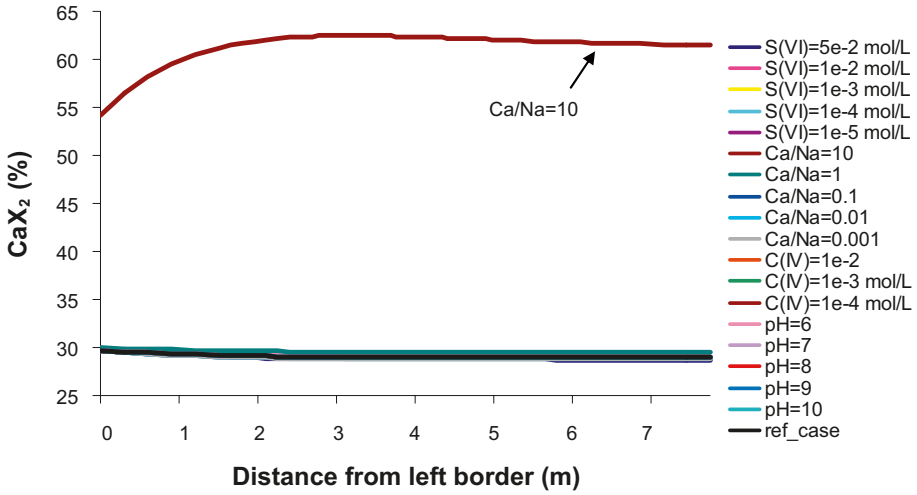

Figure 6-56. *Computed profiles for the concentration of calcium in the montmorillonite interlayer along Section 1 (see Figure 6-50) for the sensitivity cases (Table 4-9), at the end of the simulation period. Case II, MX-80 bentonite buffer.*

The initial pH of the backfill and MX-80 bentonite is 7.16 and 7.19, respectively (Table 4-7). The final pH computed along Section 2 for the Case II with the MX-80 bentonite, is between 6.69 and 7.29 (Figure 6-57). Although a relatively wide range of pH values (between 6 and 10) is considered for the groundwater entering through the fracture, the continuous mixing between the fracture groundwater and the backfill porewater, together with the geochemical reactions triggered by such mixing are able to buffer the pH perturbation induced by the groundwater entering through the fracture, so that the final pH of the bentonite buffer does not change much with respect to its original value.

The remarkable amount of calcite precipitated in the backfill for the case with a Ca/Na of 10 (Figure 6-58), leads to the lowest pH profile at the end of the simulation (6.7 in Figure 6-57). The highest final pH profile (around 7.29) is computed in the case where the fracture groundwater has a pH of 10.

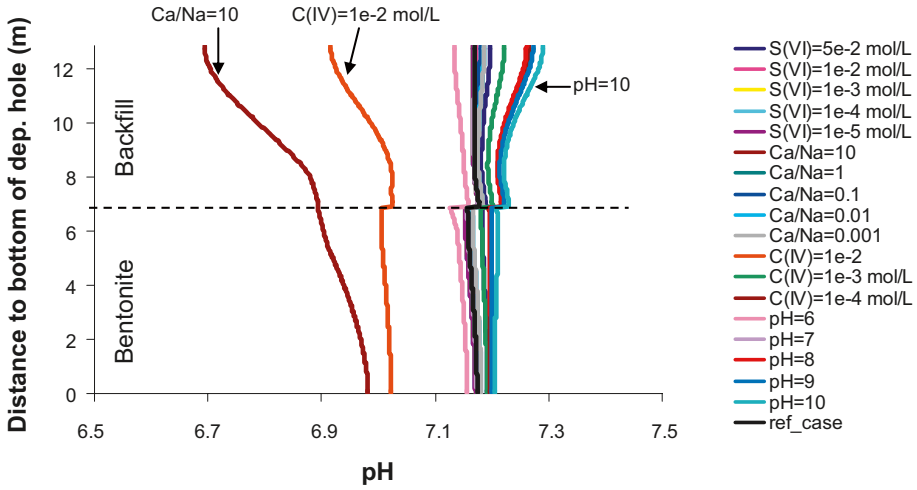

Figure 6-57. *Computed pH profiles along Section 2 (see Figure 6-50) for the sensitivity cases (Table 4-9), at the end of the simulation period. Case II, MX-80 bentonite buffer. Initial groundwater compositions are listed in Table 4-7.*

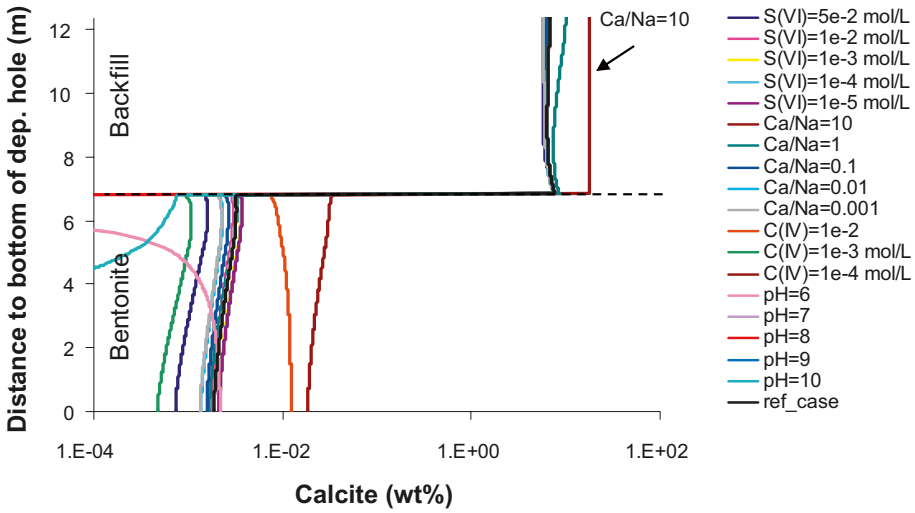

Figure 6-58. *Computed profiles for the amount of calcite along Section 2 (see Figure 6-50) for the sensitivity cases (Table 4-9), at the end of the simulation period. Case II, MX-80 bentonite buffer. Initial contents are listed in Table 3-2 and in Table 4-3.*

The MX-80 bentonite is initially depleted in carbonate minerals, while the backfill has an initial amount of calcite and dolomite of 5.56 and 11.11 wt%, respectively. The continuous inflow of most of the groundwater compositions analysed here leads to the precipitation of calcite in the MX-80 bentonite (Figure 6-58). In addition, the backfill material also enriches in calcite in some of the sensitivity cases. There is only one case where calcite is not predicted to precipitate in the MX-80 bentonite buffer. This is the case where the groundwater entering through the fracture has a pH of 9. In addition, if the pH of the inflowing groundwater is 10, calcite precipitates in the MX-80 bentonite only in the area close to contact with the backfill, on the upper part of the deposition hole.

The predicted calcite precipitation in the two engineered barriers is mainly triggered by the dissolution of gypsum which is initially present in both materials (Figure 6-59), and dolomite which is only present in the backfill (Figure 6-60).

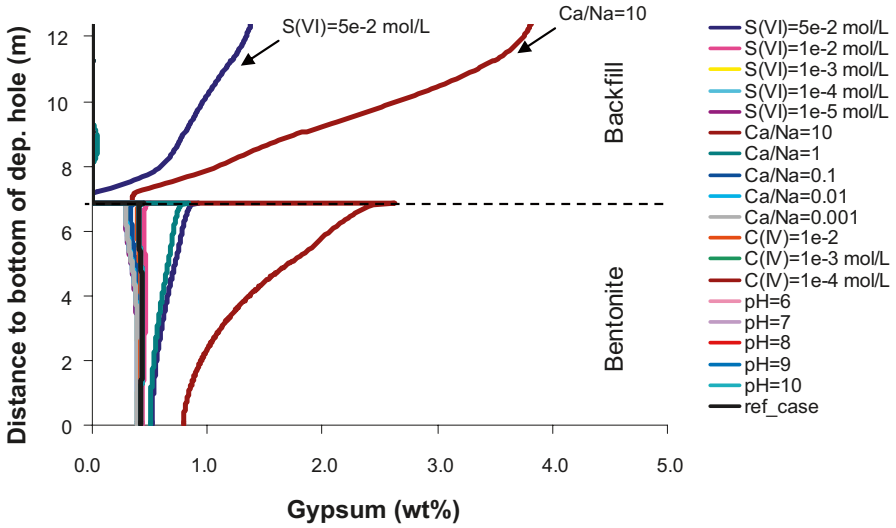

Figure 6-59. *Computed profiles for the amount of gypsum along Section 2 (see Figure 6-50) for the sensitivity cases (Table 4-9), at the end of the simulation period. Case II, MX-80 bentonite buffer. Initial contents are listed in Table 3-2 and in Table 4-3.*

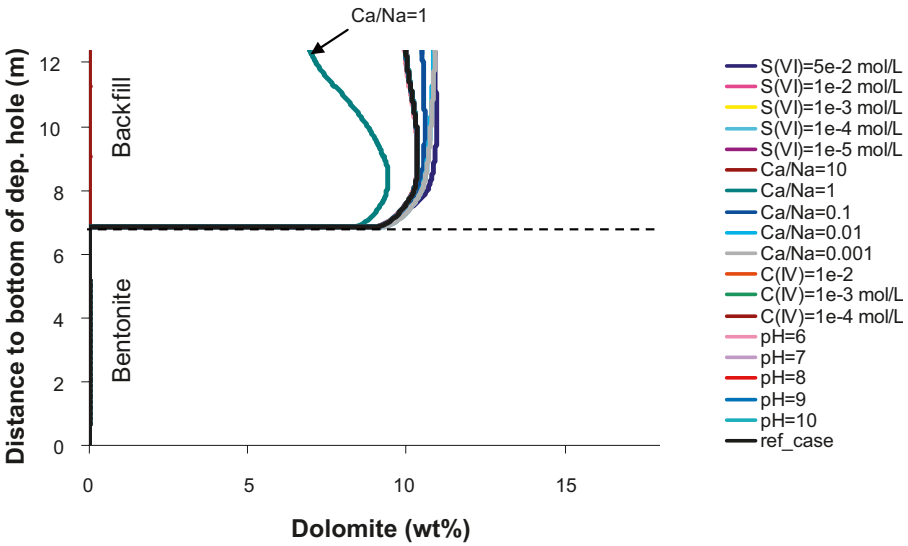

Figure 6-60. *Computed profiles for the amount of dolomite along Section 2 (see Figure 6-50) for the sensitivity cases (Table 4-9), at the end of the simulation period. Case II, MX-80 bentonite buffer. Initial contents are listed in Table 3-2 and in Table 4-3.*

The initial amount of gypsum in the backfill and MX-80 bentonite is 0.56 and 0.7 wt%, respectively. In all the sensitivity cases analysed, gypsum is predicted to be dissolved in the backfill material. The computed gypsum dissolution leads to its exhaustion in most of the sensitivity cases. Exception is made for the cases where the groundwater entering through the fracture has:

- Ca/Na of 1 and 10,
- Sulphate concentration of $5 \cdot 10^{-2}$ mol/L.

In the case with a Ca/Na of 10, gypsum is predicted to precipitate on the upper part of the backfilled tunnel and to dissolve in the lower part of the tunnel, close to the contact with the MX-80 bentonite buffer. In this case, gypsum is also predicted to precipitate in the upper part of the MX-80 bentonite buffer filling the deposition hole and to dissolve in the bottom of the deposition hole (lower part of "Bentonite" domain in Figure 6-59).

Dolomite is initially present in the backfill material (11.11 wt%, Table 4-3). The inflow of groundwater through the fracture disturbs the equilibrium of the backfill porewater with dolomite, leading to its dissolution. The amount of dolomite dissolved at the end of the simulation period is relatively small in most of the sensitivity cases (Figure 6-60).

Dolomite exhaustion in the backfill material is reached in only one sensitivity case. This is the case where the Ca/Na of the groundwater entering through the fracture is 10. The excess of aqueous calcium (Figure 6-61) provided by the inflow of this groundwater triggers a relatively fast dissolution of dolomite in favour of more calcite precipitated (Figure 6-58).

In most of the sensitivity cases, the concentration of aqueous calcium both in the MX-80 bentonite buffer and the backfill does not change much with respect to its initial value ($1.83 \cdot 10^{-2}$ and $2.97 \cdot 10^{-2}$ mol/L, respectively). Exception is made for the case with a Ca/Na of 10, where the concentration of aqueous calcium increases to ~0.15 mol/L in the backfill, and to 0.095 mol/L in the MX-80 bentonite (Figure 6-61).

Initially, calcium occupies 40% of the exchange sites of montmorillonite in the backfill material, and 18% in the MX-80 bentonite buffer. At the end of the 100,000 years, and for most of the sensitivity cases, the exchanger of montmorillonite in the backfill material is depleted in calcium (final occupancy around 29%, in Figure 6-62), in favour of more sodium adsorbed, while the montmorillonite in the MX-80 bentonite buffer is enriched in calcium (final occupancy between 29 and 31%, in Figure 6-62).

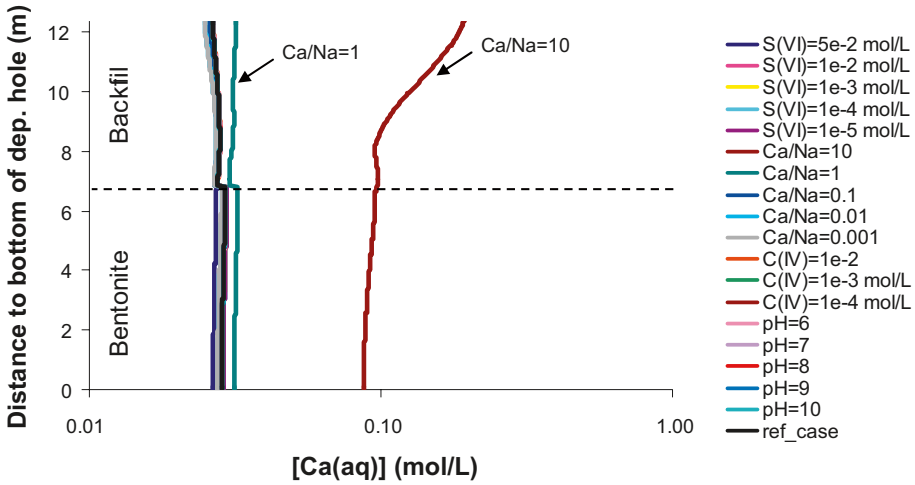

Figure 6-61. *Computed profiles for the concentration of aqueous calcium along Section 2 (see Figure 6-50) for the sensitivity cases (Table 4-9), at the end of the simulation period. Case II, MX-80 bentonite buffer. Initial groundwater compositions are listed in Table 4-7.*

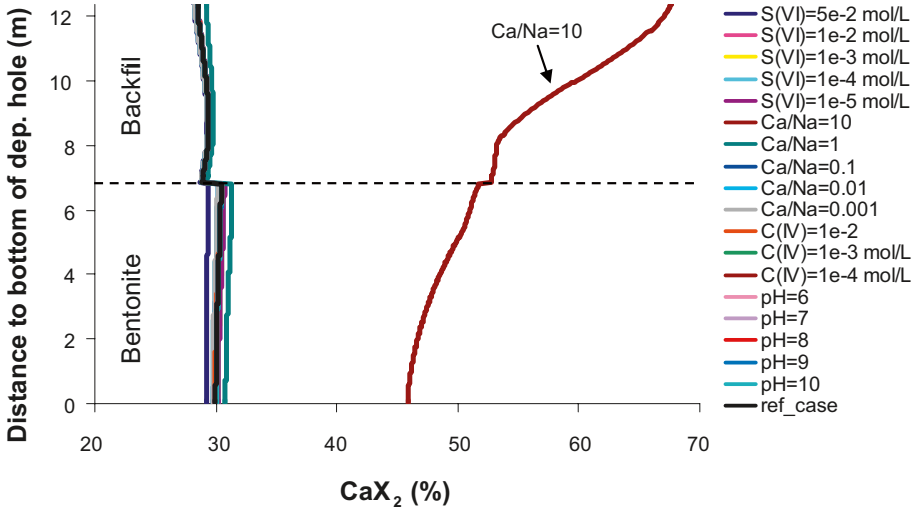

Figure 6-62. *Computed profiles for the concentration of calcium in the montmorillonite interlayer along Section 2 (see Figure 6-50) for the sensitivity cases (Table 4-9), at the end of the simulation period. Case II, MX-80 bentonite buffer.*

Again, the case with a Ca/Na of 10 leads to visibly distinct results than the remaining sensitivity cases. In this case, the exchanger of montmorillonite is enriched in calcium in both the MX-80 bentonite buffer and the backfill, at the end of the simulation period (Figure 6-62).

Besides analysing the computed results at the end of the simulation period for all the sensitivity cases considered for Case II, analysis of the time evolution of the outputs of these simulations is also performed here. In Figure 6-63, the location of the observation point for the analysis of the computed time evolution of selected chemical parameters for Case II is shown.

The initial pH of MX-80 bentonite is 7.19. It is seen in Figure 6-64 that the majority of the sensitivity cases leads to a very small decrease of the pH of the MX-80 bentonite porewater. Only two cases lead to a more visible pH decrease of the MX-80 bentonite porewater. These are the case where the carbonate concentration of the inflowing water is 10^{-2} mol/L, and the case with a Ca/Na of 10. Computed pH decrease is mostly due to the precipitation of calcite in the MX-80 bentonite buffer (Figure 6-65) which is triggered not only by the diffusion of aqueous carbonate and calcium respectively, but also by the dissolution of gypsum (Figure 6-66).

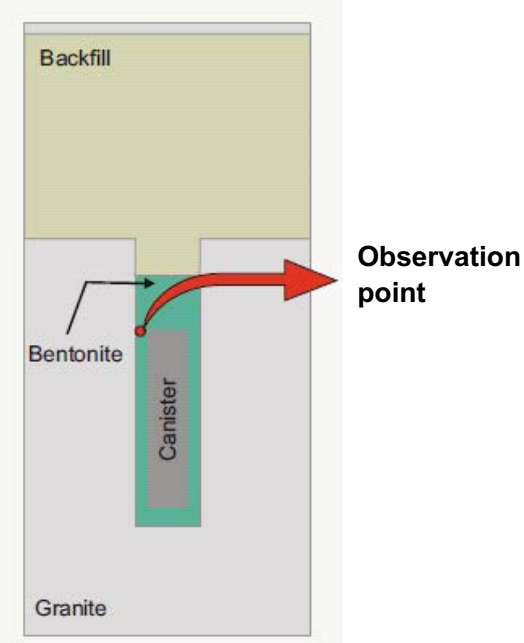

Figure 6-63. *Location of the observation point where the computed time evolution of selected chemical parameters has been analysed for the sensitivity cases considered in Case II.*

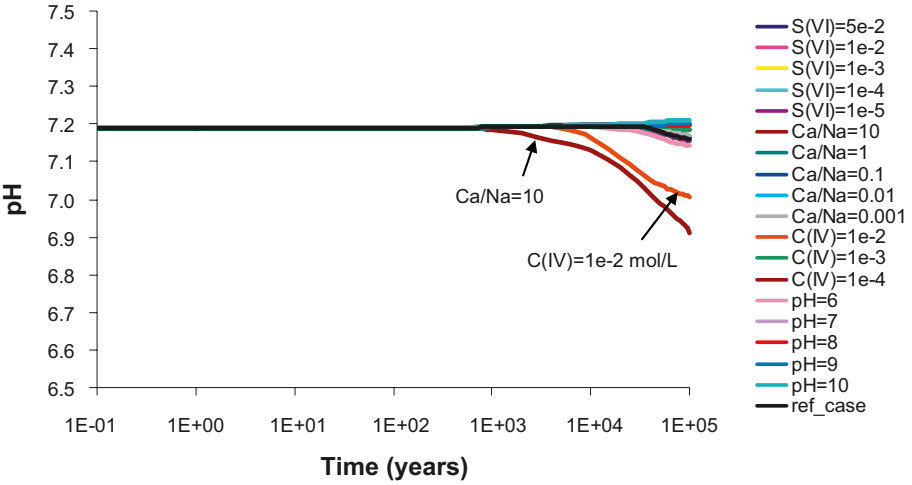

Figure 6-64. *Computed time evolution of pH in the observation point located in the bentonite (see Figure 6-63) for the nineteen inflow water compositions analysed in Case II (Table 4-9), MX-80 bentonite buffer. Initial groundwater compositions are listed in Table 4-7.*

Gypsum is predicted to be dissolved in the MX-80 bentonite in most of the sensitivity cases analysed for Case II (Figure 6-66). Only in three cases, gypsum is predicted to precipitate in the MX-80 bentonite:

- Ca/Na of the inflowing water is equal to 1 and 10,
- Sulphate concentration of the inflowing water is $5 \cdot 10^{-2}$ mol/L.

When the Ca/Na of the inflowing water is 10, gypsum precipitation along the simulated period leads to a final amount of near 1.8 wt% of gypsum in the MX-80 bentonite, while in the other two cases the final amount of gypsum is close to 0.7 wt% (Figure 6-66).

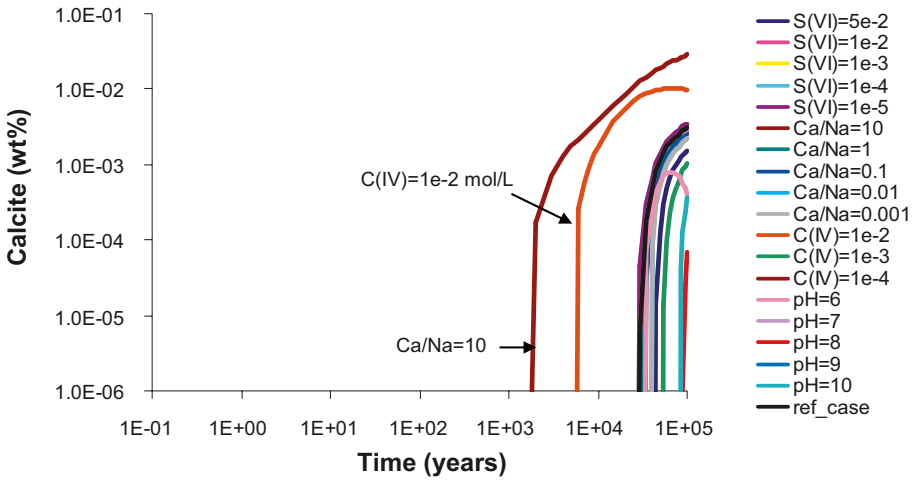

Figure 6-65. *Computed time evolution of calcite amount in the observation point located in the bentonite (see Figure 6-63) for the nineteen inflow water compositions analysed in Case II (Table 4-9), MX-80 bentonite buffer. Initial contents are listed in Table 3-2 and in Table 4-3.*

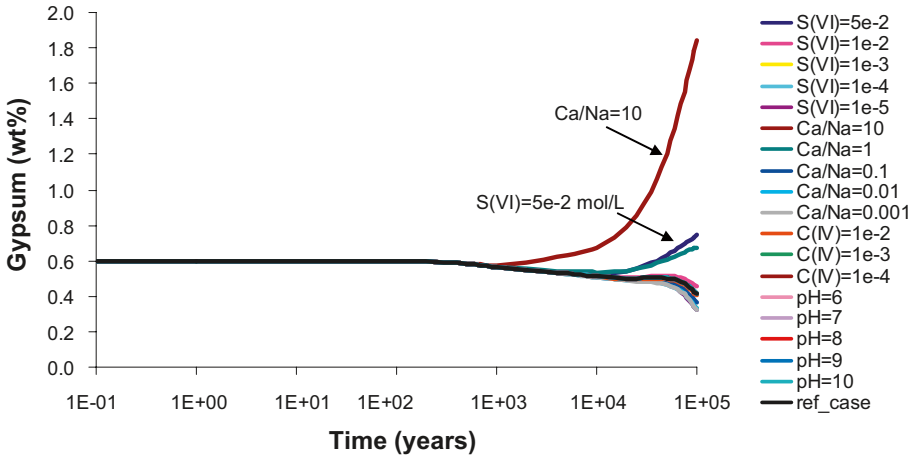

Figure 6-66. *Computed time evolution of gypsum amount in the observation point located in the bentonite (see Figure 6-63) for the nineteen inflow water compositions analysed in Case II (Table 4-9), MX-80 bentonite buffer. Initial contents are listed in Table 3-2 and in Table 4-3.*

Computed time evolution of calcium concentration in the porewater of MX-80 bentonite indicates that in the case that the Ca/Na of the inflowing water is 10, the final concentration of aqueous calcium in the MX-80 bentonite is close to 0.1 mol/L. The remaining sensitivity cases lead to a smaller increase of calcium concentration in the MX-80 bentonite porewater. In these cases, the final concentration of calcium is close to 0.03 mol/L (Figure 6-67). The computed increase of the concentration of aqueous calcium in the MX-80 bentonite in most of the sensitivity cases is due to the higher calcium concentration in the backfill porewater and to the predicted dissolution of gypsum along time (exception is made for the three above mentioned cases where gypsum is predicted to precipitate) (Figure 6-66).

Since the concentration of aqueous calcium increases in the MX-80 bentonite along time, the concentration of this cation in the montmorillonite interlayer also increases (Figure 6-68). The case leading to a more remarkable increase of calcium concentration in the montmorillonite interlayer is that where the Ca/Na of the inflowing groundwater is 10.

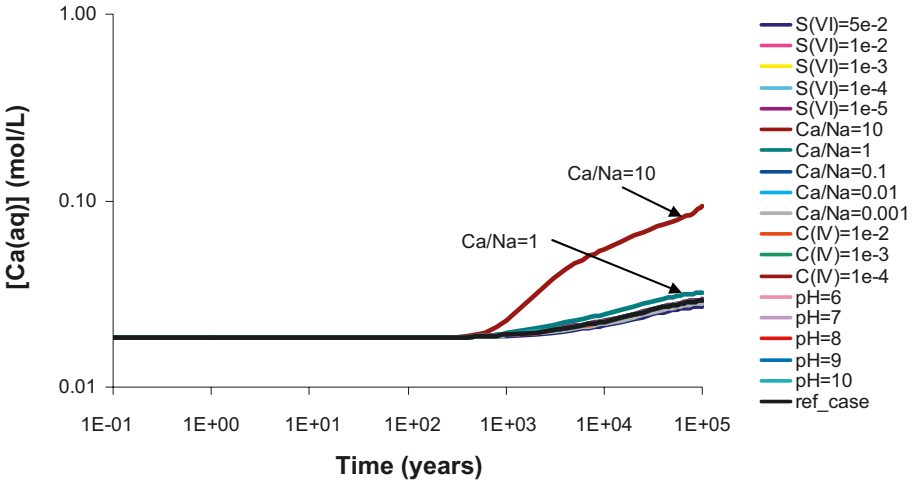

Figure 6-67. *Computed time evolution of aqueous concentration of calcium in the observation point located in the bentonite (see Figure 6-63) for the nineteen inflow water compositions analysed in Case II (Table 4-9), MX-80 bentonite buffer. Initial groundwater compositions are listed in Table 4-7.*

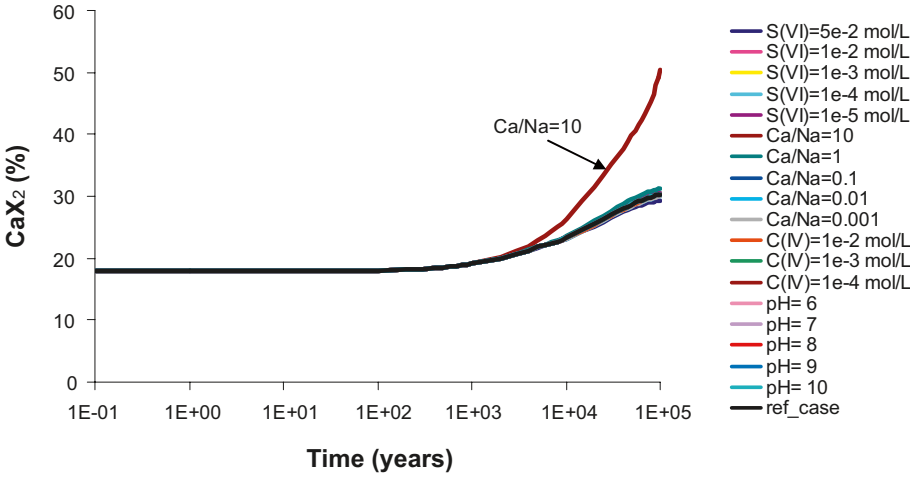

Figure 6-68. *Computed time evolution of calcium concentration in the montmorillonite interlayer in the observation point located in the bentonite (see Figure 6-63) for the nineteen inflow water compositions analysed in Case II (Table 4-9), MX-80 bentonite.*

6.2.3 Deponit CA-N bentonite buffer

The results computed for Case II with the Deponit CA-N bentonite buffer in the deposition hole are presented and discussed in the next paragraphs.

The continuous inflow of Forsmark groundwater through the backfilled tunnel and the Deponit CA-N bentonite buffer for 100,000 years has almost negligible effect on the pH of both engineered barriers (Figure 6-69). This is mainly provided by the buffering effect of the carbonate minerals present in both materials, which are calcite and dolomite.

The inflow of Forsmark groundwater leads to the precipitation of calcite close to the contact between the backfilled tunnel and the fracture where Forsmark groundwater enters into the tunnel (Figure 6-70). The amount of calcite in the Deponit CA-N bentonite buffer is almost unchanged after the 100,000 years of simulation.

While the calcite amount in both engineered barriers seems relatively unchanged after the 100,000 years of simulation, the gypsum amount suffers more pronounced modifications in both materials

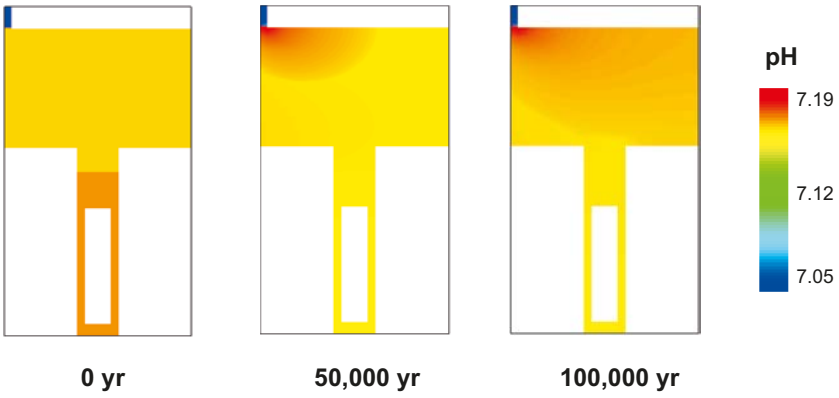

Figure 6-69. *Computed evolution of pH in the modelled domain of Reference Case II, Deponit CA-N bentonite buffer. Initial groundwater compositions are listed in Table 4-7.*

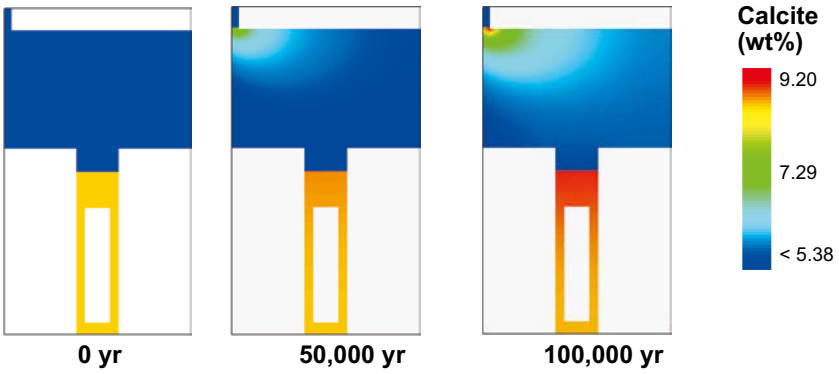

Figure 6-70. *Computed evolution of calcite content in the modelled domain of Reference Case II, Deponit CA-N bentonite buffer. Initial contents are listed in Table 3-2 and in Table 4-3.*

(Figure 6-71). It should be noted that the initial amount of carbonate minerals is much higher than the initial amount of gypsum in both materials, and therefore, for the same period of time analysed, the changes in the amount of gypsum are more visible than for the case of the carbonate minerals.

The continuous inflow of Forsmark groundwater leads to the dissolution of gypsum in the two engineered barriers that constitute the modelled domain of Case II. In the backfilled tunnel, gypsum is practically exhausted after the 100,000 years of simulation, while in the Deponit CA-N bentonite buffer the gypsum amount is visibly reduced, but not exhausted (Figure 6-71).

As for calcite, the amount of dolomite in the modelled domain of Case II seems to be relatively unchanged after the 100,000 years of simulation (Figure 6-72). The continuous inflow of Forsmark groundwater into the modelled domain leads to the dissolution of dolomite in the backfilled tunnel, while in the Deponit CA-N bentonite buffer the amount of dolomite is almost unchanged after the 100,000 years of simulation.

The results computed for the evolution of the montmorillonite exchanger in the two engineered barriers indicate that the exchanger becomes less rich in calcium due to the inflow of Forsmark groundwater (Figure 6-73). The decrease of calcium content in the exchanger is accompanied by an increase of sodium.

6.2.4 Sensitivity analysis, Case II, Deponit CA-N bentonite

In order to compare the results attained in all the sensitivity cases developed for Case II, with the Deponit CA-N bentonite buffer, the results computed at the end of the simulation period, along the vertical Section 2 of the modelled domain (see Figure 6-50) are analysed in the next paragraphs.

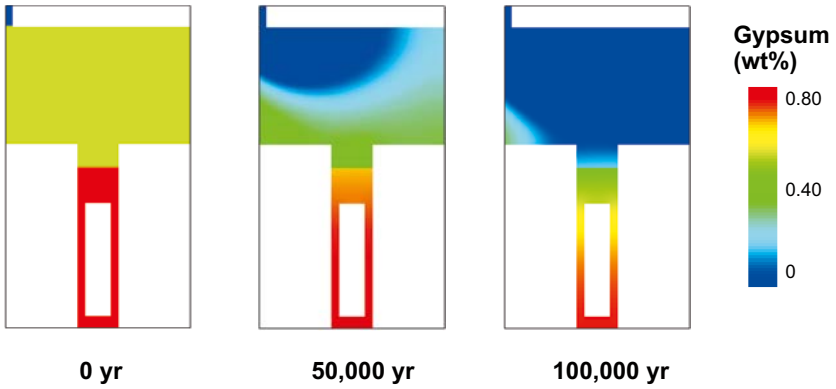

Figure 6-71. *Computed evolution of gypsum content in the modelled domain of Reference Case II, Deponit CA-N bentonite buffer. Initial contents are listed in Table 3-2 and in Table 4-3.*

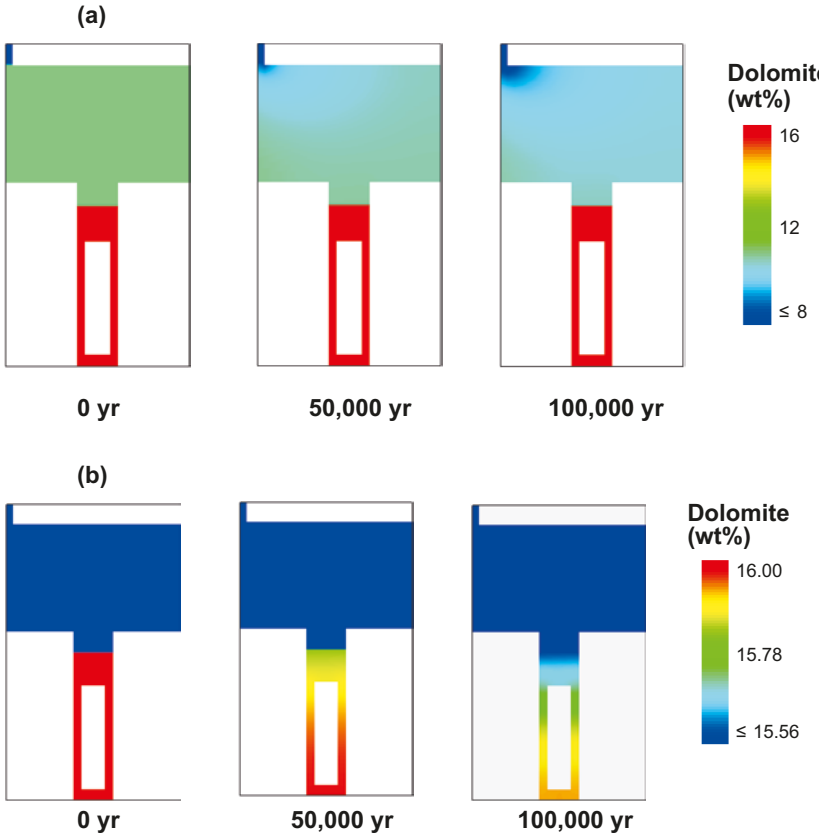

Figure 6-72. *Computed evolution of dolomite content in the modelled domain of Reference Case II, Deponit CA-N bentonite buffer. Different scales for the amount of dolomite are used in images (a) and (b), in order to visualize the changes in the backfill and in the bentonite buffer. Initial contents are listed in Table 3-2 and in Table 4-3.*

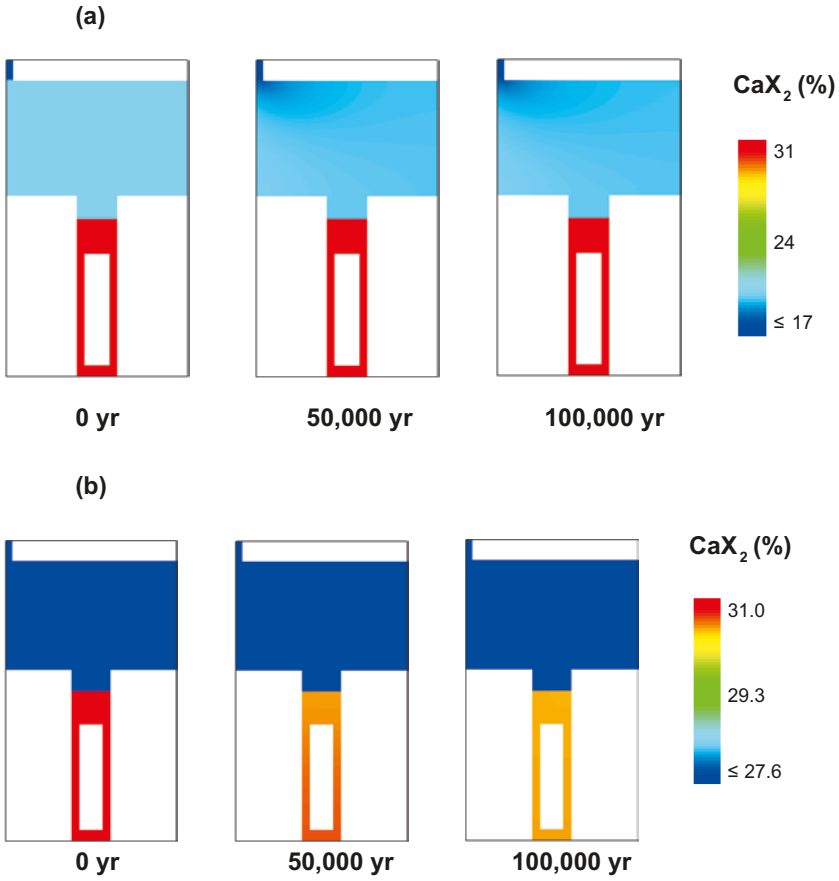

Figure 6-73. *Computed evolution calcium content in the montmorillonite interlayer in the modelled domain of Reference Case II, Deponit CA-N bentonite buffer. Different scales for the calcium content in the exchanger are used in images (a) and (b), in order to visualize the changes in the backfill and in the bentonite buffer.*

Computed pH profiles for all the sensitivity cases indicate that the initial homogenous pH value of 7.16 in the two materials (backfill and bentonite buffer) in some cases decreases, and in other cases increases. As already seen for Case II with MX-80 bentonite, the changes induced by the inflow of different types of groundwater compositions in the pH of the bentonite buffer are relatively small.

The three cases where the pH decreases are:

- pH of the inflowing water is equal to 6,
- carbonate concentration of the inflowing water is 10^{-2} mol/L,
- Ca/Na of the inflowing water is 10.

In the first of the three above-mentioned cases, the final pH of the two materials (7.14) decreases very little with respect to the initial value (7.16). In the second case, where the carbonate concentration of the inflowing water is 10^{-2} mol/L, pH decreases to ~6.9 in the backfill and ~7.0 in the bentonite buffer. In the case where the Ca/Na of the inflowing water is 10, the final pH of the backfill is between 6.7 (in the upper part of the tunnel) and 7.0 (in the lower part of the tunnel), while the final pH of the bentonite buffer is ~7.0, along the whole vertical section of the deposition hole. The pH increase predicted for the remaining sensitivity cases is mainly related to pH-buffering exerted by carbonate minerals initially present in these materials (Figure 6-75 and Figure 6-77).

The initial amount of calcite in the backfill and bentonite buffer is 5.56 and 8.00 wt%, respectively. In most of the analysed cases, the final amount of calcite in the Deponit CA-N bentonite is equal or slightly higher than the corresponding initial amount (Figure 6-75). The case leading to a more remarkable increase of the amount of calcite in the bentonite buffer is the one where the Ca/Na of

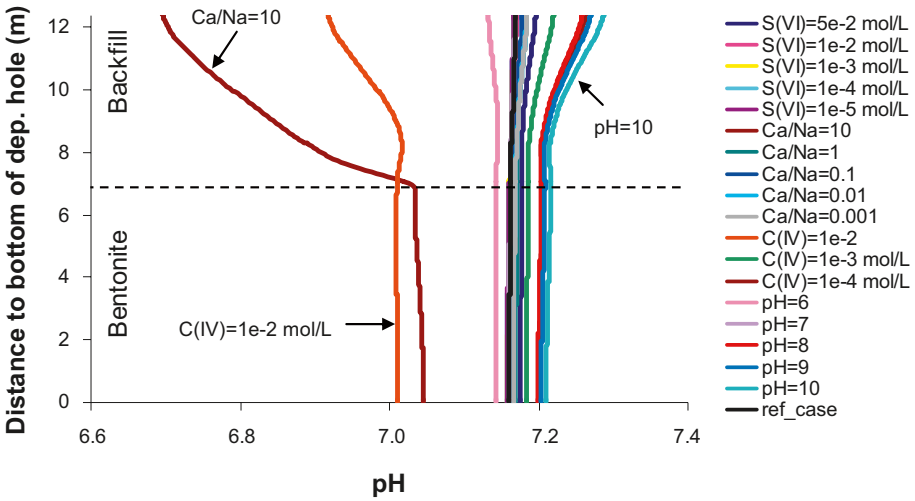

Figure 6-74. *Computed pH profiles along Section 2 (see Figure 6-50) for the sensitivity cases, at the end of the simulation period. Case II (Table 4-9), Deponit CA-N bentonite buffer. Initial groundwater compositions are listed in Table 4-7.*

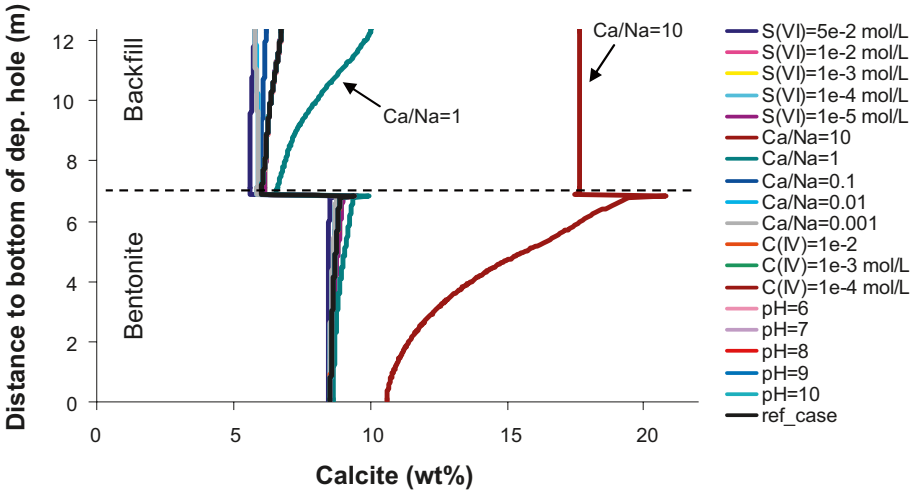

Figure 6-75. *Computed profiles for the amount of calcite along Section 2 (see Figure 6-50) for the sensitivity cases, at the end of the simulation period. Case II (Table 4-9), Deponit CA-N bentonite buffer. Initial contents are listed in Table 3-2 and in Table 4-3.*

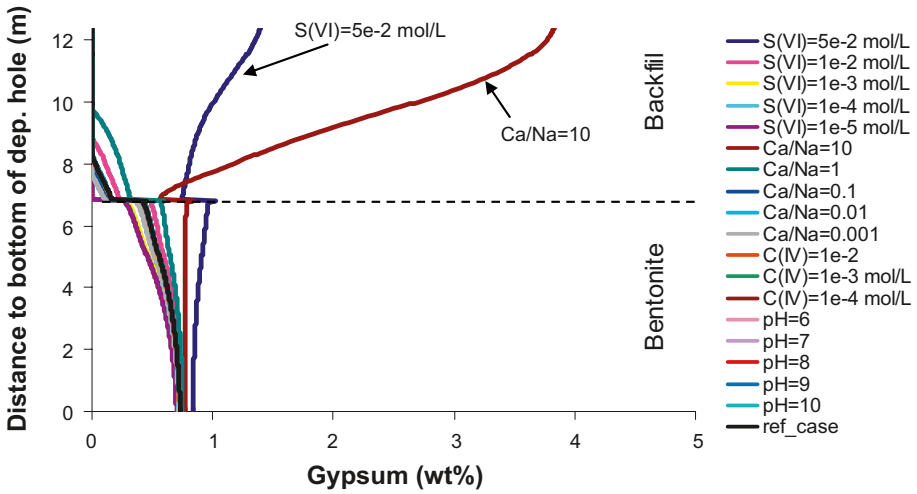

Figure 6-76. *Computed profiles for the amount of gypsum along Section 2 (see Figure 6-50) for the sensitivity cases, at the end of the simulation period. Case II (Table 4-9), Deponit CA-N bentonite buffer. Initial contents are listed in Table 3-2 and in Table 4-3.*

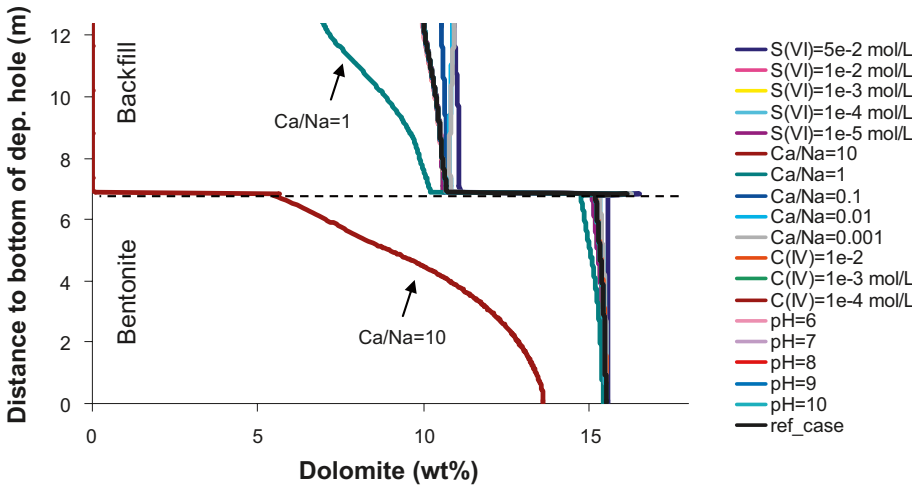

Figure 6-77. *Computed profiles for the amount of dolomite along Section 2 (see Figure 6-50) for the sensitivity cases, at the end of the simulation period. Case II (Table 4-9), Deponit CA-N bentonite buffer. Initial contents are listed in Table 3-2 and in Table 4-3.*

the inflowing water is 10. In this case, the final amount of calcite in the buffer varies between 10.6 and 22.0 wt%. In this case, the amount of calcite in the backfill material also increases remarkably, from the initial value of 11.11 wt% to 17.6 wt%.

In the backfill material, the majority of the sensitivity cases lead to a decrease of the amount of calcite (Figure 6-75). Calcite dissolution in the backfilled tunnel is mainly triggered by the continuous mixing between the groundwater entering through the fracture and the backfill porewater entering through the left boundary of the modelled domain. Although both waters are equilibrated with calcite, their mixing disturbs the initial equilibrium between calcite and the backfill porewater, leading to the dissolution of this mineral phase.

The initial amount of gypsum in the backfill and bentonite buffer is 0.56 and 0.8 wt%, respectively. The continuous inflow of the different groundwater compositions leads to the dissolution of gypsum in most of the analysed cases (Figure 6-76). Exception is made for two cases where gypsum is predicted to precipitate. These are the case where sulphate concentration of the inflowing water is $5 \cdot 10^{-2}$ mol/L and the case where the Ca/Na of the inflowing water is 10. The last of these two cases leads to a more remarkable precipitation of gypsum in the backfill.

The initial amount of dolomite in the backfill and bentonite buffer is 11.11 and 16 wt%, respectively. In all the cases analysed here, computed results indicate that dolomite is dissolved in both engineered barriers, in some cases to a lesser extent and in others to a wider extent (Figure 6-77), although in the buffer dolomite is not exhausted at the end of simulated time in any of the cases analysed. In the case where the Ca/Na of the inflowing water is 10, dissolution of dolomite leads to its exhaustion in the backfill material, while the bentonite buffer becomes considerably depleted in this mineral in the upper part of the deposition hole.

Computed results indicate that the concentration of aqueous calcium in both engineered materials is almost unchanged for most of the sensitivity cases, after 100,000 years of simulation. Exception is made for the case where the Ca/Na of the inflowing water is 10. In this case, the final concentration of aqueous calcium is remarkably higher than its initial concentration (Figure 6-78). The consequences of this case also lead to the increase of the concentration of this cation in the exchanger of montmorillonite, present in both engineered barriers (Figure 6-79).

The computed time evolution of selected parameters in the upper part of the deposition hole, filled with the Deponit CA-N bentonite (see Figure 6-63, for location of the observation point), is analysed in the next paragraphs.

Computed results indicate that the pH of the bentonite buffer changes very little along time in most of the sensitivity cases (Figure 6-80). In the cases where the pH of the inflowing water is 8, 9, and 10, the pH in the bentonite buffer slightly increases along time. In the cases where the Ca/Na of the inflowing water is 10, and where the concentration of carbonate is 10^{-2} mol/L, computed pH in the Deponit CA-N bentonite decreases to ~7.

Computed results indicate that in most of the sensitivity cases, the amount of calcite in the bentonite buffer increases very little along time. Exception is made for the case where the inflowing water has a Ca/Na of 10. In this case, calcite precipitation in the Deponit CA-N bentonite leads to a final amount of ~16 wt% (Figure 6-81).

Computed results indicate that gypsum is dissolved along time in the bentonite buffer, in most of the sensitivity cases analysed here (Figure 6-82). The two exceptional cases are the ones where the Ca/Na of the inflowing water is 10 and where the sulphate concentration of the inflowing water is $5 \cdot 10^{-2}$ mol/L. In the first of the two exceptional cases, gypsum is predicted to precipitate until 60,000 years, after which it starts to dissolve. In the case where the sulphate concentration of the inflowing water is $5 \cdot 10^{-2}$ mol/L, gypsum precipitation is computed along the whole simulation time.

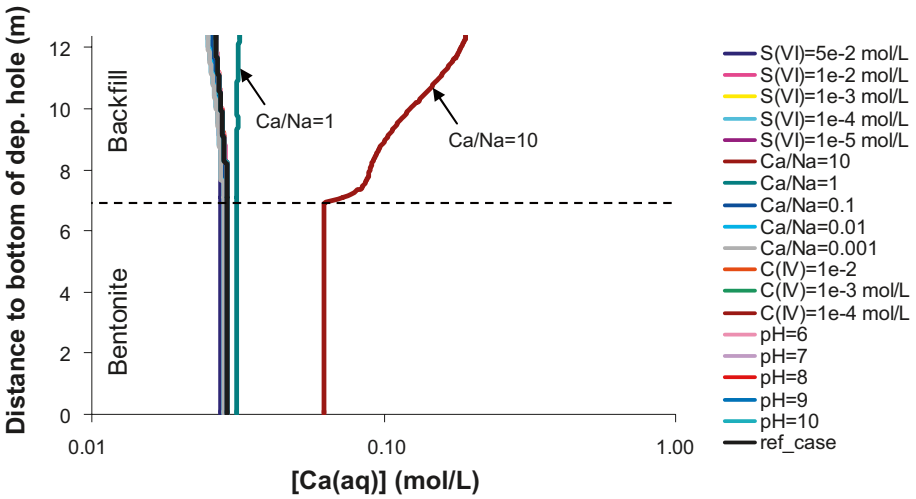

Figure 6-78. *Computed profiles for the concentration of aqueous calcium along Section 2 (see Figure 6-50) for the sensitivity cases, at the end of the simulation period. Case II (Table 4-9), Deponit CA-N bentonite buffer. Initial groundwater compositions are listed in Table 4-7.*

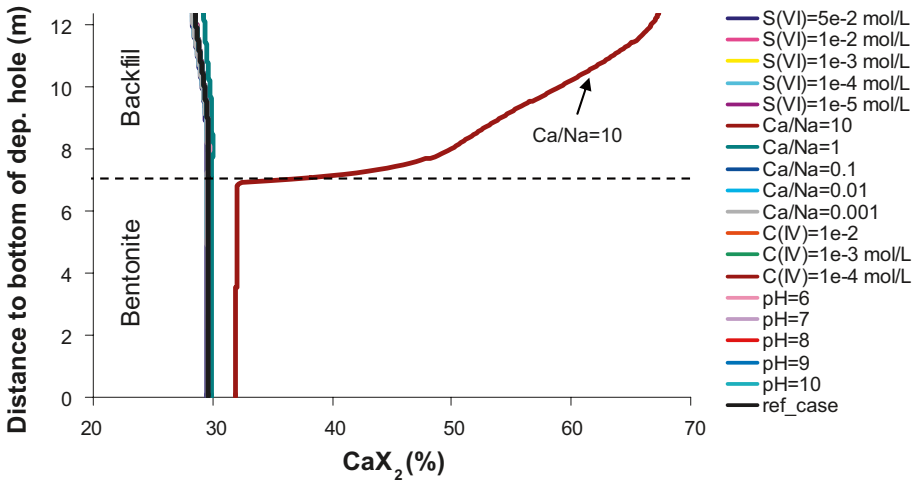

Figure 6-79. *Computed profiles for the concentration of calcium in the montmorillonite interlayer along Section 2 (Figure 6-50) for the sensitivity cases, at the end of the simulation period. Case II (Table 4-9), Deponit CA-N bentonite buffer.*

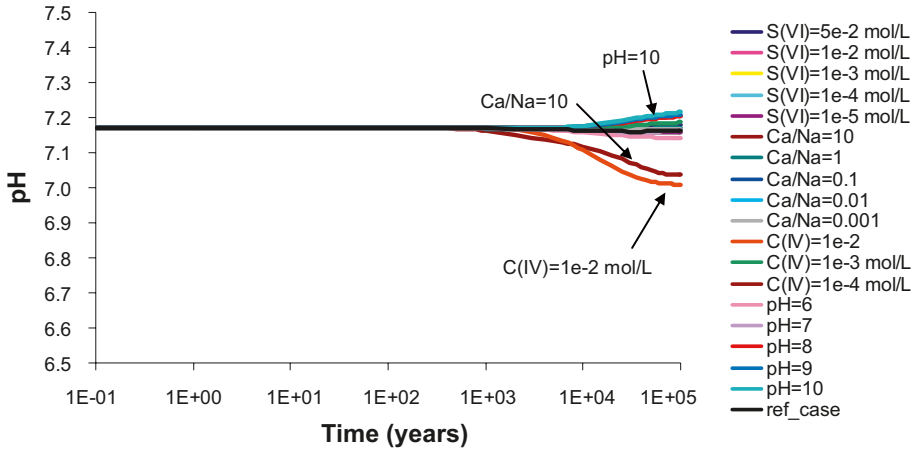

Figure 6-80. *Computed time evolution of pH in the observation point located in the bentonite (Figure 6-63) for the nineteen inflow water compositions analysed in Case II (Table 4-9), Deponit CA-N bentonite buffer. Initial groundwater compositions are listed in Table 4-7.*

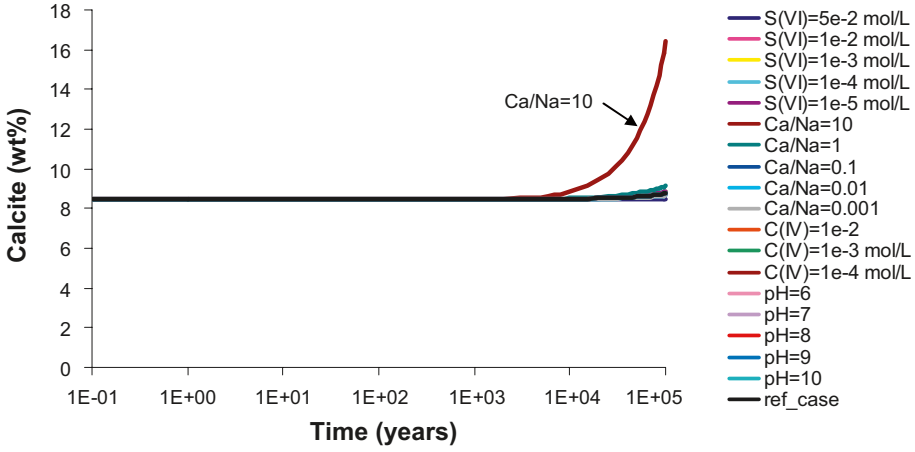

Figure 6-81. *Computed time evolution of calcite amount in the observation point located in the bentonite (see Figure 6-63) for the nineteen inflow water compositions analysed in Case II (Table 4-9), Deponit CA-N bentonite buffer. Initial contents are listed in Table 3-2 and in Table 4-3.*

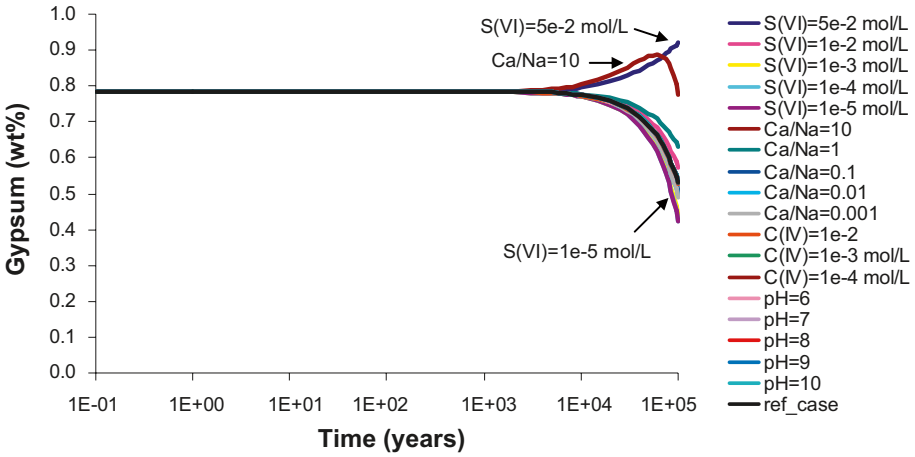

Figure 6-82. *Computed time evolution of gypsum amount in the observation point located in the bentonite (see Figure 6-63) for the nineteen inflow water compositions analysed in Case II (Table 4-9), Deponit CA-N bentonite buffer. Initial contents are listed in Table 3-2 and in Table 4-3.*

Gypsum dissolution is more pronounced in the case where the sulphate concentration of the inflowing water is 10^{-4} mol/L, and it is less pronounced in the case where the Ca/Na of the inflowing water is 1 (Figure 6-82).

The amount of dolomite in the bentonite buffer is almost unchanged after 100,000 years of simulation for most of the sensitivity cases analysed here (Figure 6-83).

Exception is made for the case where the Ca/Na of the inflowing water is 10. In this case, dolomite dissolution is much more intense which leads to a final amount of ~8 wt% of dolomite in the bentonite buffer. The perturbation induced by the inflow of a groundwater with a Ca/Na of 10 not only induces more pronounced changes on the amount of the primary minerals of the bentonite buffer, but also leads to a more visible increase of the concentration of calcium in the aqueous phase (Figure 6-84) and in the exchanger of montmorillonite (Figure 6-85).

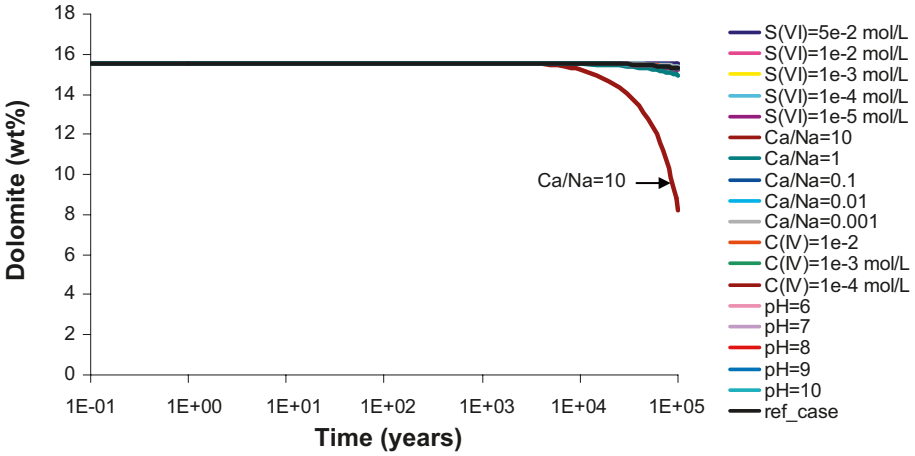

Figure 6-83. *Computed time evolution of dolomite amount in the observation point located in the bentonite (see Figure 6-63) for the nineteen inflow water compositions analysed in Case II (Table 4-9), Deponit CA-N bentonite buffer. Initial contents are listed in Table 3-2 and in Table 4-3.*

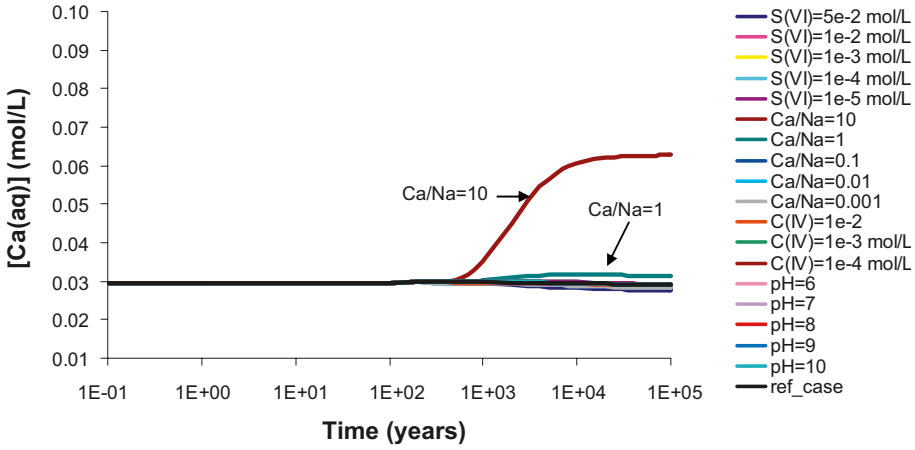

Figure 6-84. *Computed time evolution of aqueous calcium concentration in the observation point located in the bentonite (see Figure 6-63) for the nineteen inflow water compositions analysed in Case II (Table 4-9), Deponit CA-N bentonite buffer. Initial groundwater compositions are listed in Table 4-7.*

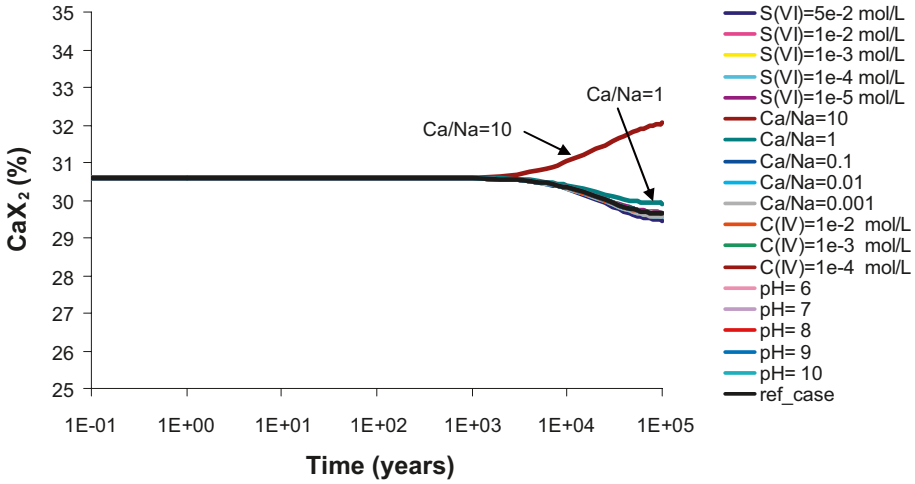

Figure 6-85. *Computed time evolution of calcium content in the montmorillonite interlayer in the observation point located in the bentonite (see Figure 6-63) for the nineteen inflow water compositions analysed in Case II (Table 4-9), Deponit CA-N bentonite buffer.*

6.2.5 Summary of Case II for the water-saturated period

In Table 6-2, a summary of the main results achieved in the sensitivity analysis developed for Case II is presented. It can be seen that although a wide range of pH values has been considered in the sensitivity analysis (from 6 to 10, Table 4-10), the final pH in the bentonite buffer of Case II does not reach such extreme values. These results reflect that the geochemical changes in the bentonite buffer, induced by the inflow of the different groundwater composition considered, are less pronounced in Case II than in Case I.

Table 6-2. Summary of the results of the sensitivity cases developed for Case II.

Bentonite	Variable	Value	Sensitivity Case
MX-80	Maximum pH	7.21	pH= 10
	Minimum pH	6.91	Ca/Na= 10
	Maximum amount of calcite	2.88E–2 wt%	Ca/Na= 10
	Minimum amount of gypsum	0.33 wt%	Ca/Na= 0.001
	Maximum amount of gypsum	1.85 wt%	Ca/Na= 10
	Maximum [Ca(aq)]	9.4E–2 mol/L	Ca/Na= 10
	Maximum [CaX_2]	50.0%	Ca/Na= 10
	Minimum [CaX_2]	29.3%	[S(VI)]= 5E–2 mol/L
Deponit CA-N	Maximum pH	7.22	pH= 10
	Minimum pH	7.01	[C(IV)]= 1E–2 mol/L
	Maximum amount of calcite	16.4 wt%	Ca/Na= 10
	Minimum amount of gypsum	0.42 wt%	[S(VI)]= 1E–5 mol/L
	Maximum amount of gypsum	0.92 wt%	[S(VI)]= 5E–2 mol/L
	Minimum amount of dolomite	8.0 wt%	Ca/Na= 10
	Maximum [Ca(aq)]	6.28E–2 mol/L	Ca/Na= 10
	Maximum [CaX_2]	32.1%	Ca/Na= 10
	Minimum [CaX_2]	29.5%	[S(VI)]= 5E–2 mol/L

6.3 Summary of the results attained in Cases I and II

A summary of the maximum deviations with respect to the initial value of selected parameters is presented for Case I and II Table 6-3 and Table 6-4, respectively). It is clear that when the hypothetical fracture intersects directly the bentonite buffer (Case I) the geochemical changes induced by the inflowing groundwater are much more pronounced than in Case II, where the hypothetical fracture intersects the backfilled tunnel.

In Case I (Table 6-3), depending on the type of bentonite buffer, the initial pH is modified by different processes in different sensitivity cases. When the MX-80 bentonite buffer is considered, the cases with pH values of 6 and high concentrations of aqueous carbonate species are characterized by more pronounced pH decreases, which are mainly related to the lack of carbonate minerals that could buffer the pH perturbation. When the Deponit CA-N bentonite buffer is considered, the cases with higher pH values and low concentration of aqueous carbonate species lead to an increase of the obtained pH values, as a consequence of the dissolution of carbonate minerals (induced by the inflow of undersaturated groundwaters). In addition, under scenarios with high concentrations of aqueous carbonate species, the precipitation of carbonate minerals is the key factor to explain the calculated pH decreases.

When the concentrations of aqueous sulphate species of the groundwater flowing through the fracture are relatively high, an increase of the amount of gypsum precipitated is computed as expected. On the other hand, the sensitivity cases with Ca/Na ratios of 10 lead to an enrichment of the aqueous solution, and the montmorillonite exchanger, in calcium.

Table 6-3. Summary of the computed maximum deviations from the initial value of selected parameters in the two types of bentonite buffer for Case I. If not mentioned, the deviation is computed for the end of the simulation (100,000 years). Initial values are listed in Table 3-2 and Table 4-7.

Variable →	pH	Calcite(wt%)	Gypsum(wt%)	Dolomite(wt%)	Ca(aq)(mol/L)	CaX_2(%)
MX-80 (initial value)	7.19	0.00	0.60	–	0.0183	18.0
Forsmark GW	–0.14 (a)	+0.0085 (a)	–0.60	–	+0.0047 (a)	+16.8 (a)
pH= 10	+1.04	0.00	–0.60	–	+0.0047	+16.8
pH= 9	+0.20	0.00	–0.60	–	+0.0047	+16.8
pH= 8	+0.09	0.00	–0.60	–	+0.0047	+16.8
pH= 7	–0.14	+0.002	–0.60	–	+0.0047	+16.7
pH= 6	–1.09	0.00	–0.60	–	+0.0047	+16.8
C(IV)= 10^{-4} mol/L	+0.01	0.00	–0.60	–	+0.0047	+16.8
C(IV)= 10^{-3} mol/L	–0.06	0.00	–0.60	–	+0.0047	+16.8
C(IV)= 10^{-2} mol/L	–0.68	+0.032	–0.60	–	+0.0047	+16.6
Ca/Na = 0.001	–0.11	0.00	–0.60	–	–0.0161	–10.4
Ca/Na = 0.01	–0.11	0.00	–0.60	–	–0.0154	–8.8
Ca/Na = 0.1	–0.10	0.00	–0.60	–	–0.0083	+4.4
Ca/Na = 1	–0.14	+0.010	–0.60	–	+0.0815	+40.9
Ca/Na = 10	–0.14	+0.010	+0.39	–	+0.9816	+66.0
S(VI)= 10^{-5} mol/L	–0.16	+0.0098	–0.60	–	+0.0047	+17.3
S(VI)= 10^{-4} mol/L	–0.16	+0.0097	–0.60	–	+0.0047	+17.3
S(VI)= 10^{-3} mol/L	–0.16	+0.0095	–0.60	–	+0.0047	+17.2
S(VI)= 10^{-2} mol/L	–0.13	+0.0073	–0.60	–	+0.0047	+16.5
S(VI)= $5 \cdot 10^{-2}$ mol/L	+0.20	+0.0010	+4.72	–	–0.0056	+4.8
Deponit CA-N (initial value)	7.16	8.48	0.78	16.	0.0334	36.0
Forsmark GW	–0.08 (b)	+7.00 (a)	–0.78	–6.48 (a)	–0.02 (a)	–14.3 (a)
pH= 10	+1.53	+5.09	–0.78	–5.20	–0.019	–14.2
pH= 9	+1.11	+5.09	–0.78	–5.23	–0.019	–14.2
pH= 8	+0.87	+5.09	–0.78	–5.21	–0.019	–14.2
pH= 7	+0.05	+5.09	–0.78	–5.16	–0.019	–14.2
pH= 6	–0.18	+5.11	–0.78	–5.40	–0.019	–14.1
C(IV)= 10^{-4} mol/L	+0.96	+5.09	–0.78	–5.23	–0.019	–14.2
C(IV)= 10^{-3} mol/L	+0.35	+5.09	–0.78	–5.18	–0.019	–14.2
C(IV)= 10^{-2} mol/L	–0.58	+5.10	–0.78	–5.24	–0.019	–14.3
Ca/Na = 0.001	+0.42	–2.05	–0.78	+1.37	–0.029	–21.7
Ca/Na = 0.01	+0.39	–1.77	–0.78	+1.12	–0.029	–21.2
Ca/Na = 0.1	+0.21	+1.00	–0.78	–1.41	–0.025	–17.6
Ca/Na = 1	+0.13 (c)	+16.88	–0.78	–16.00	0.060	+19.2
Ca/Na = 10	–0.10	+16.89	–0.63	–16.00	0.967	+48.0
S(VI)= 10^{-5} mol/L	–0.09	+5.05	–0.78	–5.12	–0.019	–13.9
S(VI)= 10^{-4} mol/L	–0.09	+5.05	–0.78	–5.12	–0.019	–13.9
S(VI)= 10^{-3} mol/L	–0.09	+5.06	–0.78	–5.12	–0.019	–13.9
S(VI)= 10^{-2} mol/L	+0.07	+5.10	–0.78	–5.16	–0.019	–14.4
S(VI)= $5 \cdot 10^{-2}$ mol/L	+0.26	+2.52	3.35	–2.78	–0.021	–17.4

Positive values an increase with respect to the initial value; Negative values a decrease with respect to the initial value; Cells in white refer to results computed for a flow rate of 0.1 m^3/yr; Cells in grey refer to results computed for a flow rate of 1E–3 m^3/yr; The more pronounced deviations from the initial value are in yellow cells. (a) flow rate of 10 m^3/yr; (b) flow rate of 10 m^3/yr, at 200 years; (c) value reached at 50,000 years;

Table 6-4. Summary of the computed maximum deviations from the initial value of selected parameters in the two types of bentonite buffer for Case II. Initial values are listed in Table 3-2 and Table 4-7.

Variable →	pH	Calcite (wt%)	Gypsum (wt%)	Dolomite (wt%)	Ca(aq) (mol/L)	CaX_2 (%)
MX-80 (initial value)	7.19	0.0	0.60	–	0.0184	18.0
Forsmark GW	–0.03	+0.0031	–0.19	–	+0.0108	+12.4
pH= 10	+0.02	+0.0004	–0.18	–	+0.0108	+12.4
pH= 9	+0.01	0.0	–0.18	–	+0.0108	+12.4
pH= 8	+0.01	+0.0001	–0.19	–	+0.0108	+12.3
pH= 7	–0.03	+0.0030	–0.19	–	+0.0108	+12.4
pH= 6	–0.05	+0.0004	–0.18	–	+0.0108	+12.4
C(IV)= 10^{-4} mol/L	+0.01	0.0	–0.19	–	+0.0108	+12.3
C(IV)= 10^{-3} mol/L	–0.01	+0.0010	–0.19	–	+0.0108	+12.3
C(IV)= 10^{-2} mol/L	–0.18	+0.0098	–0.19	–	+0.0108	+12.1
Ca/Na = 0.001	–0.02	+0.0022	–0.27	–	+0.0099	+12.1
Ca/Na = 0.01	+0.02	+0.0022	–0.27	–	+0.0099	+12.2
Ca/Na = 0.1	–0.02	+0.0026	–0.24	–	+0.0103	+13.2
Ca/Na = 1	–0.03	+0.0030	+0.07	–	+0.0138	+13.2
Ca/Na = 10	–0.28	+0.0288	+1.24	–	+0.0758	+32.3
S(VI)= 10^{-5} mol/L	–0.03	+0.0035	–0.28	–	+0.0112	+12.6
S(VI)= 10^{-4} mol/L	–0.03	+0.0035	–0.28	–	+0.0112	+12.6
S(VI)= 10^{-3} mol/L	–0.03	+0.0034	–0.26	–	+0.0111	+12.6
S(VI)= 10^{-2} mol/L	–0.03	+0.0029	–0.15	–	+0.0106	+12.2
S(VI)= $5 \cdot 10^{-2}$ mol/L	–0.01	+0.0015	+0.14	–	+0.0088	+11.3
Deponit CA-N (initial value)	7.16	8.48	0.78	16.	0.0334	36.0
Forsmark GW	–0.01	+0.29	–0.25	–0.27	–0.0007	–0.9
pH= 10	+0.04	+0.29	–0.25	–0.27	–0.0007	–0.9
pH= 9	+0.04	+0.29	–0.25	–0.27	–0.0007	–0.9
pH= 8	+0.03	+0.29	–0.25	–0.27	–0.0007	–0.9
pH= 7	–0.01	+0.29	–0.25	–0.27	–0.0007	–0.9
pH= 6	–0.03	+0.29	–0.25	–0.27	–0.0007	–0.9
C(IV)= 10^{-4} mol/L	+0.03	+0.29	–0.25	–0.27	–0.0007	–0.9
C(IV)= 10^{-3} mol/L	+0.02	+0.29	–0.25	–0.27	–0.0007	–0.9
C(IV)= 10^{-2} mol/L	–0.16	+0.29	–0.26	–0.26	–0.0007	–0.9
Ca/Na = 0.001	0.00	+0.19	–0.29	–0.17	–0.0015	–1.0
Ca/Na = 0.01	0.00	+0.19	–0.29	–0.18	–0.0014	–1.0
Ca/Na = 0.1	0.00	+0.23	–0.27	–0.21	–0.0012	–1.0
Ca/Na = 1	0.00	+0.65	–0.15	–0.60	+0.0017	–0.7
Ca/Na = 10	–0.13	+7.96	–0.01	–7.23	+0.0331	+1.5
S(VI)= 10^{-5} mol/L	–0.01	+0.37	–0.36	–0.34	–0.0005	–0.9
S(VI)= 10^{-4} mol/L	–0.01	+0.37	–0.36	–0.34	–0.0005	–0.9
S(VI)= 10^{-3} mol/L	–0.01	+0.36	–0.34	–0.33	–0.0006	–0.9
S(VI)= 10^{-2} mol/L	–0.01	+0.26	–0.21	–0.24	–0.0008	–1.0
S(VI)= $5 \cdot 10^{-2}$ mol/L	+0.01	+0.01	+0.14	–0.01	–0.0021	–1.1

Positive values an increase with respect to the initial value; Negative values a decrease with respect to the initial value; The more pronounced deviations from the initial value are in yellow cells.

7 Conclusions

The numerical results obtained for the thermal period indicate that during the saturation of the partially saturated bentonite, the groundwater circulating along a hypothetical fracture that intersects a deposition hole progressively saturates the bentonite. Regardless the velocity of saturation of the bentonite, a piston-like flow is predicted for this process regarding the solutes of the system. In addition, due to the thermal conditions imposed by the heat released from the HLNW canister, evaporation of the bentonite porewater could occur temporarily around the canister. Nevertheless, the capillary forces within the bentonite pores and also the hydraulic gradient imposed by the groundwater that penetrates the bentonite pores minimize the drying effect triggered by the vapour pressure.

The main conclusions reached for the thermal period are:

- The mineralogical changes of accessory minerals in the bentonite are mainly controlled by: (1) the dependence of mineral solubilities on the thermal evolution of the near-field and (2) the solute transport and mass transfer between the groundwater flowing along the fracture and the bentonite porewater which dictate the evolution of the concentration gradients.
- Solute transport within the bentonite pores is controlled by advection during the saturation of the bentonite. Afterwards, diffusion becomes more important. Nevertheless, for a slow saturation of the bentonite (1,000 and 2,000 years), diffusion may also be important during the saturation stage.
- If the flow rate along the fracture is high, the composition of Forsmark groundwater is not affected by the composition of the bentonite porewater, and therefore, the concentration gradients are constant at the granite/bentonite interface. In this scenario, the composition of bentonite porewater approaches that of Forsmark groundwater faster than if the flow rate along the fracture is low.
- In both bentonite types analysed (MX-80 and Deponit CA-N), primary anhydrite and quartz are predicted to dissolve and secondary calcite precipitates.
- In the MX-80 bentonite, precipitation of calcite is practically negligible and it is re-dissolved in the long-term. For higher flow rates along the fracture, calcite precipitation becomes more important due to the higher concentration gradient established at the granite/bentonite interface. The montmorillonite exchanger of the MX-80 bentonite becomes richer in calcium at the expense of sodium. And, as higher the advective flow along the fracture, more pronounced will be the replacement of sodium by calcium.
- In the Deponit CA-N bentonite, primary dolomite is dissolved in the outer (cold) part of the bentonite, and it precipitates in the inner (hot) boundary. But, during the cooling stage dolomite re-dissolves until its exhaustion. Secondary calcite precipitates replacing the dissolved dolomite. If the flow rate along the fracture is low, the montmorillonite exchanger is predicted to be depleted in calcium in favour of more magnesium adsorbed. On the other hand, if the advective flow along the fracture is high, sodium is predicted to replace calcium in the montmorillonite exchanger.

Computed results for the water-saturated period of the near-field indicate that the interaction between the minerals that constitute the MX-80 bentonite and the Forsmark groundwater that occurs nowadays at the depth of the future repository leads to an overall depletion in gypsum in favour of more calcite. In addition, the initially Na-rich montmorillonite interlayer is predicted to enrich in calcium.

In the case that the bentonite buffer is composed of Deponit CA-N bentonite, the inflow of Forsmark groundwater leads to the dissolution of gypsum and dolomite in favour of more calcite precipitated. In addition, the initially Mg and Ca-rich montmorillonite interlayer becomes depleted in these cations and enriched in sodium.

In both bentonite types, the inflow of Forsmark groundwater leads to relatively small changes on the pH of the near-field with respect to the pH values expected for the initial porewater of the engineered barriers.

Several sensitivity cases were developed for the water-saturated period of the near-field, which encompass distinct advective and chemical scenarios. The results of the sensitivity analysis performed for Case I (a water conductive fracture intersecting the deposition hole) indicate that:

- For higher flow rates in the fracture, more pronounced geochemical changes occur. In both bentonite types analysed, gypsum is exhausted earlier in the cases with a higher flow rate. More calcite precipitates in these cases (in both bentonite types), and therefore, the pH drops to lower values (around 7) in the MX-80 bentonite. Because dolomite, that is present in the Deponit CA-N bentonite, dissolves faster in the cases with a higher flow rate, the pH does not decrease (like in the cases with the MX-80 bentonite), but it increases to 7.23.
- The lowest pH value computed for the MX-80 bentonite buffer is 6.10 which is reached in the case where the inflowing groundwater has a pH of 6. The computed pH drop is mainly related to the lack of carbonate minerals in this type of bentonite. On the other hand, the lowest pH value computed for the Deponit CA-N bentonite is 6.53 which is reached in the case where the inflowing groundwater has a high concentration of aqueous carbonate (10^{-2} mol/L). The computed pH drop is related to the enhanced precipitation of carbonate minerals induced by the excess of aqueous carbonate.
- The highest pH value computed for the MX-80 bentonite is 8.23 which is reached in the case where the inflowing groundwater has a pH of 10, and the flow rate along the fracture is 0.1 m^3/yr. The highest pH value computed for the Deponit CA-N bentonite is 8.66 and it is reached in the same case as for the MX-80 bentonite. The computed pH increase is mainly due to diffusion of high-pH into the bentonite pores.
- When the inflowing water has a Ca/Na of 10, the excess of calcium in the bentonite buffer leads to the highest amount of calcite precipitated, and the highest concentration of calcium in the aqueous phase and in the montmorillonite interlayer.
- Gypsum is predicted to dissolve in most of the sensitivity cases, except when the inflowing water has a Ca/Na of 10 and when it has a high sulphate concentration ($5 \cdot 10^{-2}$ mol/L).
- Dolomite is predicted dissolve in most of the sensitivity cases with the Deponit CA-N bentonite, except in the cases where the inflowing groundwater has a Ca/Na of 0.0001 and also when it has a high sulphate concentration ($5 \cdot 10^{-2}$ mol/L).

By comparing the results computed for the thermal period and the water-saturated period (Case I), it is seen that the evolution of the amount of Ca-sulphate in the buffer is similar for both periods. Ca-sulphate minerals tend to dissolve due to the inflow of Forsmark groundwater. Nevertheless, during the warming period, anhydrite is predicted to precipitate close to the copper canister, but as soon as the temperature drops it will tend to dissolve. When the reference Forsmark groundwater is considered, secondary calcite precipitation in the MX-80 bentonite is predicted to be very small and temporary in both periods analysed.

The sensitivity cases developed for the Case II indicate that:

- The geochemical evolution of the bentonite buffer is similar to that computed for Case I, but it evolves at a much slower rate, since mixing of the groundwater entering through the fracture with the backfill porewater buffers the disturbing effect of the inflowing "foreign" groundwater.
- The geochemical evolution of the backfill does not change much regardless of the type of bentonite considered in the deposition hole.
- Calcite is predicted to precipitate in the backfilled tunnel in all the sensitivity cases considered. The highest amounts of calcite precipitated are computed in the cases where the inflowing water has a Ca/Na > 1. Therefore, the lowest pH computed for the backfill is 6.76, in the case where the inflowing water has a Ca/Na of 10.
- The highest concentration of calcium in the backfill ($1.4 \cdot 10^{-1}$ mol/L), at the end of the simulation period, is computed for the case with Ca/Na of 10.

8 References

SKB's (Svensk Kärnbränslehantering AB) publications can be found at www.skb.se/publications.

Arcos D, Grandia F, Domènech C, 2006. Geochemical evolution of the near-field of a KBS-3 repository. SKB TR-06-16 report.

Arcos D, Grandia F, Domènech C, Fernández A M, Villar M V, Muurinen A, Carlsson T, Sellin P, Hernán P, 2008. Long-term geochemical evolution of the near field repository: Insights from reactive transport modelling and experimental evidences. Journal of Contaminant Hydrology, 102: 196–209.

Birgersson M, Karnland O, 2009. Ion equilibrium between montmorillonite interlayer space and an external solution – Consequences for diffusional transport. Geochimica et Cosmochimica Acta, 73: 1908–1923.

Bourg IC, Bourg ACM, Sposito G, 2003. Modeling diffusion and adsorption in compacted bentonite: a critical review. Journal of Contaminant Hydrology, 61: 293–302.

Dershowitz W, Winberg A, Hermansson J, Byegard J, Tullborg E-L, Andersson P, Mazurek M, 2003. Äspö Hard Rock Laboratory. Äspö Task Force on modelling of groundwater flow and transport of solutes. Task 6C. A semi-synthetic model of block scale conductive structures at the Äspö HRL. SKB IPR-03-13, Svensk Kärnbränslehantering AB.

Duro L, Grivé M, Cera E, Domènech C, Bruno J, 2006. Update of a thermodynamic database for radionuclides to assist solubility limits calculation for performance assessment. SKB TR-06-17, Svensk Kärnbränslehantering AB.

Fernández AM, Villar MV, 2010. Geochemical behaviour of a bentonite barrier in the laboratory after up to 8 years of heating and hydration. Applied Geochemistry, 25(6): 809–824.

Follin S, Stigsson M, Svensson U, 2005. Regional hydrogeological simulations for Forsmark – numerical modelling using DarcyTools. Preliminary site description Forsmark area – version 1.2. SKB R-05-60, Svensk Kärnbränslehantering AB.

Fripiat J, Cases J, Franñois M, Letellier M, 1982. Thermodynamic and microdynamic behavior of water in clay suspensions and gels. Journal of Colloid and Interface Science 89, 378–400.

Hartley L, Hoch A, Jackson P, Joyce S, McCarthy R, Rodwell W, Swift B, Marsic N, 2006. Groundwater flow and transport modelling during the temperate period for the SR-Can assessment. Forsmark area – version 1.2. SKB R-06-98, Svensk Kärnbränslehantering AB.

Karnland O, Olsson S, Dueck A, Birgersson M, Nilsson U, Hernan-Hakansson T, Pedersen K, Nilsson S, Eriksen T-E, Rosborg B, 2009. Long-term test of buffer material at the Äspö Hard Rock Laboratory, LOT project – Final report on the A2 test parcel. SKB TR-09-29, Svensk Kärnbränslehantering AB.

Kipp K-L, 1997. Guide to the revised heat and solute transport simulator HST3D-Version 2. U.S. Geological Survey Water-Resources Investigations Report, 97-4157, 149 p.

Laaksoharju M, Smellie J, Nilsson AC, Skårman C, 1995. Groundwater sampling and chemical characterisation of the Laxemar deep borehole KLX02. SKB TR-95-05, Svensk Kärnbränslehantering.

Laaksoharju M, Gimeno M, Auqué L, Gómez J, Smellie J, Tullborg E-L, Gurban I, 2004. Hydrogeochemical Evaluation of the Forsmark Site, Model Version, 1.1. SKB R-04-05, Svensk Kärnbränslehantering AB.

Molera M, Eriksen T, Jansson M, 2003. Anion diffusion pathways in bentonite clay compacted to different dry densities. Applied Clay Science, 23: 69–76.

Muurinen A, Karnland O, Lehikoinen J, 2004. Ion concentration caused by an external solution into the porewater of compacted bentonite. Physics and Chemistry of the Earth, 29: 119–127.

Ochs M, Lothenbach B, Wanner H, 2001. An integrated sorption–diffusion model for the calculation of consistent distribution and diffusion coefficients in compacted bentonite. Journal of Contaminant Hydrology, 47: 283–296.

Ochs M, Talerico C, 2004. SR-Can. Data and uncertainty assessment. Migration parameters for the bentonite buffer in the KBS-3 concept. SKB TR-04-18, Svensk Kärnbränslehantering AB.

Olivella S, Gens A, Carrera J, Alonso, E-E, 1996. Numerical formulation for a simulator (CODE-BRIGHT) for the coupled analysis of saline media. Engineering Computations 13 (7), 87–112.

Olsson S, Karnland O, 2009. Characterisation of bentonites from Kutch, India and Milos, Greece – some candidate tunnel back-fill materials? SKB R-09-53, Svensk Kärnbränslehantering AB.

Parkhurst D-L, Appelo C-A-J, 1999. User's guide to PHREEQC (version 2) – A computer program for speciation, batch-reaction, one-dimensional transport and inverse geochemical calculations. U.S. Geological Survey Water Resources investigations report 99-4259.

Parkhurst D-L, Kipp K-L, Engesgaard P, Charlton S-R, 2004. PHAST – A program for simulating ground-water flow, solute transport, and multicomponent geochemical reactions. U.S. Geological Survey Techniques and Methods 6-A8, 154 pp.

Pedersen K, 2000. Microbial processes in radioactive waste disposal. SKB TR-00-04, Svensk Kärnbränslehantering AB.

Saaltink MW, Batlle F, Ayora C, Carrera J, Olivella S, 2004. RETRASO, a code for modeling reactive transport in saturated and unsaturated porous media, Geologica Acta, 2(3): 235–251.

Sandström B, Savolainen M, Tullborg E-L, 2004. Fracture mineralogy. Results from fracture minerals and wall rock alteration in boreholes KFM01A, KFM02A, KFM03A and KFM03B. Forsmark site investigation. SKB P-04-149, Svensk Kärnbränslehantering AB.

Sandström B, Tullborg E-L, Smellie J, MacKenzie A, Suksi J, 2008. Fracture mineralogy of the Forsmark site SDM-Site Forsmark. SKB R-08-102, Svensk Kärnbränslehantering AB.

Sena C, Salas J, Arcos D, 2010. Thermo-hydro-geochemical modelling of the bentonite buffer. The LOT-A2 experiment. SKB TR-10-65, Svensk Kärnbränslehantering AB.

SKB, 2004a. Interim process report for the safety assessment SR-Can. SKB R-04-33, Svensk Kärnbränslehantering AB.

SKB, 2004b. Interim main report of the safety assessment SR-Can. SKB TR-04-11, Svensk Kärnbränslehantering AB.

SKB, 2006. Long-term safety for KBS-3 repositories at Forsmark and Laxemar – a first evaluation. Main Report of the SR-Can project. SKB TR-06-09, Svensk Kärnbränslehantering AB.

SKB, 2010. Design, production and initial state of the backfill and plug in deposition tunnels, SKB TR-10-16, Svensk Kärnbränslehantering AB.

Van Loon LR, Glaus MA, Müller W, 2007. Anion exclusion effects in compacted bentonites: Towards a better understanding of anion diffusion. Applied Geochemistry , 22: 2536–2552.

Villar MV, Sánchez M, Gens A, 2008. Behaviour of a bentonite barrier in the laboratory: Experimental results up to 8 years and numerical simulation. Physics and Chemistry of the Earth, 33, S476-S485.

Wersin P, 2003. Geochemical modelling of bentonite porewater in high-level waste repositories. Journal of Contaminant Hydrology, 61: 405–422.

Wolery TJ, 1992. EQ3/6, A Software Package for Geochemical Modeling of Aqueous Systems: Package Overview and Installation Guide (Version 7.0). LLNL report UCRL-MA-110662 PT I.

Xu T, Pruess K, 2001. Modeling multiphase non-isothermal fluid flow and reactive geochemical transport in variably saturated fractured rocks: 1. Methodology. American Journal of Science, 301: 16–33.

Xu T, Sonnenthal E, Spycher N, Pruess K, 2008. TOUGHREACT User's Guide: A simulation program for non-isothermal multiphase reactive geochemical transport in variably saturated geologic media. Lawrence Berkeley National Laboratory, University of California, Berkeley.

Åkesson M, Kristensson O, Börgeson L, Dueck A, Hernelind J, 2010. THM modelling of buffer, backfill and other system components. Critical processes and scenarios. SKB TR-10-11, Svensk Kärnbränslehantering AB**.**